On Backus average in modelling guided waves

by

©David Raymond Dalton

A Dissertation submitted to the School of Graduate Studies in partial fulfillment of the
requirements for the degree of

Doctor of Philosophy

Department of Earth Sciences

Memorial University of Newfoundland

May 2018

St. John's   Newfoundland

Abstract

This thesis is a collection of five research papers. The first two are related to the Backus average. The second two are about guided waves. The fifth ties the two topics together.

In the first paper we derive expressions for elasticity parameters of a homogeneous generally anisotropic medium that is long-wave-equivalent to a stack of thin generally anisotropic layers, and examine the mathematical underpinnings of the formulation.

In the second paper we examine commutativity and noncommutativity of translational averages over a spatial variable and rotational averages over a symmetry group at a point. In general there is no commutativity but for weak anisotropy, which is common in near-surface seismology, there is approximate commutativity.

In the third paper we review forward-modelling expressions for Love and quasi-Rayleigh waves and examine the sensitivity of Love and quasi-Rayleigh waves to model parameters.

In the fourth paper we perform a Pareto Joint Inversion, using Particle Swarm Optimization, of synthetic dispersion curve data to obtain model parameters including densities, elasticity parameters, and layer thickness.

In the fifth paper we tie together the two topics of Backus average and guided waves by examining the applicability of the Backus average in modelling of guided waves. As expected, the Backus average is applicable only for low frequencies and/or thin layers and the results become worse when there is a strong nonalternating vertical inhomogeneity with near-surface low-velocity layers.

Acknowledgments

Table of Contents

List of Tables

List of Figures

xiii

List of Symbols

Mathematical relations and operators

ι $\sqrt{-1}$

$=$ equality

$\equiv$ equivalence

$:=$ definition

$\approx$ approximation

$\overline{f}$ average of f

$\lesssim$ slightly less than

$\ll$ much less than

∇ gradient

$\nabla\cdot$ divergence

$\nabla\times$ curl

∇^2 Laplacian

Physical quantities

Greek letters

α *P*-wave speed

β *S*-wave speed

δ a Thomsen parameter

ε_{kl} strain tensor

ε a Thomsen parameter

γ a Thomsen parameter

κ wavenumber

λ wavelength

ρ mass density

σ_{ij} stress tensor

ω angular frequency

Roman letters

c_{ijkl} elasticity tensor in $\mathbb{R}^3$

C_{mn} elasticity matrix; elasticity tensor in $\mathbb{R}^6$

$\mathcal{C}$ commutator

D_{ℓ} Love-wave dispersion determinant

D_r quasi-Rayleigh-wave dispersion determinant

G symmetry group

l' averaging width

$\mathcal{P}$ scalar potential

$\mathcal{S}$ vector potential

t time

T traction vector

u displacement

v_{ℓ} Love-wave speed

v_r quasi-Rayleigh-wave speed

w weight function

Z layer thickness

Chapter 1

Introduction and Overview

1.1 Lay summary

This thesis is a collection of five research papers. The first two are related to the Backus average. The second two are about guided waves. The fifth ties the two topics together.

The Backus average is a procedure whereby a stack of thin geological layers can be approximated, for long wavelength seismic waves, by a single thick layer. Mavko et al. [1998] suggest the necessity for layers to be at least ten times smaller than the seismic wavelength. Liner and Fei [2006] recommend the averaging length be less than or equal to one-third of the dominant seismic wavelength. For isotropic thin layers the thick layer is transversely isotropic. For all other symmetries of the thin layers the thick layer has the same symmetry as the thin layers. Transverse isotropy, in which the material is invariant to rotation about an axis, can be intrinsic, as in the case of shale or hexagonal crystals, or extrinsic, when it is due to a Backus average of a stack of parallel layers. Orthotropic symmetry, which exhibits three orthogonal symmetry planes, can be due to parallel horizontal layering combined with vertical fracturing. Monoclinic symmetry, which exhibits one symmetry plane, can be due to parallel horizontal layering combined with oblique fractures.

The guided waves that we study are Love and quasi-Rayleigh waves, which both propagate in the same model of a layer over a halfspace. Their propagation can be described in terms of total internal reflection within the layer as a waveguide. Love waves have a displacement that is parallel to the surface and perpendicular to the direction of propagation. Quasi-Rayleigh waves have displacement that is elliptical in the vertical plane containing the direction of propagation, so at the surface they have a component parallel to the surface and parallel to the direction of propagation, and a vertical component. Both Love and quasi-Rayleigh waves are dispersive, i.e. they exhibit a variation of speed with frequency, and that variation can be plotted as dispersion curves.

In the fifth paper we compare two approaches to solving for dispersion curves. One is the propagator matrix formulation, whereby the dispersion relation, which can be solved to obtain the dispersion curves, can be formulated as a product of layer matrices for a stack of layers. In the other approach we take the Backus average of the stack of layers and calculate the dispersion curves for the resulting thicker layer over the halfspace. It turns out that, as expected, the Backus average solution matches the propagator matrix solution only for low frequencies or thin layers.

1.2   Summary

This thesis is in manuscript format and consists of a collection of five related research papers: two about the Backus average, two about guided Love and quasi-Rayleigh waves, and a fifth paper which ties the two topics together. This section is based on the abstracts of the five papers, with a little added material.

In the first paper (Chapter 2), following the Backus [1962] approach, my coauthors and I derive a matrix formulation for elasticity parameters of a homogeneous generally anisotropic medium that is long-wave-equivalent to a stack of thin generally anisotropic layers.

We use this formulation to derive equivalent-medium elasticity parameters for the cases of stacks of monoclinic and of orthotropic layers. These expressions reduce to the results of Backus [1962] for the case of isotropic and transversely isotropic layers. In the over half-a-century since the publication of Backus [1962] there have been numerous publications applying and extending that formulation. However, my coauthors and I are unaware of further examinations of the mathematical foundations of the original formulation; hence this paper. We prove that—within the long-wave approximation—if the thin layers obey stability conditions, then so does the equivalent medium. We examine—within the Backus-average context—the approximation of the average of a product as the product of averages. This approximation underlies the averaging process. In the presented examination we use the expression of Hooke's law as a tensor equation; in other words, we use Kelvin's—as opposed to Voigt's—notation. In general, this tensorial notation allows us to conveniently examine effects due to rotations of coordinate systems.

In the second paper (Chapter 3), my coauthors and I show that, in general, the translational average over a spatial variable—discussed by Backus [1962], and referred to as the equivalent-medium average—and the rotational average over a symmetry group at a point—discussed by Gazis et al. [1963], and referred to as the effective-medium average—do not commute. However, they do commute in special cases of particular symmetry classes, which correspond to special relations among the elasticity parameters. We also show that the noncommutativity is a function of the strength of anisotropy. Surprisingly, a perturbation of the elasticity parameters about a point of weak anisotropy results in the commutator of the two types of averaging being of the order of the *square* of this perturbation. Thus, these averages nearly commute in the case of weak anisotropy, which is of interest in such disciplines as quantitative seismology, where the weak-anisotropy assumption results in empirically adequate models.

In the third paper (Chapter 4), my coauthors and I examine the sensitivity of the Love

and the quasi-Rayleigh waves to model parameters. Both waves are guided waves that propagate in the same model of an elastic layer above an elastic halfspace. We study their dispersion curves without any simplifying assumptions such as those made by some past authors, beyond the standard approach of elasticity theory in isotropic media. We examine the sensitivity of both waves to elasticity parameters, frequency and layer thickness, for varying frequency and different modes. In the case of Love waves, we derive and plot the absolute value of a dimensionless sensitivity coefficient in terms of partial derivatives, and perform an analysis to find the optimum frequency for determining the layer thickness. For a coherency of the background information, we briefly review the Love-wave dispersion relation and provide details of the less common derivation of the quasi-Rayleigh relation in an appendix. We compare that derivation to past results in the literature, finding certain discrepancies among them.

In the fourth paper (Chapter 5), my coauthors and I use the Pareto Joint Inversion, together with the Particle Swarm Optimization, to invert Love and quasi-Rayleigh surface-wave speeds, obtained from dispersion curves, to infer the elasticity parameters, mass densities and layer thickness of the model for which these curves are generated. For both waves, we use the dispersion relations derived by Dalton et al. [2017]. All computations are done for three angular frequencies, 15, 60 and 100 s^{-1}, and for two, five and seven modes, respectively. Results for all these frequencies are similar so detailed results and their discussion are presented for 15 s^{-1} and 60 s^{-1} selected solutions as representative examples. Comparisons of the model parameters with the values inverted with error-free input indicate an accurate process with potential for practical application. If, however, we introduce a constant error to the input, the results become significantly less accurate, which indicates that the inverse operation is error-sensitive. The results suggest that the layer parameters are more sensitive to input errors than the halfspace parameters. In agreement with Dalton et al. [2017], the fundamental mode is mainly sensitive to the layer parameters

4

whereas higher modes are sensitive to both the layer and halfspace properties; for the second mode, the results for the halfspace are more accurate for low frequencies. Additionally, strong correlations are observed between the inverted elasticity parameters for the layer.

In the fifth paper (Chapter 6), my coauthors and I tie together the two topics of Backus average and guided waves. We study the Backus [1962] average of a stack of layers overlying a halfspace to examine its applicability for the quasi-Rayleigh and Love wave dispersion curves. We choose these waves since both propagate in the same model. We compare these curves to values obtained for the stack of layers using the propagator matrix. In contrast to the propagator matrix, the Backus [1962] average is applicable only for thin layers or low frequencies. This is true for both a weakly inhomogeneous stack of layers resulting in a weakly anisotropic medium and a strongly inhomogeneous stack of alternating layers resulting in a strongly anisotropic medium. We also compare the strongly anisotropic and weakly anisotropic media, given by the Backus [1962] averages, to results obtained by the isotropic Voigt [1910] averages of these media. As expected, we find only a small difference between these results for weak anisotropy and a large difference for strong anisotropy. We perform the Backus [1962] average for a stack of alternating transversely isotropic layers that is strongly inhomogeneous to evaluate the dispersion relations for the resulting medium. We compare the resulting dispersion curves to values obtained using a propagator matrix for that stack of layers. Again, there is a good match only for thin layers or low frequencies. Finally, we perform the Backus [1962] average for a stack of non-alternating transversely isotropic layers that is strongly inhomogeneous, and evaluate the quasi-Rayleigh wave dispersion relations for the resulting transversely isotropic medium. We compare the resulting curves to values obtained using the propagator matrix for the stack of layers. In this case, the Backus [1962] average performs less well, but—for the fundamental mode—remains adequate for low frequencies or thin layers.

Another factor, other than the examination in Chapter 6, that ties together the two topics

5

of Backus average and guided waves is that both topics deal with seismic wave propagation in horizontally layered elastic media. Indeed, Backus [1962] suggests that his results might be obtained by taking the small-wave-number limit of the matrix products of Thomson [1950] and Haskell [1953], but we are unaware of anyone having done so.

1.3   Literature review

In this thesis, particularly in Chapters 2, 3, and 6, we build on the work of Backus [1962] on equivalent-medium parameters for the propagation of long wavelength waves in a finely layered, horizontally stratified medium. Backus [1962] built on the earlier work of Riznichenko [1949], White and Angona [1955], Postma [1955], Rytov [1956], and Helbig [1958], all of whom considered a periodic medium and did not consider the case where the individual layers are intrinsically anisotropic.

Our equivalent medium results for generally anisotropic layers in Section 2.3 were independently derived, but a literature review showed that they are similar to the results of Schoenberg and Muir [1989], Helbig and Schoenberg [1987, Appendix], Helbig [1998], Carcione et al. [2012] and Kumar [2013]. The novelty of our formulation is the use of Kelvin's notation instead of Voigt's notation for the elasticity matrix. This notation allows for a convenient study of rotations, which arise in the study of elasticity tensors expressed in coordinate systems of arbitrary orientations.

The results of our Section 2.4.1 differ from the results of Kumar [2013, Appendix B] because Kumar [2013] uses a vertical $(x_1 x_3)$ symmetry plane whereas we use a horizontal $(x_1 x_2)$ symmetry plane, which—since it is parallel to the layering—produces simpler equations, which we have not found elsewhere in the literature.

The results of our Section 2.4.2 agree with the results of Tiwary [2007, expression (5.1)] except for the fifth equation of that expression, which contains a typographical error: C_{13}

instead of C_{23}. Tiwary [2007] references that expression to Shermergor [1977, expression (2.4)], a book in Russian. An anonymous reviewer has informed us that the error is not in Shermergor [1977] but originates in Tiwary [2007]. The results of that section also agree with the results of Kumar [2013, Appendix B] and of Slawinski [2018, Exercise 4.6].

Other papers relevant to the Backus average are Berryman [1997], Helbig [2000], Brisco [2014], Danek and Slawinski [2016], Bos et al. [2017b], and Liner and Fei [2006].

Also, Backus's results have been extended to the more general case of two-scale homogenization for non-periodic media by Capdeville et al. [2010a,b, 2013], Guillot et al. [2010]. Capdeville et al. [2013] show that the result of a full-waveform inversion is equivalent to the homogenized residual model, the equivalent medium of the difference between a reference model and a 'real' model.

In Chapter 3, we also draw on papers related to effective media obtained using a rotational average over a symmetry group at a point. The computationally simplest case of this is finding the nearest isotropic tensor to a given elasticity tensor, which was derived by Voigt [1910]. The theory for other effective medium symmetry classes was developed by Gazis et al. [1963] and is reviewed in Slawinski [2018]. In Chapter 3 we assume that all tensors are expressed in the same orientation of their coordinate systems. Otherwise, the process of averaging become more complicated, as discussed—for the Gazis et al. [1963] average—by Danek et al. [2015a], Kochetov and Slawinski [2009a,b].

In Chapter 4, we present the Love-wave dispersion relation and refer the reader to Slawinski [2018, Chapter 6] and references therein for details of its derivation. However we do present the less-common details of the derivation of the quasi-Rayleigh-wave dispersion relation and compare it to earlier results of Love [1911], who considers the incompressible case, and Lee [1932], Fu [1946], Udías [1999], and Ben-Menahem and Singh [2000]. We found some errors in some of the equations of Udías [1999] though his plots seem fine, and the other formulations matched ours within multiplicative factors. Unlike Love [1911],

who assumes incompressibility, Udías [1999], who assumes a Poisson's ratio of $1/4$, and Fu [1946], who studies limiting cases, we do not make any simplifying assumptions prior to calculations for the study of sensitivity.

Some other approaches of studying sensitivities of Love and quasi-Rayleigh waves to model parameters are presented by Lucena and Taioli [2014], who examine the response of the dispersion curves to shifts in parameter values. and Novotný [1976], who investigates methods of computing the partial derivatives of dispersion curves.

In Chapter 5, we use Pareto Joint Inversion using Particle Swarm Optimization to invert dispersion curve data to obtain model parameters. Particle Swarm Optimization was first presented by Kennedy and Eberhart [1995], and Parsopoulos and Vrahatis [2002] first used it in the context of Pareto Joint Inversion.

A common technique to obtain quasi-Rayleigh wave dispersion curves is the Multichannel Analysis of Surface Waves technique [Park et al., 1999]. An approach to inverting such curves for multiple layers is given in Xia et al. [1999], who use the Levenberg-Marquardt and singular-value decomposition techniques to analyze the Jacobi matrix, and demonstrate sensitivity of material properties to the dispersion curve.

Wathelet et al. [2004] use a neighbourhood algorithm, which is a stochastic direct-search technique, to invert quasi-Rayleigh-wave dispersion curves obtained from ambient vibration measurements. Lu et al. [2007] invert quasi-Rayleigh waves in the presence of a low-velocity layer, using a genetic algorithm. Boxberger et al. [2011] perform a joint inversion, based on a genetic algorithm, using quasi-Rayleigh and Love wave dispersion curves and Horizontal-to-Vertical Spectral Ratio curves obtained from seismic noise array measurements. Fang et al. [2015] invert surface wave dispersion data without generating phase or group velocity maps, using raytracing and a tomographic inversion. Xie and Liu [2015] perform Love-wave inversion for a near-surface transversely isotropic structure, using the Very Fast Simulated Annealing algorithm.

Wang et al. [2015] use surface wave phase velocity inversion, based on first-order perturbation theory, including multiple modes and both quasi-Rayleigh and Love waves, to examine intrinsic versus extrinsic radial anisotropy in the Earth; the latter anisotropy refers to a homogenized model. Wang et al. [2015] use the classical iterative quasi-Newton method to minimize the L_2 norm misfit and introduce the Generalized Minimal Residual Method.

Dal Moro and Ferigo [2011] carry out a Pareto Joint Inversion of synthetic quasi-Rayleigh- and Love-wave dispersion curves for a multiple-layer model using an evolutionary algorithm optimization scheme. Dal Moro [2010] examines a Pareto Joint Inversion using an evolutionary algorithm of the combined quasi-Rayleigh and Love wave surface-wave dispersion curves and Horizontal-to-Vertical Spectral Ratio data. Dal Moro et al. [2015] perform a three-target Pareto Joint Inversion based on full velocity spectra, using an evolutionary algorithm optimization scheme. Unlike Dal Moro and his colleagues, we use Particle Swarm Optimization instead of an evolutionary algorithm.

Romanowicz [2002] presents an overview of progress in the last few decades of the 20th century in analysis of surface wave data to obtain Earth structure and earthquake source parameters.

In Chapter 6, we draw on the Backus [1962] average and Voigt [1910] average as well as the Thomsen [1986] parameters for quantifying the anisotropy of a transversely isotropic elasticity tensor. We also use the dispersion relations for Love and quasi-Rayleigh waves presented in Chapter 4 for an isotropic layer over an isotropic halfspace. For a transversely isotropic layer, the dispersion relations for quasi-Rayleigh and Love waves are given by setting to zero the determinants of the matrices in equations (29) and (30), respectively, of Khojasteh et al. [2008]. These relations can also be derived by setting to zero the thickness of the liquid layer in equations (22) and (23) of Bagheri et al. [2015]. For a stack of isotropic layers overlying an isotropic halfspace, the dispersion relations for Love and quasi-Rayleigh waves are based on a propagator matrix, specifically, on the delta-matrix

9

solution reviewed in Buchen and Ben-Hador [1996], which builds on the earlier work of Thomson [1950] and Haskell [1953]. For a stack of transversely isotropic layers overlying a transversely isotropic halfspace, the dispersion relation for quasi-Rayleigh waves is based on the reduced-delta-matrix solution of Ikeda and Matsuoka [2013], and the dispersion relation for Love waves is based on the delta-matrix solution reviewed in Buchen and Ben-Hador [1996] but with pseudorigidity and pseudothickness defined as in Anderson [1962].

Two other papers that deal with calculating surface-wave dispersion curves for anisotropic media are Crampin [1970], which still has the high-frequency instability problem that occurred in the original Thomson-Haskell formulation, and Ke et al. [2011].

The only reference we have found in which an equivalent medium formulation is tested in the context of dispersion curve modelling is Anderson [1962]. He extended the Haskell [1953] method for multilayered media to the case of Love waves in a stack of transversely isotropic layers. He used the results of Postma [1955] to compare dispersion curves for a laminated (periodic) stack of isotropic layers over a halfspace to those for the equivalent transversely isotropic medium over the same halfspace. He also performed calculations for an example of two such laminated stacks over a halfspace. In Chapter 6, we broaden this work to quasi-Rayleigh waves and, drawing on the work of Backus [1962], to a nonalternating stack of isotropic layers. We extend the scope to include Love waves for a stack of alternating transversely isotropic layers and quasi-Rayleigh waves for stacks of alternating and nonalternating transversely isotropic layers.

Co-authorship Statement

In writing the five papers included in this thesis, my coauthors and I have followed the practice common in mathematical journals of listing the authors alphabetically. The papers are collaborative and interdisciplinary and there is no principal author, but I did contribute significantly to each paper, and summarize my contributions below.

While I was engaged in much of the manuscript writing and literature review, there were exchanges of drafts among coauthors. Two of the papers have already been published in peer-reviewed journals and I have been engaged in the process of revision, correspondence with editors, and replies to reviewers.

Chapter 2 is a slightly modified version of L. Bos, D.R. Dalton, M.A. Slawinski, and T. Stanoev. On Backus average for generally anisotropic layers. *Journal of Elasticity*, 127(2): 179–196, 2017. I was involved with all aspects of the research. In particular, I focused on deriving the matrix formulation of the Backus average for generally anisotropic layers, including the reduction to monoclinic and orthotropic symmetries.

Chapter 3 is a slightly modified version of L. Bos, D.R. Dalton, and M.A. Slawinski. On commutativity and near commutativity of translational and rotational averages: Analytical proofs and numerical examinations. Published as arXiv: 1704.05541v3 [physics.geo-ph], 2017. Submitted to *Journal of Elasticity*, ELAS-D-17-00135, December, 2017. I was involved in all aspects of the research.

Chapter 4 is a slightly modified version of D.R. Dalton, M.A. Slawinski, P. Stachura,

and T. Stanoev. Sensitivity of Love and quasi-Rayleigh waves to model parameters. *The Quarterly Journal of Mechanics and Applied Mathematics*, 70(2): 103–130, 2017. I was engaged in the entire paper, with particular emphasis on Sections 4.2 and 4.3 and Appendices 4.A and 4.C.

Chapter 5 is a slightly modified version of A. Bogacz, D.R. Dalton, T. Danek, K. Miernik, and M.A. Slawinski. On Pareto Joint Inversion of guided waves. arXiv:1712.09850v4 [physics.geo-ph], 2018. Submitted to *Journal of Applied Geophysics*, April, 2018. I was engaged in the entire paper, with particular emphasis on the forward modelling target functions for Love and quasi-Rayleigh waves and dispersion-curve data to use as input to the inversion.

Chapter 6 is a slightly modified version of D.R. Dalton, T.B. Meehan, and M.A. Slawinski. On Backus average in modelling guided waves. arXiv:1801.05464v2 [physics.geo-ph], 2018. Submitted to *Journal of Applied Geophysics*, March, 2018. I was involved in all aspects of the research, particularly focusing on (a) forward modelling of Love and quasi-Rayleigh wave dispersion curves for an isotropic layer over an isotropic halfspace using dispersion relations presented in Dalton et al. [2017], (b) forward modelling of Love and quasi-Rayleigh wave dispersion curves for a transversely isotropic layer over an isotropic or transversely isotropic halfspace using equations given in Khojasteh et al. [2008], (c) calculating the Backus averages of the stacks of isotropic or transversely isotropic layers, (d) generating all of the plots other than Figure 6.1, and (e) supervision of undergraduate student Thomas B. Meehan, who performed the calculations of dispersion curves for the multilayer case.

The modifications made herein to the two published and three submitted papers were both in formatting, to adjust line spacing and margins for the thesis format, and in some brief responses to the final Ph.D. defence examiners' questions and comments, and in a few corrections. Some of those responses and corrections may be incorporated in the three

submitted papers at the revision stage, after we have heard from reviewers, but do not warrant errata for the two published papers.

Chapter 2

On Backus average for generally anisotropic layers[*]

Abstract

In this paper, following the Backus [1962] approach, we examine expressions for elasticity parameters of a homogeneous generally anisotropic medium that is long-wave-equivalent to a stack of thin generally anisotropic layers. These expressions reduce to the results of Backus [1962] for the case of isotropic and transversely isotropic layers.

In the over half-a-century since the publications of Backus [1962] there have been numerous publications applying and extending that formulation. However, neither George Backus nor the authors of the present paper are aware of further examinations of the mathematical underpinnings of the original formulation; hence this paper.

We prove that—within the long-wave approximation—if the thin layers obey stability conditions, which means that it takes work to deform the material, which is equivalent to positive definiteness of the elasticity tensor, then so does the equivalent medium.

14

We examine—within the Backus-average context—the approximation of the average of a product as the product of averages, which underlies the averaging process.

In the presented examination we use the expression of Hooke's law as a tensor equation; in other words, we use Kelvin's—as opposed to Voigt's—notation. In general, the tensorial notation allows us to conveniently examine effects due to rotations of coordinate systems.

2.1   Introduction and historical background

The study of properties of materials as a function of scale has occupied researchers for decades. Notably, the discipline of continuum mechanics originates, at least partially, from such a consideration. Herein, we focus our attention on the effect of a series of thin and laterally homogeneous layers on a long-wavelength wave. These layers are composed of generally anisotropic Hookean solids.

Such a mathematical formulation serves as a quantitative analogy for phenomena examined in seismology. The effect of seismic disturbances—whose wavelength is much greater than the size of encountered inhomogeneities—is tantamount to the smearing of the mechanical properties of such inhomogeneities. The mathematical analogy of this smearing is expressed as averaging. The result of this averaging is a homogeneous anisotropic medium to which we refer as an *equivalent medium.*

We refer to the process of averaging as *Backus averaging*, which is a common nomenclature in seismology. However, several other researchers have contributed to the development of this method.

Backus [1962] built on the work of Rudzki [1911], Riznichenko [1949], Thomson [1950], Haskell [1953], White and Angona [1955], Postma [1955], Rytov [1956], Helbig [1958] and Anderson [1961] to show that a homogeneous transversely isotropic medium with a vertical symmetry axis could be long-wave equivalent to a stack of thin isotropic or

transversely isotropic layers. In other words, the Backus average of thin layers appears—at the scale of a long wavelength—as a homogeneous transversely isotropic medium.

In this paper, we discuss the mathematical underpinnings of the Backus [1962] formulation. To do so, we consider a homogeneous generally anisotropic medium that is long-wave equivalent to a stack of thin generally anisotropic layers. The cases discussed explicitly by Backus [1962] are special cases of this general formulation.

2.2 Averaging Method

2.2.1 Assumptions

We assume the lateral homogeneity of Hookean solids consisting of a series of layers that are parallel to the x_1x_2-plane and have an infinite lateral extent. We subject this series of layers to the same traction above and below, independent of time or lateral position. It follows that the stress tensor components σ_{i3}, where $i \in \{1,2,3\}$, are constant throughout the strained medium, due to the requirement of equality of traction across interfaces (e.g., Slawinski [2015], pp. 430–432), and to the definition of the stress tensor,

$$T_i = \sum_{j=1}^{3} \sigma_{ij}n_j, \qquad i \in \{1,2,3\},$$

where T is traction and n is the unit normal to the interface. No such equality is imposed on the other three components of this symmetric tensor; σ_{11}, σ_{12} and σ_{22} can vary greatly along the x_3-axis due to changes of elastic properties from layer to layer.

Furthermore, regarding the strain tensor, we invoke the kinematic boundary conditions that require no slippage or separation between layers; in other words, the corresponding components of the displacement vector, u_1, u_2 and u_3, must be equal to one another across the interface (e.g., Slawinski [2015], pp. 429–430).

16

These conditions are satisfied if u is continuous. Furthermore, for parallel layers, its derivatives with respect to x_1 and x_2, evaluated along the x_3-axis, remain small. However, its derivatives with respect to x_3, evaluated along that axis, can vary wildly.

The reason for the differing behaviour of the derivatives resides within Hooke's law,

$$\sigma_{ij} = \sum_{k=1}^{3} \sum_{\ell=1}^{3} c_{ijk\ell} \varepsilon_{k\ell}, \qquad i,j \in \{1,2,3\}, \tag{2.1}$$

where

$$\varepsilon_{k\ell} := \frac{1}{2} \left(\frac{\partial u_k}{\partial x_\ell} + \frac{\partial u_\ell}{\partial x_k} \right), \qquad k,\ell \in \{1,2,3\}. \tag{2.2}$$

Within each layer, derivatives are linear functions of the stress tensor. The derivatives with respect to x_1 and x_2 remain within a given layer; hence, the linear relation remains constant. The derivatives with respect to x_3 exhibit changes due to different properties of the layers.

In view of definition (2.2), ε_{11}, ε_{12} and ε_{22} vary slowly along the x_3-axis. On the other hand, ε_{13}, ε_{23} and ε_{33} can vary wildly along that axis.

Herein, we assume that the elasticity parameters are expressed with respect to the same coordinate system for all layers. However, this *a priori* assumption can be readily removed by rotating, if necessary, the coordinate systems to express them in the same orientation.

2.2.2   Definitions

Following the definition proposed by Backus [1962], the average of the function $f(x_3)$ of "width" ℓ' is the moving average given by

$$\overline{f}(x_3) := \int_{-\infty}^{\infty} w(\zeta - x_3) f(\zeta) \, d\zeta, \tag{2.3}$$

where the weight function, $w(x_3)$, is an *approximate identity*, which is an approximate Dirac delta that acts like the delta centred at $x_3 = 0$, with the following properties:

$$w(x_3) \geqslant 0, \quad w(\pm\infty) = 0, \quad \int\limits_{-\infty}^{\infty} w(x_3)\,dx_3 = 1, \quad \int\limits_{-\infty}^{\infty} x_3 w(x_3)\,dx_3 = 0, \quad \int\limits_{-\infty}^{\infty} x_3^2 w(x_3)\,dx_3 = (\ell')^2.$$

These properties define $w(x_3)$ as a probability-density function with mean 0 and standard deviation ℓ', explaining the use of the term "width" for ℓ'.

To understand the effect of such averaging, which, as demonstrated by Liner and Fei [2006] by numerical simulation of wavefields in Backus-averaged and original earth models, is tantamount to smoothing by a wave, we may consider its effect on the pure frequency, $f(x_3) = \exp(-i\omega x_3)$,

$$\overline{f}(x_3) = \int\limits_{-\infty}^{\infty} w(\zeta - x_3) f(\zeta)\,d\zeta = \int\limits_{-\infty}^{\infty} w(\zeta - x_3)\exp(-\iota\omega\zeta)\,d\zeta = \int\limits_{-\infty}^{\infty} w(u)\exp(-\iota\omega(u + x_3))\,du.$$

where $u := \zeta - x_3$ and $\iota := \sqrt{-1}$; it follows that

$$\overline{f}(x_3) = \exp(-\iota\omega x_3) \int\limits_{-\infty}^{\infty} w(u)\exp(-\iota\omega u)\,du = \exp(-\iota\omega x_3)\widehat{w}(\omega),$$

where $\widehat{w}(\omega)$ is the Fourier transform of $w(x_3)$.

Since, in addition, $w(x_3)$ is an even function, then $\widehat{w}(\omega)$ is real-valued and we may think of $\overline{f}(x_3)$ as the pure frequency, $\exp(-\iota\omega x_3)$, whose "amplitude" is $\widehat{w}(\omega)$. The classical Riemann-Lebesgue Lemma implies that this amplitude tends to zero as the frequency goes to infinity. To examine this decay of amplitude, we may consider a common choice for $w(x_3)$, namely, the Gaussian density,

$$w(x_3) = \frac{1}{\ell'\sqrt{2\pi}}\exp\left(-\frac{x_3^2}{2(\ell')^2}\right).$$

18

As is well known, in this case,

$$\widehat{w}(\omega) = \exp\left(-\frac{(\omega\ell')^2}{2}\right),$$

which is a multiple of the Gaussian density with standard deviation $1/\ell'$. In particular, one notes the fast decay, as the product $\omega\ell'$ increases.

Perhaps it is useful to look at another example. Consider

$$w(x_3) = \frac{1}{2\sqrt{3}\,\ell'}I_{[-\sqrt{3}\ell',\sqrt{3}\ell']},$$

which is the uniform density on the interval $[-\sqrt{3}\,\ell', \sqrt{3}\,\ell']$, and which satisfies the defining properties of $w(x_3)$, as required. Its Fourier transform is

$$\widehat{w}(\omega) = \frac{\sin(\sqrt{3}\omega\ell')}{\sqrt{3}\omega\ell'},$$

and, as expected, this amplitude tends to zero as $\omega \to \pm\infty$, but at a much slower rate than in the Gaussian case; herein, the decay rate is order $1/(\omega\ell')$.

But from the above, note that if the averaging is the arithmetic average over a boxcar of height Z, then $\ell' = Z/(2\sqrt{3})$, which we will discuss again in Chapter 6.

2.2.3 Properties

To perform the averaging, we use its linearity, according to which the average of a sum is the sum of the averages, $\overline{f+g} = \overline{f} + \overline{g}$. Also, we use the following lemma, which is equivalent to equation (2) of Backus [1962]:

Lemma 2.2.1. *The average of the derivative is the derivative of the average,*

$$\overline{\frac{\partial f}{\partial x_i}} = \frac{\partial}{\partial x_i}\overline{f}, \qquad i \in \{1,2,3\}.$$

19

This lemma is proved in Appendix 2.A. In Appendix 2.B, we prove the lemma that ensures that the average of Hookean solids results in a Hookean solid, which is

Lemma 2.2.2. *If the individual layers satisfy the stability condition, so does their equivalent medium.*

The stability condition is that work is required to deform a medium, which is equivalent to positive definiteness of the elasticity tensor. The proof of this lemma invokes Lemma 2.2.3, below.

2.2.4 Approximations

In Appendix 2.C, we state and prove a result that may be paraphrased as

Lemma 2.2.3. *If $f(x_3)$ is nearly constant along x_3 and $g(x_3)$ does not vary excessively, then $\overline{fg} \approx \overline{f}\,\overline{g}$,*

which is also stated in equation (3) of Backus [1962].

An approximation—within the physical realm—is our applying the static-case properties to examine wave propagation, which is a dynamic process. As stated in Section 2.2.1, in the case of static equilibrium, σ_{i3}, where $i \in \{1,2,3\}$, are constant. We consider that these stress-tensor components remain nearly constant along the x_3-axis, for the farfield and long-wavelength phenomena. As suggested by Backus [1962], the concept of a long wavelength can be quantified as $\kappa \ell' \ll 1$, where κ is the wave number. Similarly, we consider that ε_{11}, ε_{12} and ε_{22} remain slowly varying along that axis.

Also, we assume that waves propagate perpendicularly, or nearly so, to the interfaces. Otherwise, due to inhomogeneity between layers, the proportion of distance travelled in each layer is a function of the source-receiver offset, which—in principle—entails that averaging requires different weights for each layer depending on the offset [Dalton and

Slawinski, 2016]. However traveltime results for oblique incidence of angles up to 45 degrees aren't much in error if we just do a weighting based on layer thickness. And results for guided waves in Chapter 6 are surprisingly good, perhaps since the guided waves can be expressed as interference of upgoing and downgoing totally internally reflected body waves.

2.3 Equivalent-medium elasticity parameters

Consider the constitutive equation for a generally anisotropic Hookean solid,

$$
\begin{bmatrix} \sigma_{11} \\ \sigma_{22} \\ \sigma_{33} \\ \sqrt{2}\sigma_{23} \\ \sqrt{2}\sigma_{13} \\ \sqrt{2}\sigma_{12} \end{bmatrix} = \begin{bmatrix} c_{1111} & c_{1122} & c_{1133} & \sqrt{2}c_{1123} & \sqrt{2}c_{1113} & \sqrt{2}c_{1112} \\ c_{1122} & c_{2222} & c_{2233} & \sqrt{2}c_{2223} & \sqrt{2}c_{2213} & \sqrt{2}c_{2212} \\ c_{1133} & c_{2233} & c_{3333} & \sqrt{2}c_{3323} & \sqrt{2}c_{3313} & \sqrt{2}c_{3312} \\ \sqrt{2}c_{1123} & \sqrt{2}c_{2223} & \sqrt{2}c_{3323} & 2c_{2323} & 2c_{2313} & 2c_{2312} \\ \sqrt{2}c_{1113} & \sqrt{2}c_{2213} & \sqrt{2}c_{3313} & 2c_{2313} & 2c_{1313} & 2c_{1312} \\ \sqrt{2}c_{1112} & \sqrt{2}c_{2212} & \sqrt{2}c_{3312} & 2c_{2312} & 2c_{1312} & 2c_{1212} \end{bmatrix} \begin{bmatrix} \varepsilon_{11} \\ \varepsilon_{22} \\ \varepsilon_{33} \\ \sqrt{2}\varepsilon_{23} \\ \sqrt{2}\varepsilon_{13} \\ \sqrt{2}\varepsilon_{12} \end{bmatrix},
$$

(2.4)

where the elasticity tensor, whose components constitute the 6×6 matrix, C, is positive-definite. This expression is equivalent to the canonical form of Hooke's law stated in expression (2.1). In expression (2.4), the elasticity tensor, $c_{ijk\ell}$, which in its canonical form is a fourth-rank tensor in three dimensions, is expressed as a second-rank tensor in six dimensions, and equations (2.4) constitute tensor equations (e.g., Chapman [2004, Section 4.4.2] and Slawinski [2015, Section 5.2.5]). This formulation is referred to as Kelvin's notation. A common notation, known as Voigt's notation, which does not have the factors of 2 and $\sqrt{2}$ in the entries of C, does not constitute a tensor equation.

To apply the averaging process for a stack of generally anisotropic layers, we express equations (2.4) in such a manner that the left-hand sides of each equation consist of rapidly

varying stresses or strains and the right-hand sides consist of algebraic combinations of rapidly varying layer-elasticity parameters multiplied by slowly varying stresses or strains.

First, consider the equations for σ_{33}, σ_{23} and σ_{13}, which can be written as

$$\sigma_{33} = c_{1133}\varepsilon_{11} + c_{2233}\varepsilon_{22} + c_{3333}\varepsilon_{33} + \sqrt{2}c_{3323}\sqrt{2}\varepsilon_{23} + \sqrt{2}c_{3313}\sqrt{2}\varepsilon_{13} + \sqrt{2}c_{3312}\sqrt{2}\varepsilon_{12}$$

$$\sqrt{2}\sigma_{23} = \sqrt{2}c_{1123}\varepsilon_{11} + \sqrt{2}c_{2223}\varepsilon_{22} + \sqrt{2}c_{3323}\varepsilon_{33} + 2c_{2323}\sqrt{2}\varepsilon_{23} + 2c_{2313}\sqrt{2}\varepsilon_{13} + 2c_{2312}\sqrt{2}\varepsilon_{12}$$

$$\sqrt{2}\sigma_{13} = \sqrt{2}c_{1113}\varepsilon_{11} + \sqrt{2}c_{2213}\varepsilon_{22} + \sqrt{2}c_{3313}\varepsilon_{33} + 2c_{2313}\sqrt{2}\varepsilon_{23} + 2c_{1313}\sqrt{2}\varepsilon_{13} + 2c_{1312}\sqrt{2}\varepsilon_{12},$$

which then can be written as the matrix equation,

$$
\underbrace{\begin{pmatrix} c_{3333} & \sqrt{2}c_{3323} & \sqrt{2}c_{3313} \\ \sqrt{2}c_{3323} & 2c_{2323} & 2c_{2313} \\ \sqrt{2}c_{3313} & 2c_{2313} & 2c_{1313} \end{pmatrix}}_{M}
\underbrace{\begin{pmatrix} \varepsilon_{33} \\ \sqrt{2}\varepsilon_{23} \\ \sqrt{2}\varepsilon_{13} \end{pmatrix}}_{E}
=
\underbrace{\begin{pmatrix} \sigma_{33} - c_{1133}\varepsilon_{11} - c_{2233}\varepsilon_{22} - \sqrt{2}c_{3312}\sqrt{2}\varepsilon_{12} \\ \sqrt{2}\sigma_{23} - \sqrt{2}c_{1123}\varepsilon_{11} - \sqrt{2}c_{2223}\varepsilon_{22} - 2c_{2312}\sqrt{2}\varepsilon_{12} \\ \sqrt{2}\sigma_{13} - \sqrt{2}c_{1113}\varepsilon_{11} - \sqrt{2}c_{2213}\varepsilon_{22} - 2c_{1312}\sqrt{2}\varepsilon_{12} \end{pmatrix}}_{A}
$$

$$
=
\underbrace{\begin{pmatrix} \sigma_{33} \\ \sqrt{2}\sigma_{23} \\ \sqrt{2}\sigma_{13} \end{pmatrix}}_{G}
-
\underbrace{\begin{pmatrix} c_{1133} & c_{2233} & \sqrt{2}c_{3312} \\ \sqrt{2}c_{1123} & \sqrt{2}c_{2223} & 2c_{2312} \\ \sqrt{2}c_{1113} & \sqrt{2}c_{2213} & 2c_{1312} \end{pmatrix}}_{B}
\underbrace{\begin{pmatrix} \varepsilon_{11} \\ \varepsilon_{22} \\ \sqrt{2}\varepsilon_{12} \end{pmatrix}}_{F}.
$$

$$(2.5)$$

M is invertible, since it is positive-definite and, hence, its determinant is strictly positive. This positive definiteness follows from the positive definiteness of C, given in expression (2.4), for $x \in \mathbb{R}^3 \backslash \{0\}$ and $y := [0,0,x^t,0]^t$, $x^t M x = y^t C y > 0$ as $y \neq 0$. This follows only if C is in Kelvin notation, and allows us to conclude that—since the positive definiteness is the sole constraint on the values of elasticity parameters—the Backus average is allowed for any sequence of layers composed of Hookean solids.

Notably, determinants of M, in expression (2.5), differ by a factor of four between Voigt's notation and Kelvin's notation, used herein. The final expressions for the equivalent

medium, however, appear to be the same for both notations.

Multiplying both sides of equation (2.5) by M^{-1}, we express the rapidly varying E as

$$E = M^{-1}A = M^{-1}(G - BF) = M^{-1}G - (M^{-1}B)F, \qquad (2.6)$$

which means that

$$M^{-1}G = E + (M^{-1}B)F,$$

and can be averaged to get

$$\overline{M^{-1}G} \approx \overline{E} + \overline{(M^{-1}B)}\,\overline{F},$$

and, hence, effectively,

$$\overline{G} = \overline{(M^{-1})}^{-1}\left[\overline{E} + \overline{(M^{-1}B)}\,\overline{F}\right] = \overline{(M^{-1})}^{-1}\overline{E} + \overline{(M^{-1})}^{-1}\overline{(M^{-1}B)}\,\overline{F}. \qquad (2.7)$$

Comparing expression (2.7) with the pattern of the corresponding three lines of C in expression (2.4), we obtain formulæ for the equivalent-medium elasticity parameters.

To obtain the remaining formulæ, let us examine the equations for the rapidly varying σ_{11}, σ_{22} and σ_{12}, which, from equation (2.4), can be written as

$$\underbrace{\begin{pmatrix} \sigma_{11} \\ \sigma_{22} \\ \sqrt{2}\sigma_{12} \end{pmatrix}}_{H} = \underbrace{\begin{pmatrix} c_{1111} & c_{1122} & \sqrt{2}c_{1112} \\ c_{1122} & c_{2222} & \sqrt{2}c_{2212} \\ \sqrt{2}c_{1112} & \sqrt{2}c_{2212} & 2c_{1212} \end{pmatrix}}_{J} \underbrace{\begin{pmatrix} \varepsilon_{11} \\ \varepsilon_{22} \\ \sqrt{2}\varepsilon_{12} \end{pmatrix}}_{F} + \underbrace{\begin{pmatrix} c_{1133} & \sqrt{2}c_{1123} & \sqrt{2}c_{1113} \\ c_{2233} & \sqrt{2}c_{2223} & \sqrt{2}c_{2213} \\ \sqrt{2}c_{3312} & 2c_{2312} & 2c_{1312} \end{pmatrix}}_{K} \underbrace{\begin{pmatrix} \varepsilon_{33} \\ \sqrt{2}\varepsilon_{23} \\ \sqrt{2}\varepsilon_{13} \end{pmatrix}}_{E}.$$

(2.8)

Note that $K = B^t$. Substituting expression (2.6) for E, we get

$$H = JF + KM^{-1}(G - BF) = JF + KM^{-1}G - KM^{-1}BF.$$

23

Averaging, we get

$$\overline{H} \approx \overline{J}\,\overline{F} + \overline{KM^{-1}}\,\overline{G} - \overline{KM^{-1}B}\,\overline{F}$$

$$= (\overline{J} - \overline{KM^{-1}B})\overline{F} + \overline{KM^{-1}}\left\{ \overline{(M^{-1})}^{\,-1}\left[\overline{E} + \overline{(M^{-1}B)}\,\overline{F}\right]\right\}$$

$$= \left[\overline{J} - \overline{KM^{-1}B} + \overline{KM^{-1}}\,\overline{(M^{-1})}^{\,-1}\overline{(M^{-1}B)}\right]\overline{F} + \overline{KM^{-1}}\,\overline{(M^{-1})}^{\,-1}\overline{E}\,. \qquad (2.9)$$

Comparing equation (2.9) with the pattern of the corresponding three lines in equation (2.4), we obtain formulæ for the remaining equivalent-medium parameters.

We do not list in detail the formulæ for the twenty-one equivalent-medium elasticity parameters of a generally anisotropic solid, since just one such parameter takes about half-a-dozen pages. However, a symbolic-calculation software can be used to obtain those parameters. In Section 2.4, we use the monoclinic symmetry to exemplify the process and list in detail the resulting formulæ, and we also summarize the results for orthotropic symmetry.

The results of this section are similar to the results of Schoenberg and Muir [1989], Helbig and Schoenberg [1987, Appendix], Helbig [1998], Carcione et al. [2012] and Kumar [2013], except that the tensorial form of equation (2.4) requires factors of 2 and $\sqrt{2}$ in several entries of M, B, J and K. This use of Kelvin's notation instead of Voigt's notation allows for a convenient study of rotations, which arise in the study of elasticity tensors expressed in coordinate systems of arbitrary orientations.

2.4 Reduction to higher symmetries

2.4.1 Monoclinic symmetry

Let us reduce the expressions derived for general anisotropy to higher material symmetries. To do so, let us first consider the case of monoclinic layers.

The components of a monoclinic tensor can be written in a matrix form as

$$
C^{mono} = \begin{pmatrix}
c_{1111} & c_{1122} & c_{1133} & 0 & 0 & \sqrt{2}c_{1112} \\
c_{1122} & c_{2222} & c_{2233} & 0 & 0 & \sqrt{2}c_{2212} \\
c_{1133} & c_{2233} & c_{3333} & 0 & 0 & \sqrt{2}c_{3312} \\
0 & 0 & 0 & 2c_{2323} & 2c_{2313} & 0 \\
0 & 0 & 0 & 2c_{2313} & 2c_{1313} & 0 \\
\sqrt{2}c_{1112} & \sqrt{2}c_{2212} & \sqrt{2}c_{3312} & 0 & 0 & 2c_{1212}
\end{pmatrix} ; \qquad (2.10)
$$

this expression corresponds to the coordinate system whose x_3-axis is normal to the symmetry plane. Inserting these components into expression (2.5), we write

$$
M = \begin{pmatrix}
c_{3333} & 0 & 0 \\
0 & 2c_{2323} & 2c_{2313} \\
0 & 2c_{2313} & 2c_{1313}
\end{pmatrix}, \qquad
M^{-1} = \begin{pmatrix}
\dfrac{1}{c_{3333}} & 0 & 0 \\
0 & \dfrac{c_{1313}}{D} & -\dfrac{c_{2313}}{D} \\
0 & -\dfrac{c_{2313}}{D} & \dfrac{c_{2323}}{D}
\end{pmatrix},
$$

where $D \equiv 2(c_{2323}c_{1313} - c_{2313}^2)$. Then, we have

$$
\overline{M^{-1}} = \begin{pmatrix}
\overline{\dfrac{1}{c_{3333}}} & 0 & 0 \\
0 & \overline{\dfrac{c_{1313}}{D}} & -\overline{\dfrac{c_{2313}}{D}} \\
0 & -\overline{\dfrac{c_{2313}}{D}} & \overline{\dfrac{c_{2323}}{D}}
\end{pmatrix}, \qquad
\overline{(M^{-1})}^{-1} = \begin{pmatrix}
\left(\overline{\dfrac{1}{c_{3333}}}\right)^{-1} & 0 & 0 \\
0 & \dfrac{\left(\overline{\dfrac{c_{2323}}{D}}\right)}{D_2} & \dfrac{\left(\overline{\dfrac{c_{2313}}{D}}\right)}{D_2} \\
0 & \dfrac{\left(\overline{\dfrac{c_{2313}}{D}}\right)}{D_2} & \dfrac{\left(\overline{\dfrac{c_{1313}}{D}}\right)}{D_2}
\end{pmatrix},
$$

25

where $D_2 \equiv \overline{(c_{1313}/D)}\,\overline{(c_{2323}/D)} - \overline{(c_{2313}/D)}^2$. We also have

$$
B = \begin{pmatrix} c_{1133} & c_{2233} & \sqrt{2}c_{3312} \\ 0 & 0 & 0 \\ 0 & 0 & 0 \end{pmatrix},
$$

which leads to

$$
M^{-1}B = \begin{pmatrix} \dfrac{c_{1133}}{c_{3333}} & \dfrac{c_{2233}}{c_{3333}} & \dfrac{\sqrt{2}c_{3312}}{c_{3333}} \\ 0 & 0 & 0 \\ 0 & 0 & 0 \end{pmatrix}, \qquad \overline{M^{-1}B} = \begin{pmatrix} \overline{\dfrac{c_{1133}}{c_{3333}}} & \overline{\dfrac{c_{2233}}{c_{3333}}} & \overline{\dfrac{\sqrt{2}c_{3312}}{c_{3333}}} \\ 0 & 0 & 0 \\ 0 & 0 & 0 \end{pmatrix}.
$$

Furthermore,

$$
\overline{(M^{-1})}^{-1}\overline{(M^{-1}B)} = \begin{pmatrix} \overline{\left(\dfrac{1}{c_{3333}}\right)}^{-1}\overline{\left(\dfrac{c_{1133}}{c_{3333}}\right)} & \overline{\left(\dfrac{1}{c_{3333}}\right)}^{-1}\overline{\left(\dfrac{c_{2233}}{c_{3333}}\right)} & \overline{\left(\dfrac{1}{c_{3333}}\right)}^{-1}\overline{\left(\dfrac{\sqrt{2}c_{3312}}{c_{3333}}\right)} \\ 0 & 0 & 0 \\ 0 & 0 & 0 \end{pmatrix}.
$$

Then, if we write equation (2.7) as

$$
\begin{pmatrix} \overline{\sigma_{33}} \\ \overline{\sqrt{2}\sigma_{23}} \\ \overline{\sqrt{2}\sigma_{13}} \end{pmatrix} = \overline{(M^{-1})}^{-1}\begin{pmatrix} \overline{\varepsilon_{33}} \\ \overline{\sqrt{2}\varepsilon_{23}} \\ \overline{\sqrt{2}\varepsilon_{13}} \end{pmatrix} + \overline{(M^{-1})}^{-1}\overline{(M^{-1}B)}\begin{pmatrix} \overline{\varepsilon_{11}} \\ \overline{\varepsilon_{22}} \\ \overline{\sqrt{2}\varepsilon_{12}} \end{pmatrix}
$$

and compare it to equation (2.4), we obtain

$$
\langle c_{3333} \rangle = \overline{\left(\frac{1}{c_{3333}} \right)}^{-1}, \qquad \langle c_{2323} \rangle = \frac{\overline{\left(\dfrac{c_{2323}}{D} \right)}}{2D_2},
$$

$$
\langle c_{1313} \rangle = \frac{\overline{\left(\dfrac{c_{1313}}{D} \right)}}{2D_2}, \quad \langle c_{2313} \rangle = \frac{\overline{\left(\dfrac{c_{2313}}{D} \right)}}{2D_2}, \quad \langle c_{1133} \rangle = \overline{\left(\frac{1}{c_{3333}} \right)}^{-1} \overline{\left(\frac{c_{1133}}{c_{3333}} \right)},
$$

$$
\langle c_{2233} \rangle = \overline{\left(\frac{1}{c_{3333}} \right)}^{-1} \overline{\left(\frac{c_{2233}}{c_{3333}} \right)}, \quad \langle c_{3312} \rangle = \overline{\left(\frac{1}{c_{3333}} \right)}^{-1} \overline{\left(\frac{c_{3312}}{c_{3333}} \right)},
$$

where angle brackets denote the equivalent-medium elasticity parameters.

To calculate the remaining equivalent elasticity parameters from equation (2.9), we insert components (2.10) into expression (2.8) to write

$$
J = \begin{pmatrix} c_{1111} & c_{1122} & \sqrt{2}c_{1112} \\ c_{1122} & c_{2222} & \sqrt{2}c_{2212} \\ \sqrt{2}c_{1112} & \sqrt{2}c_{2212} & 2c_{1212} \end{pmatrix}, \quad \overline{J} = \begin{pmatrix} \overline{c_{1111}} & \overline{c_{1122}} & \sqrt{2}\overline{c_{1112}} \\ \overline{c_{1122}} & \overline{c_{2222}} & \sqrt{2}\overline{c_{2212}} \\ \sqrt{2}\overline{c_{1112}} & \sqrt{2}\overline{c_{2212}} & 2\overline{c_{1212}} \end{pmatrix},
$$

$$
K = \begin{pmatrix} c_{1133} & 0 & 0 \\ c_{2233} & 0 & 0 \\ \sqrt{2}c_{3312} & 0 & 0 \end{pmatrix}, \quad KM^{-1} = \begin{pmatrix} \dfrac{c_{1133}}{c_{3333}} & 0 & 0 \\ \dfrac{c_{2233}}{c_{3333}} & 0 & 0 \\ \sqrt{2}\dfrac{c_{3312}}{c_{3333}} & 0 & 0 \end{pmatrix}, \quad \overline{KM^{-1}} = \begin{pmatrix} \overline{\left(\dfrac{c_{1133}}{c_{3333}} \right)} & 0 & 0 \\ \overline{\left(\dfrac{c_{2233}}{c_{3333}} \right)} & 0 & 0 \\ \sqrt{2}\overline{\left(\dfrac{c_{3312}}{c_{3333}} \right)} & 0 & 0 \end{pmatrix},
$$

$$
KM^{-1}B = \begin{pmatrix} \dfrac{c_{1133}^2}{c_{3333}} & \dfrac{c_{1133}c_{2233}}{c_{3333}} & \sqrt{2}\dfrac{c_{3312}c_{1133}}{c_{3333}} \\ \dfrac{c_{1133}c_{2233}}{c_{3333}} & \dfrac{c_{2233}^2}{c_{3333}} & \sqrt{2}\dfrac{c_{3312}c_{2233}}{c_{3333}} \\ \sqrt{2}\dfrac{c_{3312}c_{1133}}{c_{3333}} & \sqrt{2}\dfrac{c_{3312}c_{2233}}{c_{3333}} & 2\dfrac{c_{3312}^2}{c_{3333}} \end{pmatrix},
$$

27

$$
\overline{KM^{-1}B} = \begin{pmatrix}
\overline{\left(\dfrac{c_{1133}^2}{c_{3333}}\right)} & \overline{\left(\dfrac{c_{1133}c_{2233}}{c_{3333}}\right)} & \sqrt{2}\,\overline{\left(\dfrac{c_{3312}c_{1133}}{c_{3333}}\right)} \\[2em]
\overline{\left(\dfrac{c_{1133}c_{2233}}{c_{3333}}\right)} & \overline{\left(\dfrac{c_{2233}^2}{c_{3333}}\right)} & \sqrt{2}\,\overline{\left(\dfrac{c_{3312}c_{2233}}{c_{3333}}\right)} \\[2em]
\sqrt{2}\,\overline{\left(\dfrac{c_{3312}c_{1133}}{c_{3333}}\right)} & \sqrt{2}\,\overline{\left(\dfrac{c_{3312}c_{2233}}{c_{3333}}\right)} & 2\,\overline{\left(\dfrac{c_{3312}^2}{c_{3333}}\right)}
\end{pmatrix},
$$

$$
\overline{KM^{-1}}\,\overline{(M^{-1})}^{\,-1} = \begin{pmatrix}
\overline{\left(\dfrac{c_{1133}}{c_{3333}}\right)}\,\overline{\left(\dfrac{1}{c_{3333}}\right)}^{-1} & 0 & 0 \\[2em]
\overline{\left(\dfrac{c_{2233}}{c_{3333}}\right)}\,\overline{\left(\dfrac{1}{c_{3333}}\right)}^{-1} & 0 & 0 \\[2em]
\sqrt{2}\,\overline{\left(\dfrac{c_{3312}}{c_{3333}}\right)}\,\overline{\left(\dfrac{1}{c_{3333}}\right)}^{-1} & 0 & 0
\end{pmatrix},
$$

$$
\overline{KM^{-1}}\,\overline{(M^{-1})}^{\,-1}\overline{M^{-1}B} =
$$

$$
\begin{pmatrix}
\overline{\left(\dfrac{1}{c_{3333}}\right)}^{-1}\overline{\left(\dfrac{c_{1133}}{c_{3333}}\right)}^{2} & \overline{\left(\dfrac{1}{c_{3333}}\right)}^{-1}\overline{\left(\dfrac{c_{1133}}{c_{3333}}\right)}\overline{\left(\dfrac{c_{2233}}{c_{3333}}\right)} & \sqrt{2}\,\overline{\left(\dfrac{1}{c_{3333}}\right)}^{-1}\overline{\left(\dfrac{c_{1133}}{c_{3333}}\right)}\overline{\left(\dfrac{c_{3312}}{c_{3333}}\right)} \\[2em]
\overline{\left(\dfrac{1}{c_{3333}}\right)}^{-1}\overline{\left(\dfrac{c_{1133}}{c_{3333}}\right)}\overline{\left(\dfrac{c_{2233}}{c_{3333}}\right)} & \overline{\left(\dfrac{1}{c_{3333}}\right)}^{-1}\overline{\left(\dfrac{c_{2233}}{c_{3333}}\right)}^{2} & \sqrt{2}\,\overline{\left(\dfrac{1}{c_{3333}}\right)}^{-1}\overline{\left(\dfrac{c_{2233}}{c_{3333}}\right)}\overline{\left(\dfrac{c_{3312}}{c_{3333}}\right)} \\[2em]
\sqrt{2}\,\overline{\left(\dfrac{1}{c_{3333}}\right)}^{-1}\overline{\left(\dfrac{c_{1133}}{c_{3333}}\right)}\overline{\left(\dfrac{c_{3312}}{c_{3333}}\right)} & \sqrt{2}\,\overline{\left(\dfrac{1}{c_{3333}}\right)}^{-1}\overline{\left(\dfrac{c_{2233}}{c_{3333}}\right)}\overline{\left(\dfrac{c_{3312}}{c_{3333}}\right)} & 2\,\overline{\left(\dfrac{1}{c_{3333}}\right)}^{-1}\overline{\left(\dfrac{c_{3312}}{c_{3333}}\right)}^{2}
\end{pmatrix}.
$$

Then, if we write equation (2.9) as

$$
\begin{pmatrix} \overline{\sigma_{11}} \\[1em] \overline{\sigma_{22}} \\[1em] \sqrt{2}\overline{\sigma_{12}} \end{pmatrix} = \left[\overline{J} - \overline{KM^{-1}B} + \overline{KM^{-1}}\,\overline{(M^{-1})}^{\,-1}\overline{(M^{-1}B)} \right] \begin{pmatrix} \overline{\varepsilon_{11}} \\[1em] \overline{\varepsilon_{22}} \\[1em] \sqrt{2}\overline{\varepsilon_{12}} \end{pmatrix} + \overline{KM^{-1}}\,\overline{(M^{-1})}^{\,-1} \begin{pmatrix} \overline{\varepsilon_{33}} \\[1em] \sqrt{2}\overline{\varepsilon_{23}} \\[1em] \sqrt{2}\overline{\varepsilon_{13}} \end{pmatrix}
$$

and compare it to equation (2.4), we obtain

$$\langle c_{1133} \rangle = \overline{\left(\frac{1}{c_{3333}} \right)}^{-1} \overline{\left(\frac{c_{1133}}{c_{3333}} \right)}, \quad \langle c_{2233} \rangle = \overline{\left(\frac{1}{c_{3333}} \right)}^{-1} \overline{\left(\frac{c_{2233}}{c_{3333}} \right)}, \quad \langle c_{3312} \rangle = \overline{\left(\frac{1}{c_{3333}} \right)}^{-1} \overline{\left(\frac{c_{3312}}{c_{3333}} \right)},$$

as before, and

$$\langle c_{1111} \rangle = \overline{c_{1111}} - \overline{\left(\frac{c_{1133}^2}{c_{3333}} \right)} + \overline{\left(\frac{1}{c_{3333}} \right)}^{-1} \overline{\left(\frac{c_{1133}}{c_{3333}} \right)}^2,$$

$$\langle c_{1122} \rangle = \overline{c_{1122}} - \overline{\left(\frac{c_{1133}\, c_{2233}}{c_{3333}} \right)} + \overline{\left(\frac{1}{c_{3333}} \right)}^{-1} \overline{\left(\frac{c_{1133}}{c_{3333}} \right)} \overline{\left(\frac{c_{2233}}{c_{3333}} \right)},$$

$$\langle c_{2222} \rangle = \overline{c_{2222}} - \overline{\left(\frac{c_{2233}^2}{c_{3333}} \right)} + \overline{\left(\frac{1}{c_{3333}} \right)}^{-1} \overline{\left(\frac{c_{2233}}{c_{3333}} \right)}^2,$$

$$\langle c_{1212} \rangle = \overline{c_{1212}} - \overline{\left(\frac{c_{3312}^2}{c_{3333}} \right)} + \overline{\left(\frac{1}{c_{3333}} \right)}^{-1} \overline{\left(\frac{c_{3312}}{c_{3333}} \right)}^2,$$

$$\langle c_{1112} \rangle = \overline{c_{1112}} - \overline{\left(\frac{c_{3312}\, c_{1133}}{c_{3333}} \right)} + \overline{\left(\frac{1}{c_{3333}} \right)}^{-1} \overline{\left(\frac{c_{1133}}{c_{3333}} \right)} \overline{\left(\frac{c_{3312}}{c_{3333}} \right)},$$

$$\langle c_{2212} \rangle = \overline{c_{2212}} - \overline{\left(\frac{c_{3312}\, c_{2233}}{c_{3333}} \right)} + \overline{\left(\frac{1}{c_{3333}} \right)}^{-1} \overline{\left(\frac{c_{2233}}{c_{3333}} \right)} \overline{\left(\frac{c_{3312}}{c_{3333}} \right)}.$$

The other equivalent-medium elasticity parameters are zero. Thus, we have thirteen linearly independent parameters in the form of matrix (2.10). Hence, the equivalent medium exhibits the same symmetry as the individual layers. Also if we set c_{1112}, c_{2212}, c_{3312} and c_{2313} to zero the results of this section reduce to the results of the next section. The results of this section differ from the results of Kumar [2013, Appendix B] but that is because Kumar [2013] uses a vertical $(x_1 x_3)$ reflection symmetry plane whereas we use a horizontal $(x_1 x_2)$ reflection symmetry plane, which—since it is parallel to the layering—produces simpler results.

2.4.2 Orthotropic symmetry

Continuing the reduction of expressions derived for general anisotropy to higher material symmetries, let us consider the case of orthotropic layers. The components of an orthotropic tensor can be written as

$$
C^{\text{ortho}} = \begin{pmatrix}
c_{1111} & c_{1122} & c_{1133} & 0 & 0 & 0 \\
c_{1122} & c_{2222} & c_{2233} & 0 & 0 & 0 \\
c_{1133} & c_{2233} & c_{3333} & 0 & 0 & 0 \\
0 & 0 & 0 & 2c_{2323} & 0 & 0 \\
0 & 0 & 0 & 0 & 2c_{1313} & 0 \\
0 & 0 & 0 & 0 & 0 & 2c_{1212}
\end{pmatrix} ; \tag{2.11}
$$

this equation corresponds to the coordinate system whose axes are normal to the symmetry planes.

The equivalent medium elasticity parameters can be derived in a similar manner as in section 2.4.1 or by setting c_{1112}, c_{2212}, c_{3312} and c_{2313} to zero in the results of section 2.4.1 . In either case we obtain

$$
\langle c_{3333} \rangle = \overline{\left(\frac{1}{c_{3333}} \right)}^{-1}, \qquad
\langle c_{2323} \rangle = \overline{\left(\frac{1}{c_{2323}} \right)}^{-1}, \qquad
\langle c_{1313} \rangle = \overline{\left(\frac{1}{c_{1313}} \right)}^{-1},
$$

$$
\langle c_{1133} \rangle = \overline{\left(\frac{1}{c_{3333}} \right)}^{-1} \overline{\left(\frac{c_{1133}}{c_{3333}} \right)}, \qquad
\langle c_{2233} \rangle = \overline{\left(\frac{1}{c_{3333}} \right)}^{-1} \overline{\left(\frac{c_{2233}}{c_{3333}} \right)},
$$

$$
\langle c_{1111} \rangle = \overline{c_{1111}} - \overline{\left(\frac{c_{1133}^2}{c_{3333}} \right)} + \overline{\left(\frac{1}{c_{3333}} \right)}^{-1} \overline{\left(\frac{c_{1133}}{c_{3333}} \right)}^2,
$$

$$
\langle c_{1122} \rangle = \overline{c_{1122}} - \overline{\left(\frac{c_{1133}\, c_{2233}}{c_{3333}} \right)} + \overline{\left(\frac{1}{c_{3333}} \right)}^{-1} \overline{\left(\frac{c_{1133}}{c_{3333}} \right)} \overline{\left(\frac{c_{2233}}{c_{3333}} \right)},
$$

$$
\langle c_{2222} \rangle = \overline{c_{2222}} - \overline{\left(\frac{c_{2233}^2}{c_{3333}} \right)} + \overline{\left(\frac{1}{c_{3333}} \right)}^{-1} \overline{\left(\frac{c_{2233}}{c_{3333}} \right)}^2, \qquad
\langle c_{1212} \rangle = \overline{c_{1212}}.
$$

The other equivalent-medium elasticity parameters are zero. Thus, we have nine linearly independent parameters in the form of matrix (2.11). Hence, the equivalent medium exhibits the same symmetry as the individual layers. Subsequent reductions to transversely isotropic and isotropic layers result, respectively, in expressions (9) and (13) of Backus [1962].

Also, the results of this section agree with the results of Tiwary [2007, expression (5.1)] except for the fifth equation of that expression, which contains a typographical error: C_{13} instead of C_{23}. Tiwary [2007] references that expression to Shermergor [1977, expression (2.4)], a book in Russian. Although we do not have access to that book, an anonymous reviewer has informed us that the error is not in Shermergor [1977] but originates in Tiwary [2007]. The results of this section also agree with the results of Kumar [2013, Appendix B] and of Slawinski [2018, Exercise 4.6].

2.5 Conclusions

In this paper, using the case of the medium that is a long-wave equivalent of a stack of thin generally anisotropic layers, we examine, in our Appendices, the mathematical underpinnings of the approach of Backus [1962], whose underlying assumption remains lateral homogeneity.

Following explicit statements of assumptions and definitions, in Lemma 2.2.2, we prove—within the long-wave approximation—that if the thin layers obey stability conditions then so does the equivalent medium. Also, we show that the Backus average is allowed for any sequence of layers composed of Hookean solids. As a part of the discussion of approximations, in the proof of Lemma 2.2.3, we examine—within the Backus-average context—the approximation of the average of a product as the product of averages, and give upper bounds for their difference in Propositions 2.C.1 and 2.C.2.

2.6 Further work

The subject of Backus average was examined by several researchers, among them, Helbig and Schoenberg [1987], Schoenberg and Muir [1989], Berryman [1997], Helbig [1998, 2000], Carcione et al. [2012], Kumar [2013], Brisco [2014], and Danek and Slawinski [2016]. However, further venues of investigation remain open.

A following step is the error-propagation analysis, which is an analysis of the effect of errors in layer parameters on the errors of the equivalent medium. This step might be performed with perturbation techniques. Also, using such techniques, we could examine numerically the precise validity of $\overline{fg} \approx \overline{f}\,\overline{g}$, which is the approximation of Lemma 2.2.3.

Another numerical study could examine whether the equivalent medium for a stack of strongly anisotropic layers, whose anisotropic properties are randomly different from each other, is weakly anisotropic. If so, we might seek—using the method proposed by Gazis et al. [1963] and elaborated on by Danek et al. [2015]—an elasticity tensor of a higher symmetry that is nearest to that medium. For such a study, Kelvin's notation—used in this paper—is preferable, even though one could accommodate rotations in Voigt's notation by using the Bond [1943] transformation (e.g., Slawinski [2015], section 5.2).

A further possibility is an empirical examination of the obtained formulæ. This could be achieved with seismic data, where the layer properties are obtained from well-logging tools and the equivalent parameters from vertical seismic profiling.

Acknowledgments

2.7 References

D. L. Anderson. Elastic wave propagation in layered anisotropic media. *J. Geophys. Res.*, 66:2953–2964, 1961.

G. E. Backus. Long-wave elastic anisotropy produced by horizontal layering. *J. Geophys. Res.*, 67(11):4427–4440, 1962.

J. G. Berryman. Range of the *P*-wave anisotropy parameter for finely layered VTI media. *Stanford Exploration Project*, 93:179–192, 1997.

W. L. Bond. The mathematics of the physical properties of crystals. *Bell System Technical Journal*, 22:1–72, 1943.

L. Bos, T. Danek, M. A. Slawinski, and T. Stanoev. Statistical and numerical considerations of Backus-average product approximation. *Journal of Elasticity*, DOI 10.1007/s10659-017-9659-9:1–16, 2017.

C. Brisco. Anisotropy vs. inhomogeneity: Algorithm formulation, coding and modelling. Honours thesis, Memorial University, 2014.

J. M. Carcione, S. Picott, F. Cavallini, and J. E. Santos. Numerical test of the Schoenberg-Muir theory. *Geophysics*, 77(2):C27–C35, 2012.

C. H. Chapman. *Fundamentals of seismic wave propagation*. Cambridge University Press, 2004.

D. R. Dalton and M. A. Slawinski. On Backus average for oblique incidence. *arXiv*, [physics.geo-ph](1601.02966v1), 2016.

T. Danek and M. A. Slawinski. Backus average under random perturbations of layered media. *SIAM Journal on Applied Mathematics*, 76(4):1239–1249, 2016.

T. Danek, M. Kochetov, and M. A. Slawinski. Effective elasticity tensors in the context of random errors. *Journal of Elasticity*, 121(1):55–67, 2015.

D. C. Gazis, I. Tadjbakhsh, and R. A. Toupin. The elastic tensor of given symmetry nearest to an anisotropic elastic tensor. *Acta Crystallographica*, 16(9):917–922, 1963.

N. A. Haskell. Dispersion of surface waves on multilayered media. *Bulletin of the Seismological Society of America*, 43:17–34, 1953.

K. Helbig. Elastischen Wellen in anisotropen Medien. *Getlands Beitr. Geophys.*, 67:256–288, 1958.

K. Helbig. Layer-induced anisotropy: Forward relations between constituent parameters and compound parameters. *Revista Brasileira de Geofísica*, 16(2–3):103–114, 1998.

K. Helbig. Inversion of compound parameters to constituent parameters. *Revista Brasileira de Geofísica*, 18(2):173–185, 2000.

K. Helbig and M. Schoenberg. Anomalous polarization of elastic waves in transversely isotropic media. *J. Acoust. Soc. Am.*, 81(5):1235–1245, 1987.

D. Kumar. Applying Backus averaging for deriving seismic anisotropy of a long-wavelength equivalent medium from well-log data. *J. Geophys. Eng.*, 10:1–15, 2013.

C. L. Liner and T. W. Fei. Layer-induced seismic anisotropy from full-wave sonic logs: theory, applications and validation. *Geophysics*, 71:D183–D190, 2006.

G. W. Postma. Wave propagation in a stratified medium. *Geophysics*, 20:780–806, 1955.

Y. Y. Riznichenko. On seismic anisotropy. *Invest. Akad. Nauk SSSR, Ser. Geograf. i Geofiz.*, 13:518–544, 1949.

M. P. Rudzki. Parametrische Darstellung der elastischen Wellen in anisotropischen Medie. *Bull. Acad. Cracovie*, page 503, 1911.

S. M. Rytov. The acoustical properties of a finely layered medium. *Akust. Zhur.*, 2:71, 1956.

M. Schoenberg and F. Muir. A calculus for finely layered anisotropic media. *Geophysics*, 54(5):581–589, 1989.

T. Shermergor. *Theory of elasticity of microinhomogeneous media* (in Russian). Nauka, 1977.

M. A. Slawinski. *Waves and rays in elastic continua*. World Scientific, Singapore, 3rd edition, 2015.

M. A. Slawinski. *Waves and rays in seismology: Answers to unasked questions*. World Scientific, 2nd edition, 2018.

W. T. Thomson. Transmission of elastic waves through a stratified solid medium. *Journal of Applied Physics*, 21:89–93, 1950.

D. K. Tiwary. *Mathematical modelling and ultrasonic measurement of shale anisotropy and a comparison of upscaling methods from sonic to seismic*. PhD thesis, University of Oklahoma, 2007.

J. E. White and F. A. Angona. Elastic wave velocities in laminated media. *J. Acoust. Soc. Am.*, 27:310–317, 1955.

2.A   Average of derivatives (Lemma 2.2.1)

Proof. We begin with the definition of averaging,

$$\overline{f}(x_3) := \int\limits_{-\infty}^{\infty} w(\xi - x_3) f(\xi) \, d\xi. \tag{2.12}$$

We make the nonrestrictive assumption that $f(\xi)$ is sufficiently regular to be able to perform the standard calculus operations that we make below. The derivatives with respect to x_1 and x_2 can be written as

$$
\begin{aligned}
\frac{\partial \overline{f}}{\partial x_i} &= \frac{\partial}{\partial x_i} \int\limits_{-\infty}^{\infty} w(\xi - x_3) f(x_1, x_2, \xi) \, d\xi \\
&= \int\limits_{-\infty}^{\infty} w(\xi - x_3) \frac{\partial f(x_1, x_2, \xi)}{\partial x_i} \, d\xi =: \overline{\frac{\partial f}{\partial x_i}}, \qquad i = 1, 2,
\end{aligned}
$$

where the last equality is the statement of definition (2.12), as required. For the derivatives with respect to x_3, we need to verify that

$$\frac{\partial}{\partial x_3} \int\limits_{-\infty}^{\infty} w(\xi - x_3) f(x_1, x_2, \xi) \, d\xi = \int\limits_{-\infty}^{\infty} w(\xi - x_3) \frac{\partial f(x_1, x_2, \xi)}{\partial \xi} \, d\xi. \tag{2.13}$$

Applying integration by parts, we write the right-hand side as

$$w(\xi - x_3) f(x_1, x_2, \xi)\big|_{-\infty}^{\infty} - \int\limits_{-\infty}^{\infty} w'(\xi - x_3) \, f(x_1, x_2, \xi) \, d\xi,$$

where w is a function of a single variable. Since

$$\lim_{x_3 \to \pm\infty} w(x_3) = 0,$$

36

the product of w and f vanishes at $\pm\infty$, and we are left with

$$-\int_{-\infty}^{\infty} w'(\xi - x_3) f(x_1, x_2, \xi) \, d\xi.$$

Let us consider the left-hand side of expression (2.13). Since only w is a function of x_3, we can interchange the operations of integration and differentiation to write

$$-\int_{-\infty}^{\infty} w'(\xi - x_3) f(x_1, x_2, \xi) \, d\xi;$$

the negative sign arises from the chain rule,

$$\frac{\partial w(\xi - x_3)}{\partial x_3} = w'(\xi - x_3) \frac{\partial (\xi - x_3)}{\partial x_3} = -w'(\xi - x_3).$$

Thus, both sides of expression (2.13) are equal to one another, as required. In other words,

$$\frac{\partial \overline{f}}{\partial x_3} = \overline{\frac{\partial f}{\partial x_3}},$$

which completes the proof. $\qquad\square$

2.B Stability of equivalent medium (Lemma 2.2.2)

Proof. The stability of layers means that their deformation requires work. Mathematically, it means that, for each layer,

$$W = \frac{1}{2}\sigma \cdot \varepsilon > 0,$$

where W stands for work, and σ and ε denote the stress and strain tensors, respectively, which are expressed as columns in equation (2.4): $\sigma = C\varepsilon$. As an aside, we can say that, herein, $W > 0$ is equivalent to the positive definiteness of C, for each layer.

Performing the average of W over all layers and using—in the scalar product—the fact that the average of a sum is the sum of averages, we write

$$\overline{W} = \frac{1}{2}\overline{\sigma \cdot \varepsilon} > 0.$$

Thus, $W > 0 \implies \overline{W} > 0$.

Let us proceed to show that this implication—in turn—entails the stability of the equivalent medium, which is tantamount to the positive definiteness of $\langle C \rangle$, where $\langle C \rangle$ is the equivalent medium ($\overline{C}$ is not the equivalent medium since it would just be an average of all the matrix entries of C).

Following Lemma 2.2.3—if one of two functions is nearly constant—we can approximate the average of their product by the product of their averages,

$$\overline{W} = \frac{1}{2}\overline{\sigma} \cdot \overline{\varepsilon} > 0. \tag{2.14}$$

Herein, we use the property stated in Section 2.2.4 that σ_{i3}, where $i \in \{1,2,3\}$, are constant, and ε_{11}, ε_{12} and ε_{22} vary slowly, along the x_3-axis, together with Lemma 2.2.3, which can be invoked due to the fact that each product in expression (2.14) is such that one function is nearly constant and the other possibly varies more rapidly.

By definition of Hooke's law, $\overline{\sigma} := \langle C \rangle \overline{\varepsilon}$, expression (2.14) can be written as

$$\frac{1}{2}\left(\langle C \rangle \overline{\varepsilon}\right) \cdot \overline{\varepsilon} > 0, \qquad \forall\, \overline{\varepsilon} \neq 0,$$

which means that $\langle C \rangle$ is positive-definite, and which—in view of this derivation—proves that the equivalent medium inherits the stability of individual layers. □

2.C Approximation of product (Lemma 2.2.3)

For a fixed x_3, we may set $W(\zeta) := w(\zeta - x_3)$. Then, $W \geqslant 0$ and $\int_{-\infty}^{\infty} W(\zeta)\,d\zeta = 1$. With this notation, equation (2.3) becomes

$$\overline{f} := \int_{-\infty}^{\infty} f(x)\,W(x)\,dx.$$

Similarly,

$$\overline{g} := \int_{-\infty}^{\infty} g(x)\,W(x)\,dx \qquad \text{and} \qquad \overline{fg} := \int_{-\infty}^{\infty} f(x)\,g(x)\,W(x)\,dx.$$

Proposition 2.C.1. *Suppose that the first derivatives of f and g are uniformly bounded; that is, both*

$$\|f'\|_\infty := \sup_{-\infty < x < \infty} |f'(x)| \qquad \text{and} \qquad \|g'\|_\infty := \sup_{-\infty < x < \infty} |g'(x)|$$

are finite. Then, we have

$$|\overline{fg} - \overline{f}\,\overline{g}| \leqslant 2\,(\ell')^2\,\|f'\|_\infty \|g'\|_\infty.$$

Proof. We may calculate

$$\int_{-\infty}^{\infty} \left(f(x) - \overline{f} \right) \left(g(x) - \overline{g} \right) W(x) \, dx$$

$$= \int_{-\infty}^{\infty} f(x)g(x)W(x)\,dx - \overline{f}\int_{-\infty}^{\infty} g(x)W(x)\,dx - \overline{g}\int_{-\infty}^{\infty} f(x)W(x)\,dx + \int_{-\infty}^{\infty} \overline{f}\,\overline{g}\,W(x)\,dx$$

$$= \overline{fg} - \overline{f}\int_{-\infty}^{\infty} g(x)W(x)\,dx - \overline{g}\int_{-\infty}^{\infty} f(x)W(x)\,dx + \overline{f}\,\overline{g}$$

$$= \overline{fg} - \overline{f}\,\overline{g} - \overline{g}\,\overline{f} + \overline{f}\,\overline{g} = \overline{fg} - \overline{f}\,\overline{g};$$

that is,

$$\overline{fg} - \overline{f}\,\overline{g} = \int_{-\infty}^{\infty} \left(f(x) - \overline{f} \right) \left(g(x) - \overline{g} \right) W(x) \, dx. \tag{2.15}$$

Now,

$$f(x) - \overline{f} = f(x) - \int_{-\infty}^{\infty} f(y)W(y)\,dy = \int_{-\infty}^{\infty} \left(f(x) - f(y) \right) W(y)\,dy,$$

so that

$$\left| f(x) - \overline{f} \right| \leqslant \|f'\|_{\infty} \int_{-\infty}^{\infty} |x - y|\,W(y)\,dy, \tag{2.16}$$

and hence, by the Cauchy-Schwarz inequality,

$$\left| f(x) - \overline{f} \right|^2 \leqslant \|f'\|_{\infty}^2 \int_{-\infty}^{\infty} |x-y|^2\,W(y)\,dy \int_{-\infty}^{\infty} 1^2\,W(y)\,dy = \|f'\|_{\infty}^2 \int_{-\infty}^{\infty} |x-y|^2\,W(y)\,dy.$$

Thus,

$$\int\limits_{-\infty}^{\infty} |f(x) - \overline{f}|^2 W(x)\, dx \leqslant \|f'\|_\infty^2 \int\limits_{-\infty}^{\infty}\int\limits_{-\infty}^{\infty} |x-y|^2 W(x) W(y)\, dx\, dy$$

$$= \|f'\|_\infty^2 \int\limits_{-\infty}^{\infty}\int\limits_{-\infty}^{\infty} (x^2 - 2xy + y^2) W(x) W(y)\, dx\, dy$$

$$= \|f'\|_\infty^2 \left(2\int\limits_{-\infty}^{\infty} x^2 W(x)\, dx - 2\left(\int\limits_{-\infty}^{\infty} x W(x)\, dx\right)^2 \right).$$

It follows, by the Cauchy-Schwarz inequality applied to equation (2.15), that

$$|\overline{fg} - \overline{f}\,\overline{g}|^2 \leqslant \int\limits_{-\infty}^{\infty} |f(x) - \overline{f}|^2 W(x)\, dx \int\limits_{-\infty}^{\infty} |g(x) - \overline{g}|^2 W(x)\, dx$$

$$\leqslant \|f'\|_\infty^2 \|g'\|_\infty^2 \left(2\int\limits_{-\infty}^{\infty} x^2 W(x)\, dx - 2\left(\int\limits_{-\infty}^{\infty} x W(x)\, dx\right)^2 \right)^2.$$

Note that

$$\int\limits_{-\infty}^{\infty} x W(x)\, dx = \int\limits_{-\infty}^{\infty} x w(x - x_3)\, dx = \int\limits_{-\infty}^{\infty} (x + x_3) w(x)\, dx = x_3,$$

using the defining properties of $w(\zeta)$. Similarly

$$\int\limits_{-\infty}^{\infty} x^2 W(x)\, dx = \int\limits_{-\infty}^{\infty} x^2 w(x - x_3)\, dx = \int\limits_{-\infty}^{\infty} (x + x_3)^2 w(x)\, dx = (\ell')^2 + x_3^2.$$

Consequently,

$$2\int\limits_{-\infty}^{\infty} x^2 W(x)\, dx - 2\left(\int\limits_{-\infty}^{\infty} x W(x)\, dx\right)^2 = 2((\ell')^2 + x_3^2 - x_3^2) = 2(\ell')^2$$

41

and we have

$$|\overline{fg} - \overline{f}\,\overline{g}| \le 2\,(\ell')^2\,\|f'\|_\infty\|g'\|_\infty,$$

as claimed. □

Hence, if f and g are nearly constant, which means that $\|f'\|_\infty$ and $\|g'\|_\infty$ are small, then $\overline{fg} \approx \overline{f}\,\overline{g}$.

Corollary 2.C.1. *Since the error estimate involves the product of the norms of the derivatives, it follows that if one of them is small enough and the other is not excessively large, then their product can be small enough for the approximation, $\overline{fg} \approx \overline{f}\,\overline{g}$, to hold.*

The exact accuracy of this property will be examined further by numerical methods in a future publication. (Update: it has been examined statistically and numerically in Bos et al. [2017].)

If $g(x) \ge 0$, we can say more, even if $g(x)$ is wildly varying. If f is continuous and $g(x) \ge 0$, then, by the Mean-value Theorem for Integrals,

$$\overline{fg} = \int_{-\infty}^{\infty} f(x)g(x)W(x)\,\mathrm{d}x = f(c)\int_{-\infty}^{\infty} g(x)W(x)\,\mathrm{d}x = f(c)\overline{g},$$

for some c. Hence,

$$\overline{fg} - \overline{f}\,\overline{g} = f(c)\overline{g} - \overline{f}\,\overline{g} = (f(c) - \overline{f})\overline{g}.$$

This implies that

$$|\overline{fg} - \overline{f}\,\overline{g}| \le |f(c) - \overline{f}|\overline{g} \le \|f'\|_\infty\left(\int_{-\infty}^{\infty} |x - y|W(y)\,\mathrm{d}y\right)\overline{g}.$$

Hence, even for g wildly varying—as long as $\overline{g}$ is not too big in relation to $\|f'\|_\infty$—it is still the case that the average of the product is close to the product of the averages. A bound on $\int_{-\infty}^{\infty} |x - y|W(y)\,\mathrm{d}y$ would depend on the weight function, w, used.

An alternative estimate is provided by the following proposition.

Proposition 2.C.2. *Suppose that* $m := \inf f(x) > -\infty$ *and* $M := \sup\limits_{-\infty < x < \infty} f(x) < \infty$ *and*
$\sup\limits_{-\infty < x < \infty} |g(x)| < \infty$. *Then,*

$$\left| \overline{fg} - \overline{f}\,\overline{g} \right| \leqslant \left(\sup_{-\infty < x < \infty} |g(x)| \right) (M - m) .$$

Proof.

$$\overline{fg} = \int\limits_{-\infty}^{\infty} f(x)\,g(x)\,W(x)\,dx = \int\limits_{-\infty}^{\infty} (f(x) - m)\,g(x)\,W(x)\,dx + m \int\limits_{-\infty}^{\infty} g(x)\,W(x)\,dx,$$

which—by the definition of the average—is

$$\overline{fg} = \int\limits_{-\infty}^{\infty} (f(x) - m)\,g(x)\,W(x)\,dx + m\overline{g} .$$

Hence,

$$\left| \overline{fg} - \overline{f}\,\overline{g} \right| = \left| \int\limits_{-\infty}^{\infty} (f(x) - m)\,g(x)\,W(x)\,dx + \left(m - \overline{f} \right) \overline{g} \right|$$

$$\leqslant \left(\sup_{-\infty < x < \infty} |g(x)| \right) \int\limits_{-\infty}^{\infty} (f(x) - m)\,W(x)\,dx + \left| m - \overline{f} \right| |\overline{g}|$$

$$= \left(\sup_{-\infty < x < \infty} |g(x)| \right) \left(\overline{f} - m \right) + \left(\overline{f} - m \right) |\overline{g}|$$

$$\leqslant 2 \left(\sup_{-\infty < x < \infty} |g(x)| \right) \left(\overline{f} - m \right) . \tag{2.17}$$

Similarly,

$$\left| \overline{fg} - \overline{f}\,\overline{g} \right| \leqslant 2 \left(\sup_{-\infty < x < \infty} |g(x)| \right) \left(M - \overline{f} \right) . \tag{2.18}$$

43

Taking the average of expressions (2.17) and (2.18), we obtain

$$\left| \overline{fg} - \overline{f}\,\overline{g} \right| \leqslant 2 \left(\sup_{-\infty < x < \infty} |g(x)| \right) \frac{\left(\overline{f} - m \right) + \left(M - \overline{f} \right)}{2}$$

$$= \left(\sup_{-\infty < x < \infty} |g(x)| \right) (M - m),$$

as required. □

Consequently, if $f(x)$ is almost constant—which means that $m \approx M$—then $\overline{fg} \approx \overline{f}\,\overline{g}$.

Chapter 3

On commutativity and near commutativity of translational and rotational averages: Analytical proofs and numerical examinations[*]

Abstract

We show that, in general, the translational average over a spatial variable—discussed by Backus [1962], and referred to as the equivalent-medium average—and the rotational average over a symmetry group at a point—discussed by Gazis et al. [1963], and referred to as the effective-medium average—do not commute. However, they do commute in special cases of particular symmetry classes, which correspond to special relations among the elasticity parameters. We also show that this noncommutativity is a function of the strength of

---

anisotropy. Surprisingly, a perturbation of the elasticity parameters about a point of weak anisotropy results in the commutator of the two types of averaging being of the order of the *square* of this perturbation. Thus, these averages nearly commute in the case of weak anisotropy, which is of interest in such disciplines as quantitative seismology, where the weak-anisotropy assumption results in empirically adequate models.

3.1 Introduction

Hookean solids are defined by their mechanical property relating linearly the stress tensor, σ, and the strain tensor, ε,

$$\sigma_{ij} = \sum_{k=1}^{3} \sum_{\ell=1}^{3} c_{ijk\ell} \varepsilon_{k\ell}, \qquad i,j = 1,2,3.$$

The elasticity tensor, c, belongs to one of the eight material-symmetry classes shown in Figure 3.1.

The Backus [1962] average, which is a moving average over a spatial inhomogeneity, allows us to quantify the response of a wave propagating through a series of parallel layers whose thicknesses are much smaller than the wavelength of a signal. Each layer is a homogeneous Hookean solid exhibiting a given material symmetry with its elasticity parameters. The average results in a Hookean solid whose elasticity parameters—and, hence, its material symmetry—allow us to model a long-wavelength response. The material symmetry of a resulting medium, which we refer to as *equivalent*, is a consequence of the symmetries exhibited by the averaged layers.

As shown by Backus [1962], the medium equivalent to a stack of isotropic or transversely isotropic layers is a homogeneous, or nearly homogeneous, transversely isotropic medium, where a *nearly* homogeneous medium is a consequence of a *moving* average. The Backus [1962] formulation is reviewed and extended by Bos et al. [2017a], where formu-
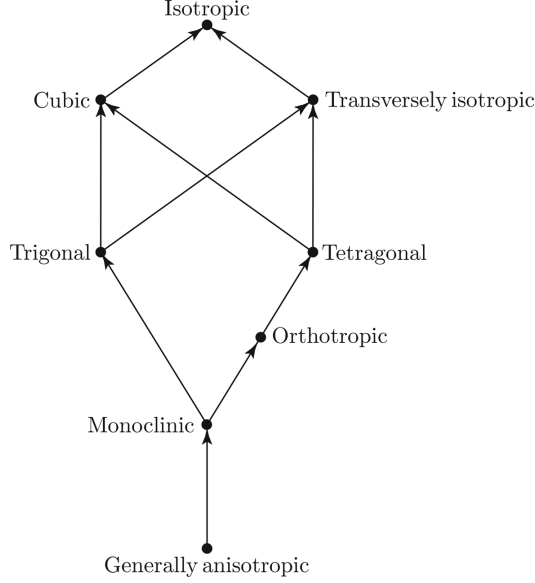
Figure 3.1: Partial ordering of material-symmetry classes of elasticity tensors: Arrows indicate subgroups. For instance, monoclinic is a subgroup of all symmetries, except general anisotropy; in particular, it is a subgroup of both orthotropic and trigonal symmetries, but orthotropic symmetry is not a subgroup of trigonal or *vice-versa*.

lations for generally anisotropic, monoclinic, and orthotropic thin layers are also derived. Also, Bos et al. [2017a] examine the underlying assumptions and approximations behind the Backus [1962] formulation, which is derived by expressing rapidly varying stresses and strains in terms of products of algebraic combinations of rapidly varying elasticity parameters with slowly varying stresses and strains. The only mathematical approximation of Backus [1962] is that the average of a product of a rapidly varying function and a slowly varying function is approximately equal to the product of the averages of these two functions. This approximation is discussed by Bos et al. [2017a,b].

According to Backus [1962], the average of $f(x_3)$ of "width" ℓ' is

$$\overline{f}(x_3) := \int\limits_{-\infty}^{\infty} w(\zeta - x_3) f(\zeta) \, \mathrm{d}\zeta, \tag{3.1}$$

47

where $w(x_3)$ is a weight function with the following properties:

$$w(x_3) \geqslant 0, \quad w(\pm\infty) = 0, \quad \int\limits_{-\infty}^{\infty} w(x_3)\, dx_3 = 1,$$

$$\int\limits_{-\infty}^{\infty} x_3 w(x_3)\, dx_3 = 0, \quad \int\limits_{-\infty}^{\infty} x_3^2 w(x_3)\, dx_3 = (\ell')^2.$$

These properties define $w(x_3)$ as a probability-density function, whose mean is zero and whose standard deviation is ℓ', thus explaining the use of the term "width" for ℓ'.

The Gazis et al. [1963] average, which is an average over an anisotropic symmetry group, allows us to obtain the closest symmetric counterpart—in the Frobenius sense—of a chosen material symmetry to a generally anisotropic Hookean solid. The average is a Hookean solid, to which we refer as *effective*, and whose elasticity parameters correspond to a symmetry chosen *a priori* in this paper, though in general one can find the nearest effective Hookean solid of any symmetry in which the Frobenius distance between the generally anisotropic Hookean solid and the effective medium lies within the range of errors.

The Gazis et al. [1963] average is a projection given by

$$\widetilde{c}^{\,\mathrm{sym}} := \int\limits_{G^{\mathrm{sym}}} (g \circ c)\, d\mu(g), \tag{3.2}$$

where the integration is over the symmetry group, G^{sym}, whose elements are g, with respect to the invariant measure, μ, normalized so that $\mu(G^{\mathrm{sym}}) = 1$; $\widetilde{c}^{\,\mathrm{sym}}$ is the orthogonal projection of c, in the sense of the Frobenius norm, onto the linear space containing all tensors of that symmetry, which are $c^{\,\mathrm{sym}}$. Integral (3.2) reduces to a finite sum for the classes whose symmetry groups are finite, which are all classes in Figure 3.1, except isotropy and transverse isotropy.

The Gazis et al. [1963] approach is reviewed and extended by Danek et al. [2013,

2015] in the context of random errors. Therein, elasticity tensors are not constrained to the same—or even different but known—orientation of the coordinate system. In other words, in general, the closest—and more symmetric counterpart—exhibits different orientation of symmetry planes and axes than does its original material.

Let us emphasize that the fundamental distinction between the two averages is their domain of operation. The Gazis et al. [1963] average is an average over symmetry groups at a point and the Backus [1962] average is a spatial average over a distance. These averages can be used separately or together. Hence, an examination of their commutativity provides us with an insight into their meaning and into allowable mathematical operations.

The interplay between anisotropy and inhomogeneity is an important factor in modelling traveltime data in seismology. Similar traveltimes, though perhaps not similar sets of traveltimes when information from different polarizations or orientations is available, can be obtained by considering anisotropy, inhomogeneity or their combination. However— since the purpose of modelling is to infer a realistic medium, not only to account for the measured traveltimes—the interplay between anisotropy and inhomogeneity is investigated in the context of symmetry increase, homogenization and their commutativity.

The commutator of two operators is defined as $[A, B] := AB - BA$ and is zero if A and B commute; more generally, the size of the commutator gives an indication of how close they are to commuting. In our case, we apply the two types of averages to a medium with a certain symmetry class with parameters that may be perturbed by a perturbation parameter, say, h. Thus we may consider the commutator $[A, B] =: F(h)$ to be a function of h. If, for no perturbation—which means that $h = 0$—the averages commute—in other words, $F(0) = 0$—we expect

$$[A, B] = F(0) + F'(0)h + \cdots = F'(0)h + \cdots$$

to be of order h. Surprisingly, we show that in certain cases, perturbing about a symmetry class for which there is commutativity, we have $[A, B] = O(h^2)$, which means that the commutator is much smaller than might originally have been expected, and we have very near commutativity.

We begin this paper by formulating analytically the commutativity diagrams between the two averages. We proceed from generally anisotropic layers to a monoclinic medium, from monoclinic layers to an orthotropic medium, and from orthotropic layers to a tetragonal medium. Also, we discuss transversely isotropic layers, which—depending on the order of operations—result in a transversely isotropic or isotropic medium. Subsequently, we examine numerically the commutativity, which allows us to consider the case of weak anisotropy. We conclude this paper with both expected and unexpected results.

3.2   Analytical formulation

3.2.1   Generally anisotropic layers and monoclinic medium

Let us consider a stack of generally anisotropic layers to obtain a monoclinic medium. To examine the commutativity between the Backus [1962] and Gazis et al. [1963] averages, let us study the following diagram,

$$
\begin{array}{ccc}
\text{aniso} & \xrightarrow{\;\;B\;\;} & \text{aniso} \\
{\scriptstyle G}\Big\downarrow & & \Big\downarrow{\scriptstyle G} \\
\text{mono} & \xrightarrow[\;\;B\;\;]{} & \text{mono}
\end{array}
\tag{3.3}
$$

and Theorem 3.2.1, as well as its corollary.

Theorem 3.2.1. *In general, the Backus [1962] and Gazis et al. [1963] averages do not commute.*

50

Proof. This is a consequence of the following more specific case.

Proposition 3.2.1. *For the generally anisotropic and monoclinic symmetries, the Backus [1962] and Gazis et al. [1963] averages do not commute.*

To understand this corollary, we invoke the following lemma, whose proof is given in Appendix 3.A.1.

Lemma 3.2.1. *For the effective monoclinic symmetry, the result of the Gazis et al. [1963] average is tantamount to replacing each $c_{ijk\ell}$, in a generally anisotropic tensor, by its corresponding $c_{ijk\ell}$ of the monoclinic tensor, expressed in the natural coordinate system, including replacements of the anisotropic-tensor components by the zeros of the corresponding monoclinic components.*

Let us first examine the counterclockwise path of Diagram (3.3). Lemma 3.2.1 entails the following corollary.

Corollary 3.2.1. *For the effective monoclinic symmetry, given a generally anisotropic tensor, C,*

$$\widetilde{C}^{\text{mono}} = C^{\text{mono}} \; ; \tag{3.4}$$

where $\widetilde{C}^{\text{mono}}$ is the Gazis et al. [1963] average of C, and C^{mono} is the monoclinic tensor whose nonzero entries are the same as for C.

According to Corollary 3.2.1, the effective monoclinic tensor is obtained simply by setting to zero—in the generally anisotropic tensor—the components that are zero for a monoclinic tensor. Then, the second counterclockwise branch of Diagram (3.3) is performed as follows. Applying the Backus [1962] average, we obtain [Bos et al., 2017a]

$$\langle c_{3333} \rangle = \overline{\left(\frac{1}{c_{3333}} \right)}^{-1}, \qquad \langle c_{2323} \rangle = \frac{\overline{\left(\dfrac{c_{2323}}{D} \right)}}{2D_2},$$

51

$$\langle c_{1313}\rangle = \frac{\overline{\left(\dfrac{c_{1313}}{D}\right)}}{2D_2}, \qquad \langle c_{2313}\rangle = \frac{\overline{\left(\dfrac{c_{2313}}{D}\right)}}{2D_2},$$

where $D \equiv 2(c_{2323}c_{1313} - c_{2313}^2)$ and $D_2 \equiv \overline{(c_{1313}/D)}\,\overline{(c_{2323}/D)} - \overline{(c_{2313}/D)}^2$. We also obtain

$$\langle c_{1133}\rangle = \overline{\left(\frac{1}{c_{3333}}\right)}^{-1}\overline{\left(\frac{c_{1133}}{c_{3333}}\right)}, \quad \langle c_{2233}\rangle = \overline{\left(\frac{1}{c_{3333}}\right)}^{-1}\overline{\left(\frac{c_{2233}}{c_{3333}}\right)},$$

$$\langle c_{3312}\rangle = \overline{\left(\frac{1}{c_{3333}}\right)}^{-1}\overline{\left(\frac{c_{3312}}{c_{3333}}\right)}, \quad \langle c_{1111}\rangle = \overline{c_{1111}} - \overline{\left(\frac{c_{1133}^2}{c_{3333}}\right)} + \overline{\left(\frac{1}{c_{3333}}\right)}^{-1}\overline{\left(\frac{c_{1133}}{c_{3333}}\right)}^2,$$

$$\langle c_{1122}\rangle = \overline{c_{1122}} - \overline{\left(\frac{c_{1133}\,c_{2233}}{c_{3333}}\right)} + \overline{\left(\frac{1}{c_{3333}}\right)}^{-1}\overline{\left(\frac{c_{1133}}{c_{3333}}\right)}\,\overline{\left(\frac{c_{2233}}{c_{3333}}\right)},$$

$$\langle c_{2222}\rangle = \overline{c_{2222}} - \overline{\left(\frac{c_{2233}^2}{c_{3333}}\right)} + \overline{\left(\frac{1}{c_{3333}}\right)}^{-1}\overline{\left(\frac{c_{2233}}{c_{3333}}\right)}^2,$$

$$\langle c_{1212}\rangle = \overline{c_{1212}} - \overline{\left(\frac{c_{3312}^2}{c_{3333}}\right)} + \overline{\left(\frac{1}{c_{3333}}\right)}^{-1}\overline{\left(\frac{c_{3312}}{c_{3333}}\right)}^2,$$

$$\langle c_{1112}\rangle = \overline{c_{1112}} - \overline{\left(\frac{c_{3312}\,c_{1133}}{c_{3333}}\right)} + \overline{\left(\frac{1}{c_{3333}}\right)}^{-1}\overline{\left(\frac{c_{1133}}{c_{3333}}\right)}\,\overline{\left(\frac{c_{3312}}{c_{3333}}\right)}$$

and

$$\langle c_{2212}\rangle = \overline{c_{2212}} - \overline{\left(\frac{c_{3312}\,c_{2233}}{c_{3333}}\right)} + \overline{\left(\frac{1}{c_{3333}}\right)}^{-1}\overline{\left(\frac{c_{2233}}{c_{3333}}\right)}\,\overline{\left(\frac{c_{3312}}{c_{3333}}\right)},$$

where angle brackets denote the equivalent-medium elasticity parameters. The other equivalent-medium elasticity parameters are zero.

Following the clockwise path of Diagram (3.3), the upper branch is derived in matrix form in Bos et al. [2017a]. Then, in accordance with Bos et al. [2017a], the result of the right-hand branch is derived by setting entries in the generally anisotropic tensor that are zero for a monoclinic tensor to zero. The nonzero entries, which are too complicated to display explicitly, are—in general—not the same as the result of the counterclockwise path. Hence, for generally anisotropic and monoclinic symmetries, the Backus [1962] and

Gazis et al. [1963] averages do not commute. □

3.2.2 Monoclinic layers and orthotropic medium

Theorem 3.2.1 remains valid for layers exhibiting higher material symmetries. For such symmetries, simpler expressions of the corresponding elasticity tensors allow us to examine special cases that result in commutativity. Let us consider the following instance of Theorem 3.2.1.

Proposition 3.2.2. *For the monoclinic and orthotropic symmetries, the Backus [1962] and Gazis et al. [1963] averages do not commute.*

To study this case, let us consider the following diagram,

$$
\begin{array}{ccc}
\text{mono} & \xrightarrow{\text{ B }} & \text{mono} \\
{\scriptstyle \text{G}}\downarrow & & \downarrow{\scriptstyle \text{G}} \\
\text{ortho} & \xrightarrow[\text{ B }]{} & \text{ortho}
\end{array}
\qquad (3.5)
$$

and the following lemma, whose proof is in Appendix 3.A.2.

Lemma 3.2.2. *For the effective orthotropic symmetry, the result of the Gazis et al. [1963] average is tantamount to replacing each $c_{ijk\ell}$, in a generally anisotropic—or monoclinic— tensor, by its corresponding $c_{ijk\ell}$ of an orthotropic tensor, expressed in the natural coordinate system, including the replacements by the corresponding zeros.*

Lemma 3.2.2 entails a corollary.

Corollary 3.2.2. *For the effective orthotropic symmetry, given a generally anisotropic—or monoclinic—tensor, C,*

$$
\widetilde{C}^{\text{ortho}} = C^{\text{ortho}}. \qquad (3.6)
$$

53

where $\widetilde{C}^{\mathrm{ortho}}$ is the Gazis et al. [1963] average of C, and C^{ortho} is an orthotropic tensor whose nonzero entries are the same as for C.

Proof. (of Proposition 3.2.2) Let us consider a monoclinic tensor and proceed counter-clockwise along the first branch of Diagram (3.5). Using the fact that the monoclinic symmetry is a special case of general anisotropy, we invoke Corollary 3.2.2 to conclude that $\widetilde{C}^{\mathrm{ortho}} = C^{\mathrm{ortho}}$, which is equivalent to setting c_{1112}, c_{2212}, c_{3312} and c_{2313} to zero in the monoclinic tensor. We perform the upper branch of Diagram (3.5), which is the averaging of a stack of monoclinic layers to get a monoclinic equivalent medium, as in the case of the lower branch of Diagram (3.3). Thus, following the clockwise path, we obtain

$$c_{1212}^{\circlearrowleft} = \overline{c_{1212}} - \overline{\left(\frac{c_{3312}^2}{c_{3333}}\right)} + \overline{\left(\frac{1}{c_{3333}}\right)}^{-1} \overline{\left(\frac{c_{3312}}{c_{3333}}\right)}^2, \qquad (3.7)$$

$$c_{1313}^{\circlearrowleft} = \frac{\overline{\left(\dfrac{c_{1313}}{D}\right)}}{2D_2}, \qquad c_{2323}^{\circlearrowleft} = \frac{\overline{\left(\dfrac{c_{2323}}{D}\right)}}{2D_2}. \qquad (3.8)$$

Following the counterclockwise path, we obtain

$$c_{1212}^{\circlearrowleft} = \overline{c_{1212}}, \quad c_{1313}^{\circlearrowleft} = \overline{\left(\frac{1}{c_{1313}}\right)}^{-1}, \quad c_{2323}^{\circlearrowleft} = \overline{\left(\frac{1}{c_{2323}}\right)}^{-1}. \qquad (3.9)$$

The other entries are the same for both paths.

In conclusion, the results of the clockwise and counterclockwise paths are the same if $c_{2313} = c_{3312} = 0$, which is a special case of monoclinic symmetry. Thus, the Backus [1962] average and Gazis et al. [1963] average commute for that case, even though they do not in general. $\qquad \square$

Now, let us consider the case of weak anisotropy, in which c_{2313} and c_{3312}, which are zero for isotropy, are small. To study the commutativity of the two averages, consider the commutator, $\mathcal{C} = [B,G] = BG - GB$, where BG is the clockwise path and GB is the

counterclockwise path. Since—if $c_{2313} = c_{3312} = 0$—the commutator is zero, it is to be expected that in a neighbourhood of this case we have near commutativity. Specifically, if both c_{2313} and c_{3312} are of order ε, then $\mathcal{C}$ should also be of order ε, which means that there is near commutativity up to this order. However, remarkably, a much stronger statement is true. It turns out that for c_{2313} and c_{3312} of order ε, $\mathcal{C}$ is of order ε^2, thus indicating a much stronger near commutativity that could expected *a priori*. This follows from the following Jacobian calculation.

In this case, $\mathcal{C} = [\mathcal{C}_1, \mathcal{C}_2, \mathcal{C}_3]$, where

$$\mathcal{C}_1 = c_{2323}^{\circlearrowleft} - c_{2323}^{\circlearrowright} = \frac{\overline{\left(\dfrac{c_{2323}}{D}\right)}}{2D_2} - \overline{\left(\dfrac{1}{c_{2323}}\right)}^{-1},$$

$$\mathcal{C}_2 = c_{1313}^{\circlearrowleft} - c_{1313}^{\circlearrowright} = \frac{\overline{\left(\dfrac{c_{1313}}{D}\right)}}{2D_2} - \overline{\left(\dfrac{1}{c_{1313}}\right)}^{-1},$$

and

$$\mathcal{C}_3 = c_{1212}^{\circlearrowleft} - c_{1212}^{\circlearrowright} = \overline{\left(\dfrac{1}{c_{3333}}\right)}^{-1} \overline{\left(\dfrac{c_{3312}}{c_{3333}}\right)}^{2} - \overline{\left(\dfrac{c_{3312}^2}{c_{3333}}\right)}.$$

The starting parameters are

$$x = c_{3333}^i, c_{2323}^i, c_{1313}^i, c_{2313}^i, c_{3312}^i, \quad i = 1, \ldots, n,$$

and we have commutativity if

$$c_{2313}^i = c_{3312}^i = 0, \quad i = 1, \ldots, n,$$

which we denote by $x = a$, such that $\mathcal{C}(a) = [0]$.

Let the average be the arithmetic average and assume that all layers have the same

55

thickness, so that

$$\overline{F} = \frac{1}{n}\sum_{i=1}^{n} F^i.$$

Also, we let the $3 \times 5n$ Jacobi matrix be

$$\mathcal{C}'(x) = \left[\frac{\partial \mathcal{C}}{\partial x}\right].$$

In Appendix 3.B we evaluate this Jacobi matrix and find that $\mathcal{C}'(a) = [0]$.

If we expand $\mathcal{C}(x)$ in a Taylor series,

$$\mathcal{C}(x) = \mathcal{C}(a) + \mathcal{C}'(a)(x-a) + \cdots = \mathcal{C}'(a)(x-a) + \cdots, \tag{3.10}$$

then we see that, near $x = a$, $||\mathcal{C}(x)|| = O\left(||x-a||^2\right)$, so that there is very near commutativity in a neighbourhood of $x = a$. In Section 3.3 we illustrate numerically this strong near commutativity.

3.2.3   Orthotropic layers and tetragonal medium

In a manner analogous to Diagram (3.5), but proceeding from the upper-left-hand corner orthotropic tensor to lower-right-hand corner tetragonal tensor by the counterclockwise path,

$$
\begin{array}{ccc}
\text{ortho} & \xrightarrow{\ \text{B}\ } & \text{ortho} \\
{\scriptstyle\text{G}}\big\downarrow & & \big\downarrow{\scriptstyle\text{G}} \\
\text{tetra} & \xrightarrow[\text{B}]{\ \ } & \text{tetra}
\end{array}
\tag{3.11}
$$

we obtain

$$c_{1111}^{\circlearrowleft} = \frac{c_{1111}+c_{2222}}{2} - \frac{\overline{\left(\dfrac{c_{1111}+c_{2222}}{2}\right)^2}}{c_{3333}} + \overline{\left(\frac{c_{1111}+c_{2222}}{2c_{3333}}\right)^2}\,\overline{\left(\frac{1}{c_{3333}}\right)}^{-1}.$$

Following the clockwise path, we obtain

$$c_{1111}^{\circlearrowright} = \overline{\frac{c_{1111}+c_{2222}}{2}} - \overline{\frac{c_{1133}^2+c_{2233}^2}{2c_{3333}}} + \frac{1}{2}\left[\overline{\left(\frac{c_{1133}}{c_{3333}}\right)^2} + \overline{\left(\frac{c_{2233}}{c_{3333}}\right)^2}\right]\overline{\left(\frac{1}{c_{3333}}\right)^{-1}}.$$

These results are not equal to one another, unless $c_{1133} = c_{2233}$, which is a special case of orthotropic symmetry. The same is true for $c_{1122}^{\circlearrowright}$ and $c_{1122}^{\circlearrowright}$. Also, c_{2323} must equal c_{1313} for $c_{2323}^{\circlearrowright} = c_{2323}^{\circlearrowright}$. The other entries are the same for both paths. Thus, the Backus [1962] average and Gazis et al. [1963] average do commute for $c_{1133} = c_{2233}$ and $c_{2323} = c_{1313}$, which is a special case of orthotropic symmetry, but they do not commute in general.

Similarly to our discussion in Section 3.2.2 and Appendix 3.B, we examine the commutator. Herein, the commutator is $\mathcal{C} = [\mathcal{C}_1, \mathcal{C}_2, \mathcal{C}_3]$, where

$$\mathcal{C}_1 = c_{1111}^{\circlearrowright} - c_{1111}^{\circlearrowleft}, \quad \mathcal{C}_2 = c_{1122}^{\circlearrowright} - c_{1122}^{\circlearrowleft}, \quad \mathcal{C}_3 = c_{2323}^{\circlearrowright} - c_{2323}^{\circlearrowleft}.$$

The starting parameters that show up in the commutator are

$$x = c_{1133}^i, c_{2233}^i, c_{3333}^i, c_{2323}^i, c_{1313}^i, \quad i = 1, \ldots, n,$$

and we have commutativity if

$$c_{1133}^i = c_{2233}^i \quad \text{and} \quad c_{2323}^i = c_{1313}^i, \quad i = 1, \ldots, n,$$

which we denote by $x = a$, such that $\mathcal{C}(a) = [0]$.

Again, as in Section 3.2.2, we let the $3 \times 5n$ Jacobi matrix be

$$\mathcal{C}'(x) = \left[\frac{\partial \mathcal{C}}{\partial x}\right].$$

In a series of calculations similar to those in Appendix 3.B we evaluate this Jacobi matrix

and again find that $\mathcal{C}'(a) = [0]$.

Let us also examine the process of combining the Gazis et al. [1963] averages, which is tantamount to combining Diagrams (3.5) and (3.11),

$$
\begin{array}{ccc}
\text{mono} & \xrightarrow{\;\;B\;\;} & \text{mono} \\
{\scriptstyle G}\big\downarrow & & \big\downarrow{\scriptstyle G} \\
\text{ortho} & \xrightarrow[\;\;B\;\;]{} & \text{ortho} \\
{\scriptstyle G}\big\downarrow & & \big\downarrow{\scriptstyle G} \\
\text{tetra} & \xrightarrow[\;\;B\;\;]{} & \text{tetra}
\end{array}
\qquad (3.12)
$$

In accordance with Theorem 3.2.1, in general, there is no commutativity. However, the outcomes are the same as for the corresponding steps in Sections 3.2.2 and 3.2.3. In general, for the Gazis et al. [1963] average, proceeding directly, $\text{aniso} \xrightarrow{G} \text{iso}$, is tantamount to proceeding along arrows in Figure 3.1, $\text{aniso} \xrightarrow{G} \cdots \xrightarrow{G} \text{iso}$. No such combining of the Backus [1962] averages is possible, since, for each step, layers become a homogeneous medium.

3.2.4   Transversely isotropic layers

Lack of commutativity between the two averages can be also exemplified by the case of transversely isotropic layers. Following the clockwise path of Diagram (3.5), the Backus [1962] average results in a transversely isotropic medium, whose Gazis et al. [1963] average, in accordance with Figure 3.1, is isotropic. Following the counterclockwise path, Gazis et al. [1963] average results in an isotropic medium, whose Backus [1962] average, however, is transverse isotropy. Thus, not only the elasticity parameters, but even the resulting material-symmetry classes differ.

Also, we could—in a manner analogous to the one illustrated in Diagram (3.12)—begin with generally anisotropic layers and obtain isotropy by the clockwise path and transverse

isotropy by the counterclockwise path, which again illustrates noncommutativity.

3.3 Numerical examination

3.3.1 Introduction

In this section, we study numerically the extent of the lack of commutativity between the Backus [1962] and Gazis et al. [1963] averages. Also, we examine the effect of the strength of the anisotropy on noncommutativity.

We are once again dealing with Diagram (3.5). Herein, B and G stand for the Backus [1962] average and the Gazis et al. [1963] average, respectively. The upper left-hand corner of Diagram (3.5) is a series of parallel monoclinic layers. The lower right-hand corner is a single orthotropic medium. The intermediate clockwise result is a single monoclinic tensor: an equivalent medium; the intermediate counterclockwise result is a series of parallel orthotropic layers: effective media.

As discussed in Section 3.2, even though, in general, the Backus [1962] average and the Gazis et al. [1963] average do not commute, except in particular cases, it is important to consider the extent of their noncommutativity. In other words, we enquire to what extent— in the context of a continuum-mechanics model and unavoidable measurement errors—the averages could be considered as approximately commutative.

To do so, we numerically examine BG and GB in two cases. In one case, we begin—in the upper left-hand corner of Diagram (3.5)—with ten strongly anisotropic layers. In the other case, we begin with ten weakly anisotropic layers.

3.3.2 Monoclinic layers and orthotropic medium

The elasticity parameters of the strongly anisotropic layers are derived by random variation of a feldspar given by Waeselmann et al. [2016]. For consistency, we express these parameters in the natural coordinate system whose x_3-axis is perpendicular to the symmetry plane, as opposed to the x_2-axis used by Waeselmann et al. [2016]. These parameters are given in Table 3.1.

Table 3.1: Ten strongly anisotropic monoclinic tensors. The elasticity parameters are density-scaled; their units are $10^6 \ \mathrm{m^2/s^2}$.

layer	c_{1111}	c_{1122}	c_{1133}	c_{1112}	c_{2222}	c_{2233}	c_{2212}	c_{3333}	c_{3312}	c_{2323}	c_{2313}	c_{1313}	c_{1212}
1	23.9	11.6	12.2	1.53	71.4	6.64	2.94	52.0	-2.89	8.00	-6.79	8.21	4.54
2	33.5	8.24	12.2	-0.98	66.9	5.65	2.02	82.3	-1.12	6.35	-5.16	17.4	7.36
3	33.2	9.79	16.9	0.57	62.1	6.19	3.81	83.4	-7.34	10.2	-2.33	16.6	4.72
4	38.1	8.33	12.2	1.51	55.0	4.87	3.11	56.8	-1.43	4.10	-0.20	8.25	11.2
5	37.4	11.5	14.4	-0.79	72.6	3.93	3.00	76.5	-6.07	9.58	-4.38	14.8	8.70
6	38.4	10.7	17.1	1.55	63.8	7.11	1.99	55.2	-0.98	9.66	-6.85	11.1	11.4
7	29.2	11.4	11.7	0.59	59.5	5.23	3.74	82.7	-3.81	10.1	-5.09	9.78	6.89
8	31.9	9.03	19.1	-0.07	71.6	4.18	1.98	70.4	-0.25	4.84	-0.33	8.21	10.9
9	37.5	10.5	19.4	0.37	76.7	5.02	3.57	76.7	-0.16	7.84	-1.62	13.8	10.7
10	36.0	9.65	18.9	-0.43	73.1	3.94	2.53	60.4	-7.20	5.44	-2.20	9.25	5.20

The elasticity parameters of the weakly anisotropic layers are derived from the strongly anisotropic ones by keeping c_{1111} and c_{2323} , which are the two distinct elasticity parameters of isotropy, approximately the same as for the corresponding strongly anisotropic layers, and by varying slightly other parameters away from isotropy. These parameters are given in Table 3.2.

Table 3.2: Ten weakly anisotropic monoclinic tensors. The elasticity parameters are density-scaled; their units are $10^6 \, \mathrm{m}^2/\mathrm{s}^2$.

layer	c_{1111}	c_{1122}	c_{1133}	c_{1112}	c_{2222}	c_{2233}	c_{2212}	c_{3333}	c_{3312}	c_{2323}	c_{2313}	c_{1313}	c_{1212}
1	24	9	9	0.2	29	7	0.3	27	-0.3	8	-1	8.2	7
2	34	15	18	-0.1	38	14	0.2	39	-0.1	6	-1	7.5	6.5
3	33	12	14	0.06	37	10	0.4	38	-0.7	10	-0.5	12	8.5
4	38	20	22	0.15	40	15	0.3	41	-0.1	4	-0.2	5	6
5	37	14	16	-0.08	42	10	0.3	41	-0.6	10	-0.8	11	9
6	38	15	18	0.16	41	14	0.2	40	-0.1	10	-1	10.5	11
7	29	9.5	9.5	0.06	32	8	0.4	34	-0.4	10	-0.8	10	9
8	32	15	19.5	-0.01	36	13	0.2	36	-0.03	5	-0.3	6	6
9	38	16	20	0.04	43	14	0.4	42	-0.02	8	-0.4	9	9
10	36	18	23	-0.04	40	15	0.3	39	-0.7	5	-0.5	6	5

Assuming that all layers have the same thickness, we use an arithmetic average for the Backus [1962] averaging; for instance,

$$\overline{c_{1212}} = \frac{1}{10} \sum_{i=1}^{10} c_{1212}^i .$$

The results of the clockwise and counterclockwise paths for the three elasticity parameters that differ from each other are calculated from Equations (3.7), (3.8) and (3.9), and given in Table 3.3. It appears that the averages nearly commute for the case of weak anisotropy. Hence, we confirm, as discussed in Section 3.2.2, that the extent of noncommutativity is a function of the strength of anisotropy.

Table 3.3: Comparison of numerical results.

anisotropy	$c_{1212}^{\circlearrowright}$	$c_{1212}^{\circlearrowleft}$	$c_{1313}^{\circlearrowright}$	$c_{1313}^{\circlearrowleft}$	$c_{2323}^{\circlearrowright}$	$c_{2323}^{\circlearrowleft}$
strong	8.06	8.16	9.13	10.84	6.36	6.90
weak	7.70	7.70	7.88	7.87	6.82	6.81

To ensure that our calculation of the Jacobi matrix being zero is correct, as obtained in Section 3.2.2 and Appendix 3.B, we perform another test. We multiply the weakly anisotropic values of c_{2313}^i and c_{3312}^i, where $i = 1, \ldots, n$, by $\frac{1}{2}$ to find that, as expected, the

commutator is multiplied by $\frac{1}{4}$.

To quantify the strength of anisotropy, we invoke the concept of distance in the space of elasticity tensors [Danek et al., 2013, 2015, Kochetov and Slawinski, 2009a,b]. In particular, we consider the closest isotropic tensor—according to the Frobenius norm—as formulated by Voigt [1910]. Examining one layer from the upper left-hand corner of Diagram (3.5), we denote its weakly anisotropic tensor as c^{w} and its strongly anisotropic tensor as c^{s}.

Using explicit expressions of Slawinski [2018], we find that the elasticity parameters of the closest isotropic tensor, $c^{\mathrm{iso_w}}$, to c^{w} is $c_{1111}^{\mathrm{iso_w}} = 25.52$ and $c_{2323}^{\mathrm{iso_w}} = 8.307$. The Frobenius distance from c^{w} to $c^{\mathrm{iso_w}}$ is 6.328. The closest isotropic tensor, $c^{\mathrm{iso_s}}$, to c^{s} is $c_{1111}^{\mathrm{iso_s}} = 39.08$ and $c_{2323}^{\mathrm{iso_s}} = 11.94$. The distance from c^{s} to $c^{\mathrm{iso_s}}$ is 49.16.

Thus, as expected, c^{s}, which represents strong anisotropy, is much further from isotropy than c^{w}, which represents weak anisotropy.

Wave propagation through the strongly anisotropic Backus medium would exhibit noticeable differences from that through the weakly anisotropic Backus medium, particularly with regards to shear-wave splitting.

3.3.3 Orthotropic layers and tetragonal medium

To examine further the commutativity of averages, we generate ten weakly anisotropic orthotropic tensors from the ten weakly anisotropic monoclinic tensors by setting appropriate entries to zero. Similarly to the weakly anisotropic case discussed in Section 3.3.2, we find that the Backus [1962] and Gazis et al. [1963] averages nearly commute.

As shown in Section 3.2.3—for orthotropic layers and a tetragonal medium—there is commutativity only if $c_{1133}^{i} = c_{2233}^{i}$ and $c_{2323}^{i} = c_{1313}^{i}$, which, in this case, corresponds to $x = a$ in expression (3.10).

If we multiply the difference between the weakly anisotropic values of c_{1133}^{i} and c_{2233}^{i}

as well as that between c_{2323}^i and c_{1313}^i by a factor of F, we find that $\mathcal{C}$ is multiplied by approximately a factor of F^2. The factors of F used in these examination are $\frac{1}{2}$, $\frac{1}{3}$, $\frac{1}{4}$ and $\frac{1}{10}$, with nearly exact values of F^2 for $\mathcal{C}_1$ and $\mathcal{C}_2$ and a close value for $\mathcal{C}_3$. Thus, again, if the differences are of order ε, the commutator is of order ε^2.

3.4   Discussion

We conclude that—in general—the Backus [1962] average, which is a spatial average over an inhomogeneity, and the Gazis et al. [1963] average, which is an average over an anisotropic symmetry group at a point, do not commute. Mathematically, this noncommutativity is stated by Proposition 3.2.1. Also, it is exemplified for several material symmetries.

There are, however, particular cases of given material symmetries for which the averaging processes commute, as discussed in Sections 3.2.2 and 3.2.3. Yet, we do not see a physical explanation for the commutativity in these special cases, which is consistent with the view that a mathematical realm—even though it allows us to formulate quantitative analogies for the physical world—has no causal connection with it.

Using the case of monoclinic and orthotropic symmetries, we numerically show that noncommutativity is a function of the strength of anisotropy. For weak anisotropy, which is a common case of seismological studies, the averages nearly commute. Furthermore, and perhaps surprisingly, a perturbation of the elasticity parameters about a point of weak anisotropy results in the commutator of the two types of averaging being of the order of the square of this perturbation.

For theoretical seismology, which is our motivation, weak anisotropy is adequate for most cases; hence, this near commutativity is welcome. In other words, the fact that the order of a sequence of these two averages is nearly indistinguishable is important information, since it implies that perform either order of operations (BG or GB).

In this study—for convenience and without appreciable loss of generality—we assume that all tensors are expressed in the same orientation of their coordinate systems. Otherwise, the process of averaging become more complicated, as discussed—for the Gazis et al. [1963] average—by Kochetov and Slawinski [2009a,b] and as mentioned—for the Backus [1962] average—by Bos et al. [2017a].

Acknowledgments

3.5   References

G. E. Backus. Long-wave elastic anisotropy produced by horizontal layering. *J. Geophys. Res.*, 67(11):4427–4440, 1962.

A. Bóna, I. Bucataru, and M. A. Slawinski. Space of $SO(3)$-orbits of elasticity tensors. *Archives of Mechanics*, 60(2):123–138, 2008.

L. Bos, D. R. Dalton, M. A. Slawinski, and T. Stanoev. On Backus average for generally anisotropic layers. *Journal of Elasticity*, 127(2):179–196, 2017a.

L. Bos, T. Danek, M. A. Slawinski, and T. Stanoev. Statistical and numerical considerations of Backus-average product approximation. *Journal of Elasticity*, DOI 10.1007/s10659-017-9659-9:1–16, 2017b.

C. H. Chapman. *Fundamentals of seismic wave propagation*. Cambridge University Press, 2004.

T. Danek, M. Kochetov, and M. A. Slawinski. Uncertainty analysis of effective elasticity tensors using quaternion-based global optimization and Monte-Carlo method. *The Quarterly Journal of Mechanics and Applied Mathematics*, 66(2):253–272, 2013.

T. Danek, M. Kochetov, and M. A. Slawinski. Effective elasticity tensors in the context of random errors. *Journal of Elasticity*, 121(1):55–67, 2015.

D. C. Gazis, I. Tadjbakhsh, and R. A. Toupin. The elastic tensor of given symmetry nearest to an anisotropic elastic tensor. *Acta Crystallographica*, 16(9):917–922, 1963.

M. Kochetov and M. A. Slawinski. On obtaining effective orthotropic elasticity tensors. *The Quarterly Journal of Mechanics and Applied Mathematics*, 62(2):149–166, 2009a.

M. Kochetov and M. A. Slawinski. On obtaining effective transversely isotropic elasticity tensors. *Journal of Elasticity*, 94:1–13, 2009b.

M. A. Slawinski. *Waves and rays in elastic continua*. World Scientific, Singapore, 3rd edition, 2015.

M. A. Slawinski. *Waves and rays in seismology: Answers to unasked questions*. World Scientific, 2nd edition, 2018.

W. Thomson. *Mathematical and physical papers: Elasticity, heat, electromagnetism*. Cambridge University Press, 1890.

W. Voigt. *Lehrbuch der Kristallphysik*. Teubner, Leipzig, 1910.

N. Waeselmann, J. M. Brown, R. J. Angel, N. Ross, J. Zhao, and W. Kamensky. The elastic tensor of monoclinic alkali feldspars. *American Mineralogist*, 101:1228–1231, 2016.

3.A Proofs of Lemmas

3.A.1 Lemma 3.2.1

Proof. For discrete symmetries, we can write integral (3.2) as a sum,

$$\widetilde{C}^{\text{sym}} = \frac{1}{n}\left(\tilde{A}_1^{\text{sym}}C\tilde{A}_1^{\text{sym}\,T} + \ldots + \tilde{A}_n^{\text{sym}}C\tilde{A}_n^{\text{sym}\,T}\right), \tag{3.13}$$

where $\widetilde{C}^{\text{sym}}$ is expressed in Kelvin's notation, in view of Thomson [1890, p. 110], as discussed in Chapman [2004, Section 4.4.2].

To write the elements of the monoclinic symmetry group as 6×6 matrices, we must consider orthogonal transformations in $\mathbb{R}^3$. Transformation $A \in SO(3)$ of $c_{ijk\ell}$ corresponds to transformation of C given by

$$\tilde{A} = \begin{bmatrix} A_{11}^2 & A_{12}^2 & A_{13}^2 & \sqrt{2}A_{12}A_{13} \\ A_{21}^2 & A_{22}^2 & A_{23}^2 & \sqrt{2}A_{22}A_{23} \\ A_{31}^2 & A_{32}^2 & A_{33}^2 & \sqrt{2}A_{32}A_{33} \\ \sqrt{2}A_{21}A_{31} & \sqrt{2}A_{22}A_{32} & \sqrt{2}A_{23}A_{33} & A_{23}A_{32}+A_{22}A_{33} \\ \sqrt{2}A_{11}A_{31} & \sqrt{2}A_{12}A_{32} & \sqrt{2}A_{13}A_{33} & A_{13}A_{32}+A_{12}A_{33} \\ \sqrt{2}A_{11}A_{21} & \sqrt{2}A_{12}A_{22} & \sqrt{2}A_{13}A_{23} & A_{13}A_{22}+A_{12}A_{23} \end{bmatrix} \tag{3.14}$$

$$\begin{matrix} \sqrt{2}A_{11}A_{13} & \sqrt{2}A_{11}A_{12} \\ \sqrt{2}A_{21}A_{23} & \sqrt{2}A_{21}A_{22} \\ \sqrt{2}A_{31}A_{33} & \sqrt{2}A_{31}A_{32} \\ A_{23}A_{31}+A_{21}A_{33} & A_{22}A_{31}+A_{21}A_{32} \\ A_{13}A_{31}+A_{11}A_{33} & A_{12}A_{31}+A_{11}A_{32} \\ A_{13}A_{21}+A_{11}A_{23} & A_{12}A_{21}+A_{11}A_{22} \end{matrix} \Bigg],$$

which is an orthogonal matrix, $\tilde{A} \in SO(6)$ [Slawinski, 2015, Section 5.2.5].[*]

The required symmetry-group elements are

$$A_1^{\text{mono}} = \begin{bmatrix} 1 & 0 & 0 \\ 0 & 1 & 0 \\ 0 & 0 & 1 \end{bmatrix} \mapsto \begin{bmatrix} 1 & 0 & 0 & 0 & 0 & 0 \\ 0 & 1 & 0 & 0 & 0 & 0 \\ 0 & 0 & 1 & 0 & 0 & 0 \\ 0 & 0 & 0 & 1 & 0 & 0 \\ 0 & 0 & 0 & 0 & 1 & 0 \\ 0 & 0 & 0 & 0 & 0 & 1 \end{bmatrix} = \tilde{A}_1^{\text{mono}}$$

and

$$A_2^{\text{mono}} = \begin{bmatrix} -1 & 0 & 0 \\ 0 & -1 & 0 \\ 0 & 0 & 1 \end{bmatrix} \mapsto \begin{bmatrix} 1 & 0 & 0 & 0 & 0 & 0 \\ 0 & 1 & 0 & 0 & 0 & 0 \\ 0 & 0 & 1 & 0 & 0 & 0 \\ 0 & 0 & 0 & -1 & 0 & 0 \\ 0 & 0 & 0 & 0 & -1 & 0 \\ 0 & 0 & 0 & 0 & 0 & 1 \end{bmatrix} = \tilde{A}_2^{\text{mono}}.$$

For the monoclinic case, expression (3.13) can be stated explicitly as

$$\widetilde{C}^{\text{mono}} = \frac{\left(\tilde{A}_1^{\text{mono}}\right) C \left(\tilde{A}_1^{\text{mono}}\right)^T + \left(\tilde{A}_2^{\text{mono}}\right) C \left(\tilde{A}_2^{\text{mono}}\right)^T}{2}.$$

---

[*]Readers interested in formulation of matrix (3.14) might also refer to Bóna et al. [2008].

Performing matrix operations, we obtain

$$
\widetilde{C}^{\text{mono}} =
\begin{bmatrix}
c_{1111} & c_{1122} & c_{1133} & 0 & 0 & \sqrt{2}c_{1112} \\
c_{1122} & c_{2222} & c_{2233} & 0 & 0 & \sqrt{2}c_{2212} \\
c_{1133} & c_{2233} & c_{3333} & 0 & 0 & \sqrt{2}c_{3312} \\
0 & 0 & 0 & 2c_{2323} & 2c_{2313} & 0 \\
0 & 0 & 0 & 2c_{2313} & 2c_{1313} & 0 \\
\sqrt{2}c_{1112} & \sqrt{2}c_{2212} & \sqrt{2}c_{3312} & 0 & 0 & 2c_{1212}
\end{bmatrix},
\tag{3.15}
$$

which exhibits the form of the monoclinic tensor in its natural coordinate system. In other words, $\widetilde{C}^{\text{mono}} = C^{\text{mono}}$, in accordance with Corollary 3.2.1. $\qquad\square$

3.A.2 Lemma 3.2.2

Proof. For orthotropic symmetry,

$$\tilde{A}_1^{\text{ortho}} = \tilde{A}_1^{\text{mono}}, \tilde{A}_2^{\text{ortho}} = \tilde{A}_2^{\text{mono}},$$

$$
A_3^{\text{ortho}} =
\begin{bmatrix}
-1 & 0 & 0 \\
0 & 1 & 0 \\
0 & 0 & -1
\end{bmatrix}
\mapsto
\begin{bmatrix}
1 & 0 & 0 & 0 & 0 & 0 \\
0 & 1 & 0 & 0 & 0 & 0 \\
0 & 0 & 1 & 0 & 0 & 0 \\
0 & 0 & 0 & -1 & 0 & 0 \\
0 & 0 & 0 & 0 & 1 & 0 \\
0 & 0 & 0 & 0 & 0 & -1
\end{bmatrix}
= \tilde{A}_3^{\text{ortho}},
$$

and

$$A_4^{\text{ortho}} = \begin{bmatrix} 1 & 0 & 0 \\ 0 & -1 & 0 \\ 0 & 0 & -1 \end{bmatrix} \mapsto \begin{bmatrix} 1 & 0 & 0 & 0 & 0 & 0 \\ 0 & 1 & 0 & 0 & 0 & 0 \\ 0 & 0 & 1 & 0 & 0 & 0 \\ 0 & 0 & 0 & 1 & 0 & 0 \\ 0 & 0 & 0 & 0 & -1 & 0 \\ 0 & 0 & 0 & 0 & 0 & -1 \end{bmatrix} = \tilde{A}_4^{\text{ortho}}.$$

For the orthotropic case, expression (3.13) can be stated explicitly as

$$\widetilde{C}^{\text{ortho}} = \left[\left(\tilde{A}_1^{\text{ortho}} \right) C \left(\tilde{A}_1^{\text{ortho}} \right)^T + \left(\tilde{A}_2^{\text{ortho}} \right) C \left(\tilde{A}_2^{\text{ortho}} \right)^T \right.$$
$$\left. + \left(\tilde{A}_3^{\text{ortho}} \right) C \left(\tilde{A}_3^{\text{ortho}} \right)^T + \left(\tilde{A}_4^{\text{ortho}} \right) C \left(\tilde{A}_4^{\text{ortho}} \right)^T \right] / 4.$$

Performing matrix operations, we obtain

$$\widetilde{C}^{\text{ortho}} = \begin{bmatrix} c_{1111} & c_{1122} & c_{1133} & 0 & 0 & 0 \\ c_{1122} & c_{2222} & c_{2233} & 0 & 0 & 0 \\ c_{1133} & c_{2233} & c_{3333} & 0 & 0 & 0 \\ 0 & 0 & 0 & 2c_{2323} & 0 & 0 \\ 0 & 0 & 0 & 0 & 2c_{1313} & 0 \\ 0 & 0 & 0 & 0 & 0 & 2c_{1212} \end{bmatrix}, \tag{3.16}$$

which exhibits the form of the orthotropic tensor in its natural coordinate system. In other words, $\widetilde{C}^{\text{ortho}} = C^{\text{ortho}}$, in accordance with Corollary 3.2.2. $\qquad \square$

3.B   Evaluation of Jacobian

$$\mathcal{C}_3 = \left[\frac{1}{n} \sum_{i=1}^{n} \frac{1}{c_{3333}^i} \right]^{-1} \left[\frac{1}{n} \sum_{i=1}^{n} \frac{c_{3312}^i}{c_{3333}^i} \right]^2 - \left[\frac{1}{n} \sum_{i=1}^{n} \frac{(c_{3312}^i)^2}{c_{3333}^i} \right].$$

$$\frac{\partial \mathcal{C}_3}{\partial c_{2323}^j} = \frac{\partial \mathcal{C}_3}{\partial c_{1313}^j} = \frac{\partial \mathcal{C}_3}{\partial c_{2313}^j} = 0.$$

$$\frac{\partial \mathcal{C}_3}{\partial c_{3312}^j} = 2 \left[\frac{1}{n} \sum_{i=1}^n \frac{1}{c_{3333}^i} \right]^{-1} \left[\frac{1}{n} \sum_{i=1}^n \frac{c_{3312}^i}{c_{3333}^i} \right] \left(\frac{1}{n} \right) \left(\frac{1}{c_{3333}^j} \right) - \frac{2}{n} \frac{c_{3312}^j}{c_{3333}^j}.$$

$$\frac{\partial \mathcal{C}_3}{\partial c_{3333}^j} = - \left[\frac{1}{n} \sum_{i=1}^n \frac{1}{c_{3333}^i} \right]^{-2} \left[\frac{1}{n} \left(\frac{-1}{(c_{3333}^j)^2} \right) \right] \left[\frac{1}{n} \sum_{i=1}^n \frac{c_{3312}^i}{c_{3333}^i} \right]^2$$
$$+ \left[\frac{1}{n} \sum_{i=1}^n \frac{1}{c_{3333}^i} \right]^{-1} \left[\frac{2}{n} \sum_{i=1}^n \frac{c_{3312}^i}{c_{3333}^i} \right] \left[\frac{1}{n} \left(\frac{-c_{3312}^j}{(c_{3333}^j)^2} \right) \right] + \frac{1}{n} \frac{\left(c_{3312}^j \right)^2}{\left(c_{3333}^j \right)^2}.$$

Examining the above two equations—where for $x = a$, $c_{2313}^j = c_{3312}^j = 0$, with $j = 1, \dots, n$—

we see that

$$\left. \frac{\partial \mathcal{C}_3}{\partial c_{3312}^j} \right|_{x=a} = \left. \frac{\partial \mathcal{C}_3}{\partial c_{3333}^j} \right|_{x=a} = 0.$$

Next, let us examine $\mathcal{C}_1$ and $\mathcal{C}_2$. First, note that

$$\frac{\partial \mathcal{C}_1}{\partial c_{3333}^j} = \frac{\partial \mathcal{C}_2}{\partial c_{3333}^j} = \frac{\partial \mathcal{C}_1}{\partial c_{3312}^j} = \frac{\partial \mathcal{C}_2}{\partial c_{3312}^j} = 0.$$

We let

$$f = \frac{1}{n} \sum_{i=1}^n \frac{c_{2323}^i}{2 \left(c_{2323}^i c_{1313}^i - \left[c_{2313}^i \right]^2 \right)},$$

$$g = \frac{1}{n} \sum_{i=1}^n \frac{c_{1313}^i}{2 \left(c_{2323}^i c_{1313}^i - \left[c_{2313}^i \right]^2 \right)}$$

and

$$h = \frac{1}{n} \sum_{i=1}^n \frac{c_{2313}^i}{2 \left(c_{2323}^i c_{1313}^i - \left[c_{2313}^i \right]^2 \right)}.$$

which leads to

$$\mathcal{C}_1 = \frac{f}{2 [fg - h^2]} - \left(\frac{1}{n} \sum_{i=1}^n \frac{1}{c_{2323}^i} \right)^{-1},$$

Thus,

$$\frac{\partial \mathcal{C}_1}{\partial c_{2323}^j} = \frac{\partial f}{\partial c_{2323}^j} \frac{1}{2[fg-h^2]} - \frac{f}{2} \left[fg - h^2\right]^{-2} \left[g \frac{\partial f}{\partial c_{2323}^j} + f \frac{\partial g}{\partial c_{2323}^j} - 2h \frac{\partial h}{\partial c_{2323}^j}\right]$$

$$+ \left(\frac{1}{n} \sum_{i=1}^{n} \frac{1}{c_{2323}^i}\right)^{-2} \frac{1}{n} \frac{-1}{\left[c_{2323}^j\right]^2},$$

$$\frac{\partial f}{\partial c_{2323}^j} = \frac{1}{n} \frac{1}{2 \left(c_{2323}^j c_{1313}^j - \left[c_{2313}^j\right]^2\right)} - \frac{c_{2323}^j}{2n} c_{1313}^j \left(c_{2323}^j c_{1313}^j - \left[c_{2313}^j\right]^2\right)^{-2},$$

$$\frac{\partial g}{\partial c_{2323}^j} = \frac{-\left[c_{1313}^j\right]^2}{2n} \left(c_{2323}^j c_{1313}^j - \left[c_{2313}^j\right]^2\right)^{-2},$$

$$\frac{\partial h}{\partial c_{2323}^j} = \frac{c_{2313}^j}{2n} \left(2c_{1313}^j\right) \left(c_{2323}^j c_{1313}^j - \left[c_{2313}^j\right]^2\right)^{-2}.$$

$$\left.\frac{\partial f}{\partial c_{2323}^j}\right|_{x=a} = \frac{1}{2n c_{2323}^j c_{1313}^j} - \frac{c_{2323}^j c_{1313}^j}{2n \left(c_{2323}^j c_{1313}^j\right)^2} = 0.$$

$$\left.\frac{\partial g}{\partial c_{2323}^j}\right|_{x=a} = \frac{-\left(c_{1313}^j\right)^2}{2n \left(c_{2323}^j\right)^2 \left(c_{1313}^j\right)^2} = \frac{-1}{2n \left(c_{2323}^j\right)^2}.$$

$$\left.\frac{\partial h}{\partial c_{2323}^j}\right|_{x=a} = 0.$$

$$\left.\frac{\partial \mathcal{C}_1}{\partial c_{2323}^j}\right|_{x=a} = 0 - \frac{f}{2} \left[fg - h^2\right]^{-2} \left[0 - \frac{f}{2n(c_{2323}^j)^2} - 0\right] + \left(\frac{1}{n} \sum_{i=1}^{n} \frac{1}{c_{2323}^i}\right)^{-2} \frac{1}{n} \frac{-1}{\left(c_{2323}^j\right)^2}.$$

$$\left.\frac{f^2}{4n \left[fg - h^2\right]^2}\right|_{x=a} = \frac{\left[\frac{1}{n} \sum_{i=1}^{n} \left(\frac{1}{2c_{1313}^i}\right)\right]^2}{4n \left(\frac{1}{4n^2} \sum_{i=1}^{n} \frac{1}{c_{1313}^i} \sum_{i=1}^{n} \frac{1}{c_{2323}^i}\right)^2} = \frac{n}{\left(\sum_{i=1}^{n} \frac{1}{c_{2323}^i}\right)^2}.$$

71

So,

$$\left.\frac{\partial \mathcal{C}_1}{\partial c_{2323}^j}\right|_{x=a} = \frac{n}{\left(\sum_{i=1}^{n} \frac{1}{c_{2323}^i}\right)^2 \left(c_{2323}^j\right)^2} - \frac{n}{\left(\sum_{i=1}^{n} \frac{1}{c_{2323}^i}\right)^2 \left(c_{2323}^j\right)^2} = 0.$$

Similarly, by symmetry of the equations,

$$\left.\frac{\partial \mathcal{C}_2}{\partial c_{1313}^j}\right|_{x=a} = 0.$$

Next, we consider the derivative with respect to c_{1313}^j.

$$\frac{\partial \mathcal{C}_1}{\partial c_{1313}^j} = \frac{\partial f}{\partial c_{1313}^j} \frac{1}{2 \left[fg - h^2\right]} - \frac{f}{2} \left[fg - h^2\right]^{-2} \left[g \frac{\partial f}{\partial c_{1313}^j} + f \frac{\partial g}{\partial c_{1313}^j} - 2h \frac{\partial h}{\partial c_{1313}^j}\right].$$

$$\frac{\partial f}{\partial c_{1313}^j} = \frac{-\left[c_{2323}^j\right]^2}{2n} \left(c_{2323}^j c_{1313}^j - \left[c_{2313}^j\right]^2\right)^{-2},$$

$$\frac{\partial g}{\partial c_{1313}^j} = \frac{1}{n} \frac{1}{2 \left(c_{2323}^j c_{1313}^j - \left[c_{2313}^j\right]^2\right)} - \frac{c_{1313}^j}{2n} c_{2323}^j \left(c_{2323}^j c_{1313}^j - \left[c_{2313}^j\right]^2\right)^{-2},$$

$$\frac{\partial h}{\partial c_{1313}^j} = \frac{c_{2313}^j}{2n} \left(2 c_{2323}^j\right) \left(c_{2323}^j c_{1313}^j - \left[c_{2313}^j\right]^2\right)^{-2}.$$

These lead to

$$\left.\frac{\partial f}{\partial c_{1313}^j}\right|_{x=a} = \frac{-1}{2n \left(c_{1313}^j\right)^2},$$

$$\left.\frac{\partial g}{\partial c_{1313}^j}\right|_{x=a} = \frac{1}{2n c_{2323}^j c_{1313}^j} - \frac{c_{1313}^j c_{2323}^j}{2n \left(c_{2323}^j c_{1313}^j\right)^2} = 0,$$

$$\left.\frac{\partial h}{\partial c_{1313}^j}\right|_{x=a} = 0.$$

So,

$$\left.\frac{\partial \mathcal{C}_1}{\partial c_{1313}^j}\right|_{x=a} = \left.\frac{\partial f}{\partial c_{1313}^j}\frac{1}{2\left[fg-h^2\right]}\left[1-\frac{fg}{fg-h^2}\right]\right|_{x=a} = 0$$

and, similarly,

$$\left.\frac{\partial \mathcal{C}_2}{\partial c_{2323}^j}\right|_{x=a} = 0.$$

Next, we consider the derivative with respect to c_{2313}^j.

$$\frac{\partial \mathcal{C}_1}{\partial c_{2313}^j} = \frac{\partial f}{\partial c_{2313}^j}\frac{1}{2\left[fg-h^2\right]} - \frac{f}{2}\left[fg-h^2\right]^{-2}\left[g\frac{\partial f}{\partial c_{2313}^j}+f\frac{\partial g}{\partial c_{2313}^j}-2h\frac{\partial h}{\partial c_{2313}^j}\right].$$

$$\left.\frac{\partial f}{\partial c_{2313}^j}\right|_{x=a} = \left.\frac{-2c_{2313}^j c_{2323}^j}{2n\left(c_{2323}^j c_{1313}^j - \left[c_{2313}^j\right]^2\right)^2}\right|_{x=a} = 0,$$

$$\left.\frac{\partial g}{\partial c_{2313}^j}\right|_{x=a} = \left.\frac{-2c_{2313}^j c_{1313}^j}{2n\left(c_{2323}^j c_{1313}^j - \left[c_{2313}^j\right]^2\right)^2}\right|_{x=a} = 0,$$

$$\left.\frac{\partial h}{\partial c_{2313}^j}\right|_{x=a} = \left.\frac{1}{2n\left(c_{2323}^j c_{1313}^j - \left[c_{2313}^j\right]^2\right)}\right|_{x=a} + \left.\frac{2(c_{2313}^j)^2}{2n\left(c_{2323}^j c_{1313}^j - \left[c_{2313}^j\right]^2\right)^2}\right|_{x=a}$$

$$= \frac{1}{2nc_{2323}^j c_{1313}^j}.$$

Thus,

$$\left.\frac{\partial \mathcal{C}_1}{\partial c_{2313}^j}\right|_{x=a} = 0 - \frac{f}{2}\left[fg-h^2\right]^{-2}[0+0-0] = 0,$$

and, similarly,

$$\left.\frac{\partial \mathcal{C}_2}{\partial c_{2313}^j}\right|_{x=a} = 0\,.$$

Hence, $\mathcal{C}'(a) = [0]$; the Jacobi matrix is the zero matrix.

Chapter 4

Sensitivity of Love and quasi-Rayleigh waves to model parameters*

Abstract

We examine the sensitivity of the Love and the quasi-Rayleigh waves to model parameters. Both waves are guided waves that propagate in the same model of an elastic layer above an elastic halfspace. We study their dispersion curves without any simplifying assumptions, beyond the standard approach of elasticity theory in isotropic media. We examine the sensitivity of both waves to elasticity parameters, frequency and layer thickness, for varying frequency and different modes. In the case of Love waves, we derive and plot the absolute value of a dimensionless sensitivity coefficient in terms of partial derivatives, and perform an analysis to find the optimum frequency for determining the layer thickness. For a coherency of the background information, we briefly review the Love-wave dispersion relation and provide details of the less common derivation of the quasi-Rayleigh relation

---

in an appendix. We compare that derivation to past results in the literature, finding certain discrepancies among them.

4.1 Introduction

In this paper, we examine the sensitivity of the Love and quasi-Rayleigh waves to model parameters. This study provides insight into the reliability of inferences of model properties from data. Herein, sensitivity refers to relations between the wave properties and model parameters in the context of dispersion relations. It does not refer to a misfit between a model and experimental data.

Both waves propagate within an elastic isotropic layer over an elastic isotropic half-space. This provides a redundancy of information, since both waves are described in terms of the same model parameters, and can be jointly inverted to obtain those parameters, which is studied in Chapter 5. To examine the sensitivity—given the elasticity parameters, mass densities and the thickness of the layer, as well as the frequency of the signal—we study expressions for the speeds of the waves that correspond to different modes for either wave. In general, each wave has an infinite number of modes and each mode propagates with a different speed. However, for a given frequency, there is a finite number of modes, and hence, speeds.

On the surface, the two waves exhibit displacements that are perpendicular to each other. The displacements of the Love wave are in the horizontal plane and perpendicular to the direction of propagation. The displacements of the quasi-Rayleigh wave are elliptical and in the vertical plane, and—on the surface—have a horizontal component parallel to the direction of propagation. Thus, different speeds and displacement directions render these waves and their modes empirically distinguishable.

The quasi-Rayleigh wave shares many similarities with the classical Rayleigh wave,

but is not restricted to the halfspace alone. In literature, the quasi-Rayleigh wave has been also referred to as Rayleigh-type wave, Rayleigh-like wave, generalized Rayleigh wave, Rayleigh-Lamb wave and Rayleigh wave in inhomogeneous media.

Seismological information, such as wave speeds measured on the surface, allows us to infer properties of the subsurface. Herein, to gain insight into such an inverse problem, we examine the sensitivity of the forward one. Wave speeds corresponding to different modes of either wave exhibit different sensitivities to model parameters.

Motivated by the accuracy of modern seismic measurements and availability of computational tools, we study the Love and quasi-Rayleigh dispersion curves without any simplifying assumptions, beyond the standard approach of elasticity theory in isotropic media.

The presented concept of studying sensitivities exhibits certain similarities to the recent work of Lucena and Taioli [2014], but with a different approach and scope. The novelty of this study consists of an analysis of the sensitivity of the dispersion relation to elasticity parameters and layer thickness for both Love and quasi-Rayleigh waves for varying frequencies and different modes. Furthermore, we formulate a dimensionless sensitivity coefficient analysis from which we obtain the optimum frequency of Love waves for determining layer thickness.

We begin this paper by examining Love waves and proceed to quasi-Rayleigh waves. In either case, we discuss the sensitivity of the dispersion relations to elasticity parameters and layer thickness for varying frequencies and different modes. We highlight the sensitivity results in Section 4.4.2 and suggest further research directions in Section 4.5. This paper contains three appendices, which consist, respectively, of the derivation of the quasi-Rayleigh dispersion relation, calculations of its determinant and a comparison to literature results.

4.2 Love waves

4.2.1 Material properties

We wish to examine the sensitivity of guided *SH* waves to model parameters. For this purpose, we consider an elastic layer with mass density, ρ^u, elasticity parameter, C_{44}^u, and hence, *S*-wave propagation speed, $\beta^u = \sqrt{C_{44}^u/\rho^u}$. Also, we consider an elastic halfspace with ρ^d, C_{44}^d and $\beta^d = \sqrt{C_{44}^d/\rho^d}$. We set the coordinate system in such a manner that the surface is at $x_3 = 0$ and the interface is at $x_3 = Z$, with the x_3-axis positive downwards.

For details of the derivation of the Love wave dispersion relation, see, for instance, Slawinski [2018, Chapter 6] and references therein. The dispersion relation for Love waves, where v_ℓ is the speed of Love waves and ω is the angular frequency, can be written as

$$
\tan\left(\omega\sqrt{\frac{1}{(\beta^u)^2} - \frac{1}{v_\ell^2}}\, Z\right) = \frac{C_{44}^d\sqrt{\dfrac{1}{v_\ell^2} - \dfrac{1}{(\beta^d)^2}}}{C_{44}^u\sqrt{\dfrac{1}{(\beta^u)^2} - \dfrac{1}{v_\ell^2}}}. \tag{4.1}
$$

To plot expression (4.1), we rewrite it as an expression equal to zero, where

$$
D_\ell = 2\left(C_{44}^u\sqrt{\left(\frac{v_\ell}{\beta^u}\right)^2 - 1}\,\sin\left(\frac{\omega Z}{\beta^u}\sqrt{1 - \left(\frac{\beta^u}{v_\ell}\right)^2}\right) - C_{44}^d\sqrt{1 - \left(\frac{v_\ell}{\beta^d}\right)^2}\,\cos\left(\frac{\omega Z}{\beta^u}\sqrt{1 - \left(\frac{\beta^u}{v_\ell}\right)^2}\right)\right) = 0. \tag{4.2}
$$

We plot expression (4.2) within a model in which we set the layer thickness $Z = 500\,\text{m}$, the two elasticity parameters, $C_{44}^u = 0.88 \times 10^{10}\,\text{N/m}^2$ and $C_{44}^d = 4.16 \times 10^{10}\,\text{N/m}^2$, and mass densities, $\rho^u = 2200\,\text{kg/m}^3$ and $\rho^d = 2600\,\text{kg/m}^3$. It follows that the *S*-wave propagation speeds in the layer and the halfspace are $\beta^u = 2000\,\text{m/s}$ and $\beta^d = 4000\,\text{m/s}$, respectively. Such a model could represent a sandstone layer over a granite halfspace.

Examining the left and right plots of Figure 4.1, as well as the dispersion curves in Figure 4.2, we see that, for high frequency, $\omega = 60\,\text{s}^{-1}$, the speed of the fundamental
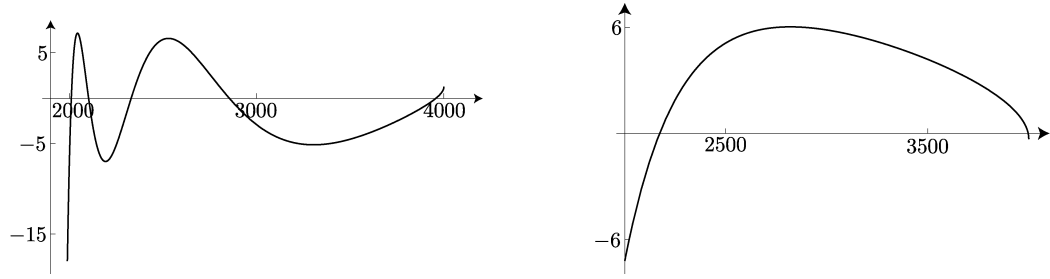
Figure 4.1: D_ℓ, defined in expression (4.2), as a function of speed, v_ℓ. On the left, for $\omega = 60 \text{ s}^{-1}$, there are five roots: $v_\ell^1 = 2010.7 \text{ m/s}$, $v_\ell^2 = 2102.76 \text{ m/s}$, $v_\ell^3 = 2330.44 \text{ m/s}$, $v_\ell^4 = 2853.13 \text{ m/s}$ and $v_\ell^5 = 3958.53 \text{ m/s}$. On the right, for $\omega = 15 \text{ s}^{-1}$, there are two roots: $v_\ell^6 = 2172.48 \text{ m/s}$ and $v_\ell^7 = 3997.01 \text{ m/s}$. The values on the vertical axes are to be multiplied by 10^{10}.
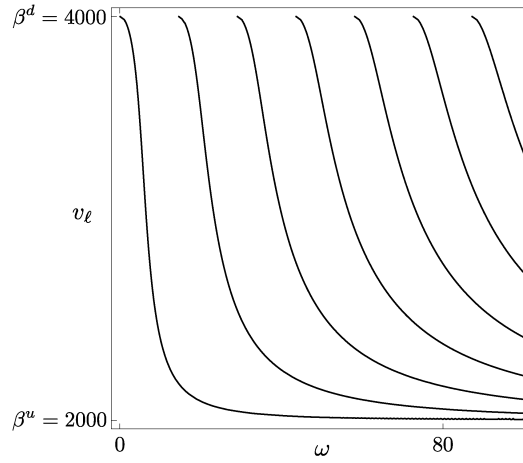
Figure 4.2: The Love-wave dispersion curves, $D_\ell = 0$, defined in expression (4.2), as a function of speed, v_ℓ, and frequency, ω.

mode of the Love wave, $v_\ell^1 = 2011$ m/s, approaches β^u, from above. The values of v_ℓ are computed numerically. This result is in agreement with Udías [1999, p. 196], and with the general theory of Love waves.

4.2.2 Sensitivity of dispersion relation

We wish to examine effects of elasticity parameters and layer thickness on the dispersion relation, for various frequencies and different modes. To do so, we examine effects of these quantities on the value of D_ℓ, defined in expression (4.2). Specifically, we examine D_ℓ as a function of C_{44}^d and C_{44}^u, for two distinct frequencies and for fixed values of v_ℓ, which correspond to particular modes.

In the contour maps of Figures 4.3–4.6, the sensitivity of the dispersion relation is illustrated by the slope of the zero contour line, where a vertical line implies no sensitivity to the parameter on the vertical axis and a horizontal line implies no sensitivity to the parameter on the horizontal axis. In other words, a parallel line does not restrict the values on the corresponding axis. The zero contour line is the combination of elasticity parameters that result in a solution, $D_\ell = 0$. Hence, from a vertical line we infer that the horizontal axis parameter is fixed but the vertical axis parameter is not constrained. Our approach differs from the approach of Lucena and Taioli [2014], who examine the response of the dispersion curves to shifts in parameter values.

Let us examine the numerical solutions of speed for the Love wave dispersion relation for the high-frequency and low-frequency cases. We use these solutions to investigate the relative sensitivities of Love waves to the elasticity parameters in the upper layer and in the lower halfspace, as well as to the elasticity parameter in the upper layer and to the layer thickness.

We begin by considering the layer and halfspace elasticity parameters. For the high-speed case, we consider the fifth root of the left plot of Figure 4.1, which is $v_\ell^5 = 3959$ m/s,
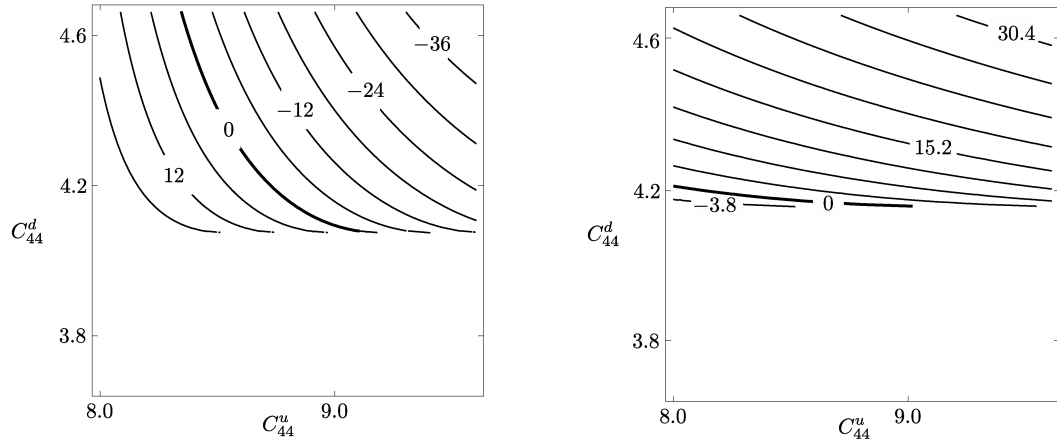
Figure 4.3: $D_\ell / 10^9$, defined in expression (4.2), as a function of the elasticity parameters, C_{44}^u and C_{44}^d, for $\omega = 60$ s^{-1} and $v_\ell^5 = 3958.53$ m/s, on the left, and for $\omega = 15$ s^{-1} and $v_\ell^7 = 3997.01$ m/s, on the right. The values on the horizontal and vertical axes are to be multiplied by 10^9 and 10^{10}, respectively. Both plots demonstrate sensitivity to C_{44}^u and C_{44}^d but the right plot, for lower frequency, demonstrates a greater sensitivity to C_{44}^d.
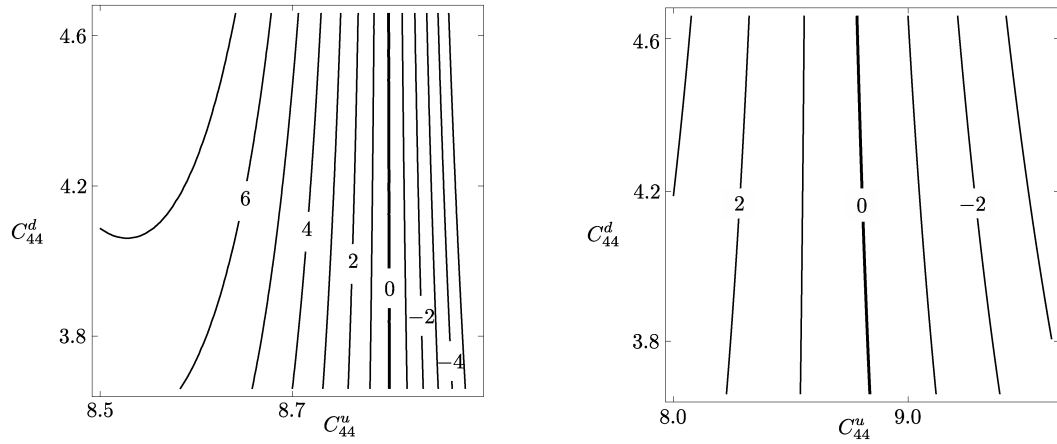
Figure 4.4: $D_\ell / 10^{10}$, defined in expression (4.2), as a function of the elasticity parameters, C_{44}^u and C_{44}^d, where $\omega = 60$ s^{-1} and $v_\ell^1 = 2010.7$ m/s, and where $\omega = 15$ s^{-1} and $v_\ell^6 = 2172.48$ m/s, for left and right, respectively. The values on the horizontal and vertical axes are to be multiplied by 10^9 and 10^{10}, respectively. We see from the zero contours, which are near vertical, that there is sensitivity to C_{44}^u and not to C_{44}^d, and this contrast is slightly more pronounced for the higher frequency case.

and the second root of the right plot of Figure 4.1, which is $v_\ell^7 = 3997$ m/s. The left and right plots of Figure 4.3 are the corresponding contour plots of $D_\ell/10^9$ with varying C_{44}^u and C_{44}^d. In both cases, D_ℓ is sensitive to variations in both C_{44}^u and C_{44}^d. However, the right plot of Figure 4.3 indicates a greater sensitivity to C_{44}^d for the lower frequency, which is tantamount to longer wavelength.

For the low-speed case, we observe different sensitivities. Let us examine the first root of the left plot of Figure 4.1, which is $v_\ell^1 = 2011$ m/s, and the first root of the right plot of Figure 4.1, which is $v_\ell^6 = 2172$ m/s. Following the corresponding plots in Figure 4.4, we see that there are near vertical lines at $C_{44}^u = 0.88 \times 10^{10}$. This indicates a sensitivity toward C_{44}^u but not toward C_{44}^d, and we observe that it is more pronounced for the left plot. Thus, for a given wavelength, a solution whose speed is closer to β^u is less sensitive to C_{44}^d than a solution with greater speed.

Next, we consider the layer elasticity parameter and layer thickness. Using the high-speed roots of expression (4.2), we observe sensitivity to both C_{44}^u and Z, in the high-frequency and low-frequency cases, which are depicted in Figure 4.5. Using low-speed roots in Figure 4.6, we see that there is less sensitivity to Z for higher frequencies than lower frequencies. Note that, in the left plot of Figure 4.5, the groups of contours in the upper left and lower right are due to the periodicity of D_ℓ in Z, as discussed is section 4.2.3, below.

Additionally, the two plots of Figure 4.6, along with the left plot of Figure 4.4, approach a maximum value of C_{44}^u, whereas the two plots of Figure 4.5 do not. To understand this behaviour, we recall that, as a consequence of the allowable range of Love-wave speeds, $\beta^u < v_\ell < \beta^d$, there is a maximum value of C_{44}^u whose value is $v_\ell^2 \rho^u$.
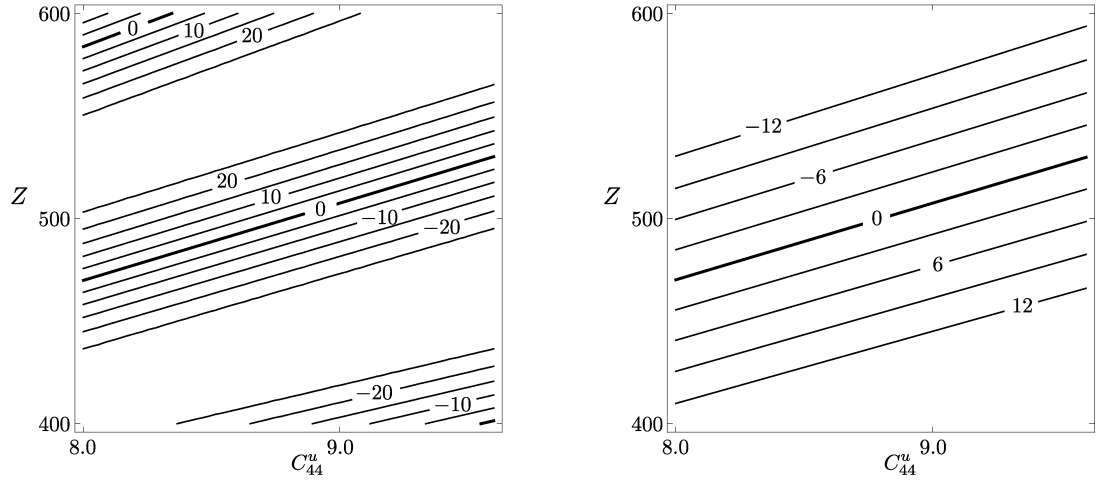
Figure 4.5: $D_\ell/10^9$, defined in expression (4.2), as a function of C_{44}^u and Z, for $\omega = 60$ s^{-1} and $v_\ell^5 = 3958.53$ m/s, on the left, and for $\omega = 15$ s^{-1} and $v_\ell^7 = 3997.01$ m/s, on the right. The values on the horizontal axis are to be multiplied by 10^9. In each case, there is sensitivity to both C_{44}^u and Z.
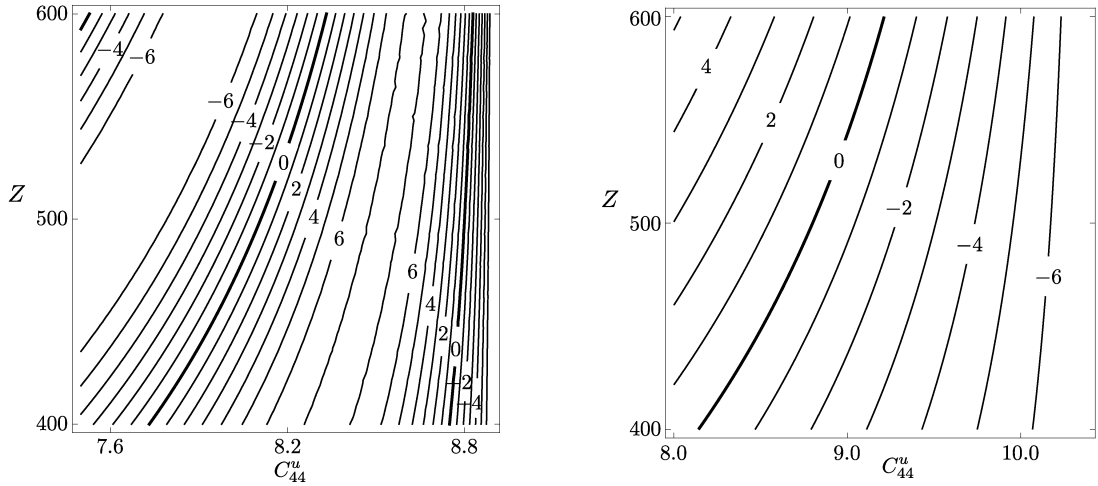
Figure 4.6: $D_\ell/10^{10}$, defined in expression (4.2), as a function of C_{44}^u and Z, where $\omega = 60$ s^{-1} and $v_\ell^1 = 2010.7$ m/s, and where $\omega = 15$ s^{-1} and $v_\ell^6 = 2172.48$ m/s, for left and right, respectively. In the left plot, the zero contour of interest is the near-vertical one on the right side of the plot, near the maximum C_{44}^u. The values on the horizontal axis are to be multiplied by 10^9. In each case, there is sensitivity to both C_{44}^u and Z, but the higher frequency case has less sensitivity to Z.

4.2.3 Love wave as superposition of *SH* waves

The ridge and valley behaviour, shown in Figures 4.5 and 4.6, can be explained by examining the nonzero component of the displacement, taken from the derivation of the Love-wave dispersion relation in Slawinski [2018],

$$u_2^u(x_1, x_3, t) = C_1 \exp\left(-\iota \kappa s^u x_3\right) \exp[\iota(\kappa x_1 - \omega t)] + C_2 \exp\left(\iota \kappa s^u x_3\right) \exp[\iota(\kappa x_1 - \omega t)],$$

where $s^u := \sqrt{(v_\ell/\beta^u)^2 - 1}$. This expression can be interpreted as a superposition of two *SH* waves within the elastic layer. Both waves travel obliquely with respect to the surface and interface; one wave travels upwards, the other downwards. Their wave vectors are $\overline{k}_\pm := (\kappa, 0, \pm \kappa s^u)$. Thus, since

$$|\overline{k}_\pm| = \sqrt{\kappa^2 + (\kappa s^u)^2},$$

we have

$$|\overline{k}_\pm| = \kappa \sqrt{1 + (s^u)^2} = \kappa \frac{v_\ell}{\beta^u},$$

where

$$\frac{\beta^u}{v_\ell} = \frac{\kappa}{|\overline{k}_\pm|} = \sin\theta,$$

with θ representing the angle between $\overline{k}_\pm$ and the x_3-axis. Thus, θ is the angle between the x_3-axis and a wavefront normal, which implies that it is the propagation direction of a wavefront. Hence, for the case where v_ℓ is only slightly larger than β^u, it follows that both the upgoing and downgoing *SH* waves propagate nearly horizontally. In other words, their propagation directions are nearly parallel to the interface. In such a case, the resulting Love wave is less sensitive to the material properties below the interface than for the case of $\beta^u/v_\ell \ll 1$.

Depending on the propagation direction, θ, of the *SH* waves, there is a distinction in the sensitivity to the material properties of the halfspace. This distinction is more pronounced for short wavelengths, in comparison with the layer thickness. For any angle, the longer the wavelength the more sensitivity of the wave to material properties below the interface, and thus the distinction—as a function of the propagation direction—is diminished.

Also, the superposition helps us understand the requirement of $\beta^u < v_\ell < \beta^d$. The lower limit, which we can write as $\sin\theta = \beta^u/\beta^u = 1$, corresponds to waves that propagate along the x_1-axis, and hence, do not exhibit any interference associated with the presence of the horizontal surface or interface. Formally, the lower limit is required by the real value of the sine function.

The upper limit is introduced to ensure an exponential amplitude decay in the halfspace. Herein, we can write the upper limit as $\sin\theta = \beta^u/\beta^d$, which—in general—implies that the *SH* waves propagate obliquely. In the extreme case, if $\beta^d \to \infty$, the waves propagate vertically. Also, this case is tantamount to total internal reflection, since it corresponds to a rigid halfspace, $C_{44}^d \to \infty$; such a case is discussed by Slawinski [2018, Section 6.3.1].

Update: even in the case of a non-rigid halfspace, but still with $\beta^d > \beta^u$, the Love wave can be viewed as the superposition of upgoing and downgoing obliquely propagating totally internally reflected *SH* waves, and in the halfspace there is just an evanescent wave.

4.2.4 Optimum frequency for layer-thickness determination

In this section, we search for the best frequency for inferring the depth of the interface. Given the values of the elasticity parameters and layer thickness, for a specific frequency, we deduce the corresponding propagation speed. For a given mode, this speed depends on Z, which means that Z is a function of speed. Since, experimentally, the speed is measured with only finite accuracy, we inherit that finite accuracy for any inference of the value of Z.

As a measure of sensitivity of Z to errors in speed, we take the derivative, dZ/dv_ℓ, or, more precisely, its ratio to Z, namely,

$$\tilde{A} := \frac{1}{Z}\frac{dZ}{dv_\ell}. \tag{4.3}$$

For convenience, we write relation (4.2) using dimensionless quantities. If we let

$$\alpha := \sqrt{\frac{C_{44}^d \rho^u}{C_{44}^u \rho^d}} = \frac{\beta^d}{\beta^u} > 1, \quad E := \sqrt{\frac{C_{44}^d \rho^d}{C_{44}^u \rho^u}}, \quad \theta := \frac{v_\ell}{\beta^u}, \quad v := \frac{\omega Z}{\beta^u}, \tag{4.4}$$

then relation (4.2) becomes

$$F(v,\theta) := \sqrt{\theta^2 - 1}\sin\left(v\sqrt{1 - \frac{1}{\theta^2}}\right) - E\sqrt{\alpha^2 - \theta^2}\cos\left(v\sqrt{1 - \frac{1}{\theta^2}}\right) = 0, \tag{4.5}$$

where $1 < \theta < \alpha$ and $v > 0$. Using the Implicit Function Theorem, which in its most basic form says that a relation $F(x,y) = 0$ can be converted to $y(x)$ or $x(y)$, the following properties are shown.

○ $F(v,\theta) = 0$ defines locally θ as a function of v, and, reciprocally, v as a function of θ.

○ $F(v,\theta) = 0$ has a solution $1 < \theta < \alpha$ for any $v > 0$. The smallest such solution is the fundamental mode; it is a smooth and strictly decreasing function of v; it is invertible and defines v as a function of θ.

○ Higher modes start at $v_k > 0$, $k = 1, 2, \ldots$, and define θ as strictly decreasing functions of v.

The Implicit Function Theorem is also used in a related study by Novotný [1976] except his dispersion relation remains in its tangent form.

Following the definition of $\tilde{A}$, in expression (4.3), it is convenient to measure speed in units of β^u so that θ is used instead of v_ℓ. Thus, we define the dimensionless coefficient as

$$A := \frac{1}{Z}\frac{dZ}{d\theta}. \tag{4.6}$$

$Z(\theta)$, which appears in definition (4.6), is given by

$$Z(\theta) := \frac{\beta^u}{\omega}v(\theta), \tag{4.7}$$

and $v(\theta)$ is a mode defined by expression (4.5). Hence,

$$A = \frac{1}{v}\frac{dv}{d\theta} = \frac{1}{v}\frac{1}{\frac{d\theta}{dv}}, \qquad \text{where} \qquad \frac{d\theta}{dv} = -\frac{\frac{\partial F}{\partial v}}{\frac{\partial F}{\partial \theta}}. \tag{4.8}$$

To calculate and plot $A(\omega)$, given Z, we calculate $v = (\omega Z)/\beta^u$, given Z and ω, and numerically find the minimum solution, $\theta(v)$, for $F = 0$.

Calculating the partial derivatives and using

$$\sin\left(v\sqrt{1 - \frac{1}{\theta^2}}\right) = \frac{E\sqrt{\alpha^2 - \theta^2}\cos\left(v\sqrt{1 - \frac{1}{\theta^2}}\right)}{\sqrt{\theta^2 - 1}}, \tag{4.9}$$

from expression (4.5), we obtain

$$A = -\frac{1}{v}\frac{\left(\alpha^2 - 1\right)E\theta^3 + E^2v(\alpha^2 - \theta^2)^{3/2} + v\left(\theta^2 - 1\right)\sqrt{\alpha^2 - \theta^2}}{\theta\left(\theta^2 - 1\right)\sqrt{\alpha^2 - \theta^2}\left(\theta^2 - 1 + E^2(\alpha^2 - \theta^2)\right)}, \tag{4.10}$$

which is the relative dimensionless sensitivity coefficient.

In Figure 4.7, we examine the relationship between $|A|$ and ω for different layer thicknesses. In the left plot, which is the case of $Z = 100$ m, we graphically estimate from the plot a minimum $|A|$ at about $\omega_0 = 30$ s^{-1}. In the right plot, which is the case for $Z = 500$ m,
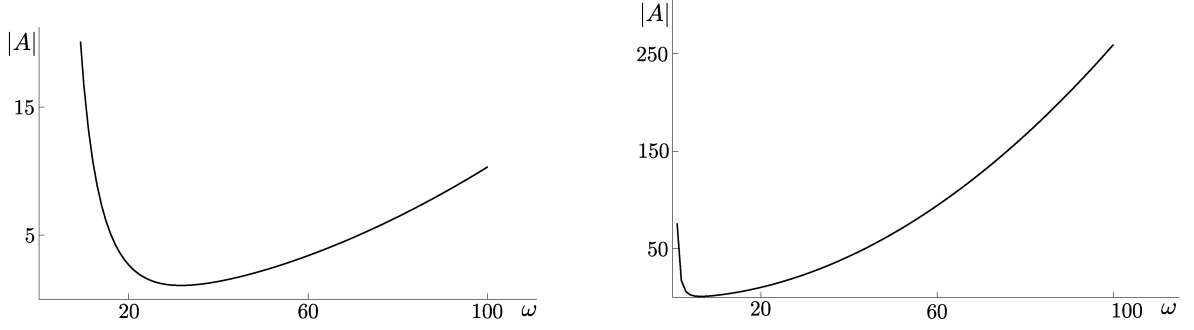
Figure 4.7: The absolute value of the relative dimensionless sensitivity coefficient, $|A|$, is plotted against ω, for $Z = 100$ m on the left, and for $Z = 500$ m on the right. Both plots begin at $\omega = 1\,\text{s}^{-1}$ due to the asymptote at $\omega = 0$. Due to the different vertical scales, the minimum $|A|$ on each plot is the same.

the same minimum $|A|$ occurs at about $\omega_0 = 7\ \text{s}^{-1}$.

We wish to calculate the minimal value of $|A|$ to find the frequency, ω_0, where the layer thickness, Z, is least sensitive to variations in speed. To find that value of $|A|$, we solve for $\text{d}A/\text{d}v = 0$ or, equivalently,

$$\frac{\text{d}}{\text{d}v}\left(\frac{1}{A}\right) = \frac{\text{d}}{\text{d}v}\left(v\frac{\text{d}\theta}{\text{d}v}\right) = \frac{\text{d}\theta}{\text{d}v} + v\frac{\text{d}^2\theta}{\text{d}v^2} = \theta' + v\theta'' = 0. \tag{4.11}$$

By differentiating $F(v, \theta(v)) = 0$ twice with respect to v, we get

$$\frac{\partial^2 F}{\partial v^2} + 2\frac{\partial^2 F}{\partial\theta\partial v}\theta' + \frac{\partial^2 F}{\partial\theta^2}(\theta')^2 + \frac{\partial F}{\partial\theta}\theta'' = 0,$$

where prime denotes derivative with respect to v. In this manner, $\theta' + v\theta'' = 0$ in expression (4.11) can be written in terms of F as

$$F_2(v, \theta) = -2\frac{\partial^2 F}{\partial\theta\partial v}\frac{\partial F}{\partial\theta} + \frac{1}{v}\left(\frac{\partial F}{\partial\theta}\right)^2 + \frac{\partial^2 F}{\partial\theta^2}\frac{\partial F}{\partial v} = 0, \tag{4.12}$$

where we use

$$\frac{\partial^2 F}{\partial v^2} = \frac{1 - \theta^2}{\theta^2}F = 0.$$

88
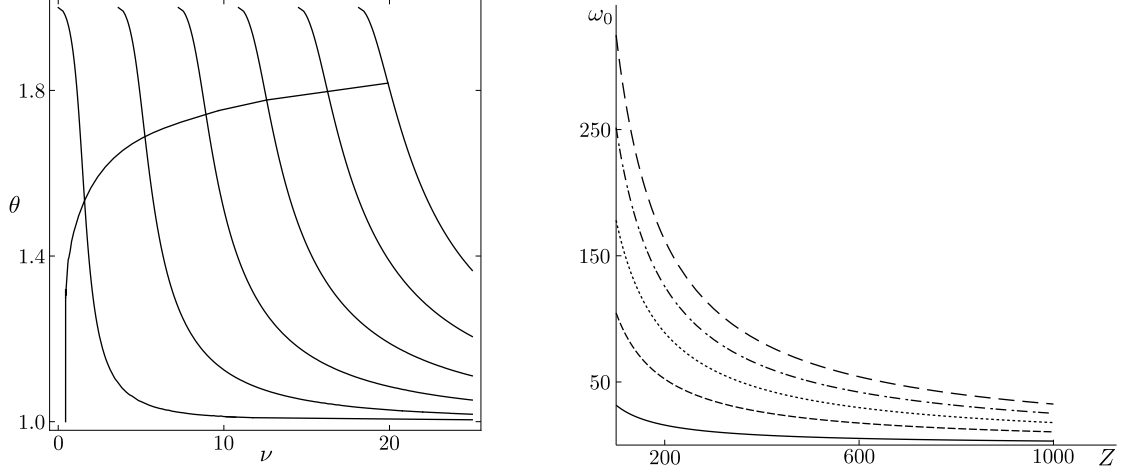
Figure 4.8: The left plot depicts intersecting zero contours of $F(\nu, \theta)$ and $F_2(\nu, \theta)$, where the curve ascending from $(0,1)$ is the zero contour of F_2. The right plot depicts the optimum frequency ω_0 plotted versus Z.

Evaluating the partial derivatives and using expression (4.9), we obtain

$$
\begin{aligned}
F_2(\nu, \theta) &= \frac{\cos^2\left(\frac{\nu\sqrt{\theta^2-1}}{\theta}\right)}{\theta^5\left(\theta^2-1\right)^2\left(\alpha^2-\theta^2\right)} \left\{ \frac{\theta\left(\left(\alpha^2-1\right)E\theta^3+E^2\nu(\alpha^2-\theta^2)^{3/2}+\nu\left(\theta^2-1\right)\sqrt{\alpha^2-\theta^2}\right)^2}{\nu} \right. \\
&+ \frac{1}{\sqrt{\alpha^2-\theta^2}}\left[\left(E^2(\alpha^2-\theta^2)+\theta^2-1\right)\left(\left(\theta^2-1\right)\left(\alpha^4 E\nu^2-\alpha^2\theta\left(\nu\left(\theta^2-2\right)\sqrt{\alpha^2-\theta^2}\right.\right.\right.\right. \\
&\quad\left.\left.+E\left(2\nu^2\theta-\theta^5+\theta^3\right)\right)+\nu\theta^3\left(\left(\theta^2-2\right)\sqrt{\alpha^2-\theta^2}+E\nu\theta\right)\right)-E(\alpha^2-\theta^2)^{3/2} \\
&\quad\left.\left.\times\left(\alpha^2 E\nu\left(3\theta^2-2\right)\theta+\sqrt{\alpha^2-\theta^2}\left(\nu^2\left(\theta^2-1\right)+\theta^4\right)-E\nu\theta^5\right)\right)\right] \\
&- \left[2\theta\left(E^2\left(\alpha^2-\theta^4\right)+\theta^4-1\right)\left(\alpha^4 E^2\nu+\alpha^2\left(E\theta^3\sqrt{\alpha^2-\theta^2}\right.\right.\right. \qquad\qquad (4.13) \\
&\quad\left.\left.\left.+\nu\left(-2E^2\theta^2+\theta^2-1\right)\right)+\theta^2\left(-E\theta\sqrt{\alpha^2-\theta^2}+\left(E^2-1\right)\nu\theta^2+\nu\right)\right)\right] \right\} = 0.
\end{aligned}
$$

Using the system of equations formed by expressions (4.5) and (4.13), we obtain ν_0 for which the absolute value of A is minimal for a given mode.

The intersection points of $F(\nu, \theta)$ and $F_2(\nu, \theta)$, on the left plot of Figure 4.8, correspond to solutions, (ν_0, θ_0), for the first six modes of A in expression (4.10). In view of the intrinsic nonlinearity, we estimate the coordinates of the intersection points and use them as starting points in a numerical search. The values of (ν_0, θ_0), for the first six modes, are

$(1.58172, 1.53806)$, $(5.23429, 1.68935)$, $(8.90672, 1.74515)$, $(12.5772, 1.7779)$, $(16.2443, 1.80044)$ and $(19.9085, 1.81731)$. Using the values in equation (4.10), we obtain values of $|A|_{\min}$ for the first six modes. They are 1.05, 0.555, 0.445, 0.392, 0.360 and 0.338, and are constant for all Z for a given mode. This is shown in Figure 4.7 for $|A|_{\min} = 1.05$ for both $Z = 100$ and $Z = 500$.

On the right plot of Figure 4.8, the relationship between the optimum frequency, ω_0, and Z for the first five modes, is illustrated, where the solid black line closest to the horizontal axis corresponds to the first mode. Using the definition of v from expression (4.4), we are able to compare values of ω_0 with those estimated in Figure 4.7. Using the fundamental mode, $v_0 = 1.58172$, we calculate, for $Z = 500$ a value of $\omega_0 = 6.33$, which compares favourably to $\omega_0 = 7$, which we estimated graphically from the right plot of Figure 4.7. For $Z = 100$, we obtain a value of $\omega_0 = 31.6$, which compares favourably to the $\omega_0 = 30$, which we estimated graphically from the left plot of Figure 4.7.

The study presented in this section, which gives the optimum frequency for measuring Z for a given mode for Love waves, could be repeated for other quantities, such as the elasticity parameters, holding Z fixed. A similar study might be performed for quasi-Rayleigh waves.

4.3 Quasi-Rayleigh waves

4.3.1 Material properties

To consider the quasi-Rayleigh wave within the model of material properties discussed in Section 4.2, we also need to specify C_{11}^u and C_{11}^d, which are the elasticity parameters for the layer and the halfspace that do not appear in the Love-wave equations. Hence, the corresponding P-wave propagation speeds are $\alpha^u = \sqrt{C_{11}^u / \rho^u}$ and $\alpha^d = \sqrt{C_{11}^d / \rho^d}$.

We invoke the wave number $\kappa = \omega / v_r$, where v_r is the propagation speed. Herein, this

speed corresponds to the quasi-Rayleigh wave. For a notational convenience, we let

$$
r^u := \sqrt{\frac{v_r^2}{(\alpha^u)^2} - 1}, \quad s^u := \sqrt{\frac{v_r^2}{(\beta^u)^2} - 1}, \quad r^d := \sqrt{1 - \frac{v_r^2}{(\alpha^d)^2}}, \quad s^d := \sqrt{1 - \frac{v_r^2}{(\beta^d)^2}}.
$$

(4.14)

Following a laborious process, shown in Appendix 4.A and Appendix 4.B, we obtain

the dispersion relation, which is expressed as the determinant of the coefficient matrix,

$$
D_r := \det[M_r] = 4C_{44}^u \det \begin{bmatrix} s^u X & s^u S \\ r^u T & r^u Y \end{bmatrix},
$$

(4.15)

where X, Y, S, T are

$$
X := \left[(s^u)^2 - 1 \right] \left[-(v_r^2 q + 2p)B' + 2pr^d \cos b' \right] + 2 \left[r^u (2p - v_r^2 \rho^d) \sin a' + r^d (2p + v_r^2 \rho^u) \cos a' \right],
$$

$$
Y := \left[(s^u)^2 - 1 \right] \left[(v_r^2 q + 2p)A' - 2ps^d \cos a' \right] + 2 \left[-s^d (2p + v_r^2 \rho^u) \cos b' - s^u (2p - v_r^2 \rho^d) \sin b' \right],
$$

$$
S := \left[(s^u)^2 - 1 \right] \left[-(v_r^2 \rho^u + 2p)s^d B' + (2p - v_r^2 \rho^d) \cos b' \right] + 2 \left[(2p + v_r^2 q) \cos a' + 2pr^u s^d \sin a' \right],
$$

$$
T := \left[(s^u)^2 - 1 \right] \left[r^d (v_r^2 \rho^u + 2p)A' - (2p - v_r^2 \rho^d) \cos a' \right] - 2 \left[(2p + v_r^2 q) \cos b' + 2s^u r^d p \sin b' \right],
$$

with q, p, a', b', A', B' given by

$$
q := \rho^u - \rho^d, \quad p := C_{44}^d - C_{44}^u, \quad a' := \kappa r^u Z, \quad b' := \kappa s^u Z,
$$

$$
A' := \begin{cases} \dfrac{\sin a'}{r^u} & r^u \neq 0 \\ \kappa Z & r^u = 0 \end{cases}, \quad B' := \begin{cases} \dfrac{\sin b'}{s^u} & s^u \neq 0 \\ \kappa Z & s^u = 0 \end{cases},
$$

where both A' and B' are real, regardless of whether or not r^u and s^u are real or imaginary.

In accordance with l'Hôpital's rule, both A' and B' are equal to κZ, for $r^u = 0$ and $s^u = 0$, in

the limit sense. From our calculations, we find that that X, Y, S, T are real, $D_r = 0$ for $s^u = 0$
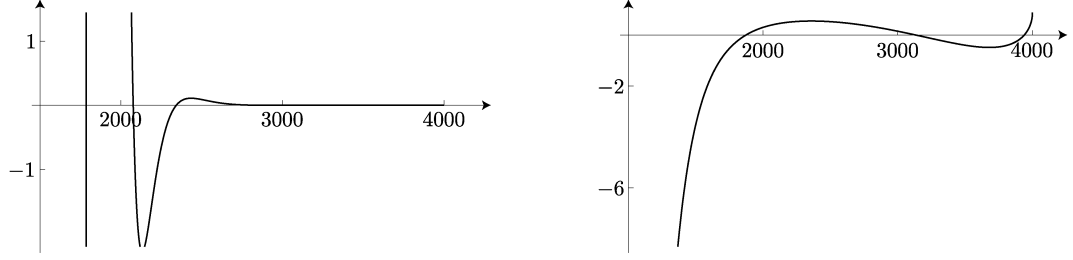
Figure 4.9: D_{r2}, defined in expression (4.17), as a function of speed v_r. On the left, for $\omega = 60\,\text{s}^{-1}$, there are seven roots: $v_r^1 = 1786\ \text{m/s}$, $v_r^2 = 2077\ \text{m/s}$, $v_r^3 = 2343\ \text{m/s}$, $v_r^4 = 2869\ \text{m/s}$, $v_r^5 = 3075\ \text{m/s}$, $v_r^6 = 3288\ \text{m/s}$ and $v_r^7 = 3705\ \text{m/s}$. On the right, for $\omega = 15\,\text{s}^{-1}$, there are three roots: $v_r^8 = 1869\ \text{m/s}$, $v_r^9 = 3143\ \text{m/s}$ and $v_r^{10} = 3937\ \text{m/s}$. The values on the vertical axes are to be multiplied by 10^{25} and 10^{22}, on the left and right plots, respectively.

or $r^u = 0$, and whether D_r is real or imaginary depends only on whether the product $s^u r^u$ is real or imaginary, which depends on the value of v_r. We express the latter dependence as

$$
D_r : \begin{cases} \text{Real} & \text{for} \quad v_r \in (0, \beta^u) \cup (\alpha^u, \beta^d) \\[2mm] \text{Imaginary} & \text{for} \quad v_r \in (\beta^u, \alpha^u) \end{cases}. \tag{4.16}
$$

Also, there are body-wave solutions for $r^u = 0$ and for $s^u = 0$, which means that $v_r = \alpha^u$, and $v_r = \beta^u$, respectively. However, from analyses of equations (4.35)–(4.38), (4.41) and (4.42), we conclude that their displacements are zero, and hence, these solutions are trivial.

To solve numerically for v_r, we let

$$
XY - ST =: D_{r2} = 0, \tag{4.17}
$$

where solutions exist for particular values of C_{11}^u, C_{44}^u, ρ^u, C_{11}^d, C_{44}^d, ρ^d, Z and ω. Note that arguments a, a', b, b' and expressions (4.14), for r^u, r^d, s^u, s^d, depend on v_r; the arguments also depend on $\kappa Z = \omega Z / v_r$. Since the matrix includes frequency dependent terms, the quasi-Rayleigh waves—like Love waves but unlike classical Rayleigh waves—

92
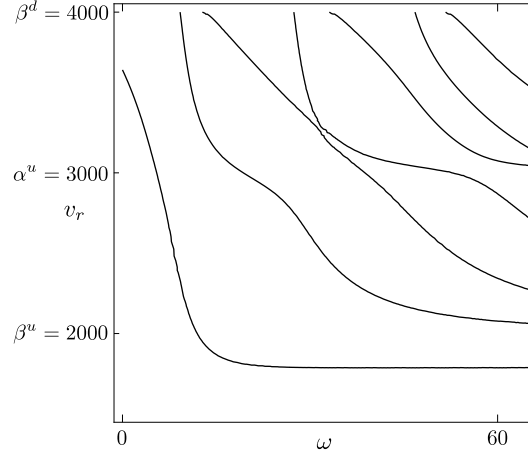
Figure 4.10: The quasi-Rayleigh-wave dispersion curves, $D_{r2} = 0$, defined in expression (4.17), as a function of speed, v_r, and frequency, ω

are dispersive.

Quasi-Rayleigh waves within the model discussed herein are reviewed by Udías [1999, Section 10.4] and Ben-Menahem and Singh [2000, Section 3.6.5]. Unlike Udías [1999], we do not restrict Poisson's ratio in the layer and in the halfspace to be $1/4$. Furthermore, in our formulation, we found six corrections to Udías's formulæ, which are stated in Appendix 4.C.4. Also, in a research paper, Fu [1946] makes certain simplifying assumptions prior to calculations, which we do not. Such an exact approach allows for the examination of details regarding the forward problem and sets the stage for a further investigation of the inverse problem.

In Figure 4.10, we plot the dispersion curves for expression (4.17), not for $D_r = 0$, to avoid the trivial solutions, $r^u = 0$ and $s^u = 0$. Also, in that manner, we avoid, for all frequencies, transitions between the real and imaginary domains, stated in expression (4.16).

The existence of Love waves requires $\beta^d > v_\ell > \beta^u$, and of quasi-Rayleigh waves, $\alpha^d > \beta^d > v_r$. However, concerning propagation speeds, Udías [1999] states that for the fundamental mode for high frequency, $v_r < \beta^u$, but for higher modes, $v_r > \beta^u$. Therefore, it is not necessary that $v_r > \beta^u$, except for higher modes. Furthermore, the fundamental mode

93

Figure 4.11: $D_{r2}/10^{19}$, defined in expression (4.17), as a function of the elasticity parameters, C_{44}^u and C_{44}^d, for $\omega = 5$ s^{-1} and $v_r = 3069$ m/s. The values on the horizontal and vertical axes are to be multiplied by 10^9 and 10^{10}, respectively. The sloping zero contour demonstrates sensitivity of the dispersion relation to both C_{44}^u and C_{44}^d.

appears at all frequencies whereas higher modes have cutoff frequencies below which they do not appear. If $v_r < \alpha^u$, then, from equations (4.22), (4.25) and (4.26), which are found in Appendix 4.A.2, there is a partially exponential variation in the layer as opposed to a purely sinusoidal variation. If $\alpha^u \geq \beta^d$, the determinant of the coefficient matrix, as defined in expression (4.15), is purely imaginary but there remains a solution for v_r in $D_r = 0$.

Let us examine, in an analogous manner to Figure 4.1, the numerical solutions of speed for the quasi-Rayleigh wave dispersion relation for high-frequency and low-frequency cases. Herein, unlike for the Love wave, we need to introduce $C_{11}^u = 1.98 \times 10^{10}$ N/m^2, which implies that $\alpha^u = 3000$ m/s, and $C_{11}^d = 10.985 \times 10^{10}$ N/m^2, which implies that $\alpha^d = 6500$ m/s.

We depict in Figure 4.9 the high-frequency case, where $\omega = 60$ s^{-1}, in the left plot and the low-frequency case, where $\omega = 15$ s^{-1}, in the right plot. Therein, we see that as ω or Z increases, the number of solutions for v_r increases. We observe that expression (4.15) is real or imaginary in the same manner as stated in expression (4.16). Yet, D_{r2}, defined in expression (4.17), is real for the entire range of v_r.
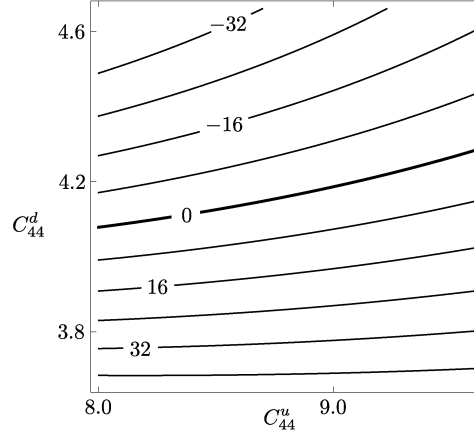
94

Figure 4.12: $D_{r2}/10^{20}$, defined in expression (4.17), as a function of the elasticity parameters, C_{44}^u and C_{44}^d, for $\omega = 60 \text{ s}^{-1}$ and $v_r^7 = 3705 \text{ m/s}$, on the left, and for $\omega = 15 \text{ s}^{-1}$ and $v_r^{10} = 3937 \text{ m/s}$, on the right. The values on the horizontal and vertical axes are to be multiplied by 10^9 and 10^{10}, respectively. The zero contour on the left plot indicates sensitivity to both C_{44}^u and C_{44}^d but the lower-frequency case, in the right plot, indicates more sensitivity to C_{44}^d than to C_{44}^u.

Consider the case of $v_r < \beta^u$ in Figure 4.10, where the fundamental mode still has a solution for v_r for higher frequencies, but the higher modes do not. For high frequency, the fundamental-mode speed asymptotically approaches the classical Rayleigh wave speed in the layer, which is $0.89\beta^u$. In the limit—as $\omega \to 0$—that fundamental mode—which unlike the higher modes has no low cutoff frequency—approaches the classical Rayleigh-wave speed in the halfspace, which is $0.91\beta^d$.

4.3.2   Sensitivity of dispersion relation

We wish to examine effects of elasticity parameters and layer thickness on the dispersion relation, for various frequencies and different modes. To do so, we examine effects of these quantities on the value of D_{r2}, defined in expression (4.17). Specifically, we examine D_{r2} as a function of C_{44}^d and C_{44}^u, for three distinct frequencies and for fixed values of v_r, which correspond to particular modes.

The contour maps of Figures 4.12, 4.13, 4.15 and 4.16 illustrate the sensitivity of the

95
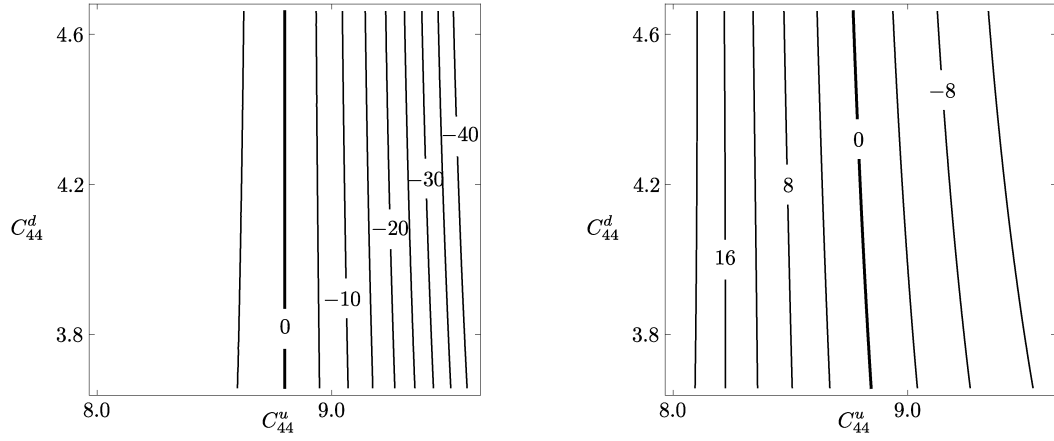
Figure 4.13: $D_{r2}/10^{27}$, on the left, and $D_{r2}/10^{20}$, on the right, defined in expression (4.17), as a function of the elasticity parameters, C_{44}^u and C_{44}^d, where $\omega = 60 \text{ s}^{-1}$ and $v_r^1 = 1786 \text{ m/s}$, and where $\omega = 15 \text{ s}^{-1}$ and $v_r^8 = 1869 \text{ m/s}$, for left and right, respectively. The values on the horizontal and vertical axes are to be multiplied by 10^9 and 10^{10}, respectively. The near vertical contours in both plots indicate sensitivity to C_{44}^u and little sensitivity to C_{44}^d.
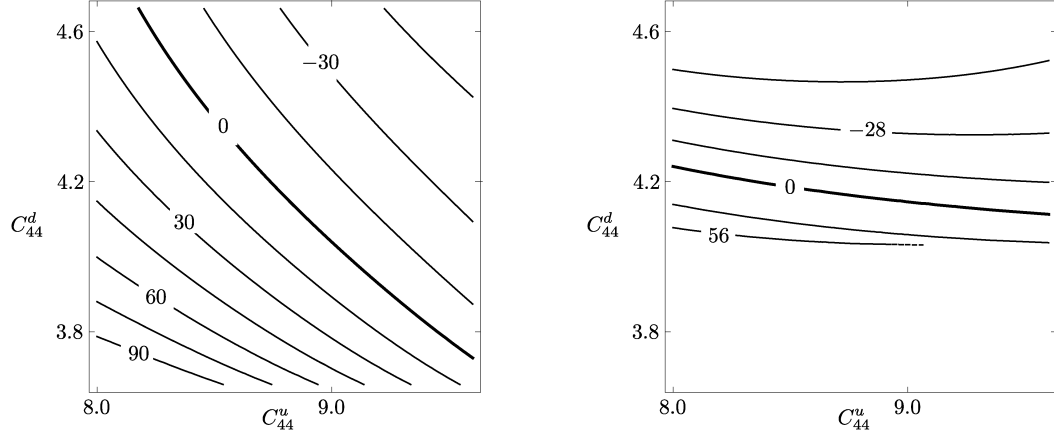

Figure 4.14: $D_{r2}/10^{20}$, defined in expression (4.17), as a function of the elasticity parameter, C_{44}^u, and layer thickness, Z, for $\omega = 5 \text{ s}^{-1}$ and $v_r = 3069 \text{ m/s}$. The values on the horizontal axis are to be multiplied by 10^9. The sloping zero contour indicate sensitivity to both C_{44}^u and Z.

dispersion relation by the slope of the zero contour line for quasi-Rayleigh waves. These plots, and their interpretation, are analogous to Figures 4.3–4.6.

Let us examine the numerical solutions for the quasi-Rayleigh wave dispersion relation for the high-frequency and low-frequency cases. We use these solutions to investigate the relative sensitivities of the quasi-Rayleigh wave to the elasticity parameter in the upper layer and in the lower halfspace, as well as to the elasticity parameter in the upper layer and to the layer thickness.

We begin by considering the layer and halfspace elasticity parameters. For the high-speed case, we consider the seventh root of the left plot of Figure 4.9, which is $v_r^7 = 3705$ m/s, and the third root of the right plot of Figure 4.9, which is $v_r^{10} = 3937$ m/s. The left and right plots of Figure 4.12 are the corresponding contour plots of $D_{r2}/10^{20}$ with varying C_{44}^u and C_{44}^d. In both cases, D_{r2} is sensitive to C_{44}^u and C_{44}^d. However, the right plot of Figure 4.12, which depicts a lower frequency and high speed, indicates a greater sensitivity to C_{44}^d.

Then, we consider Figure 4.11, which is the corresponding plot of $D_{r2}/10^{19}$, whose frequency and speed is lower than the right plot of Figure 4.12. In this case, we observe that the determinant is also sensitive to both C_{44}^u and C_{44}^d.

For the low-speed case, we observe different sensitivities. Let us examine the first root of the left plot of Figure 4.9, which is $v_r^1 = 1786$ m/s, and the first root of the right plot of Figure 4.9, which is $v_r^8 = 1869$ m/s. Following the corresponding plot of Figure 4.13, we see that there are near vertical zero lines. This indicates that there is a greater sensitivity to C_{44}^u but lower sensitivity to C_{44}^d for both frequencies.

Next, we consider the layer elasticity parameter and the layer thickness. Using the high-speed roots of expression (4.17), we observe sensitivity to both C_{44}^u and Z, in the high-frequency and low-frequency cases, which are depicted in Figure 4.15. Using low-speed roots in Figure 4.16, we observe sensitivity in the right plot to both C_{44}^u and Z. However, the

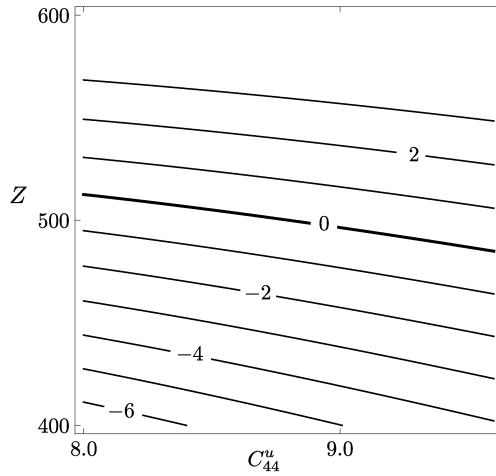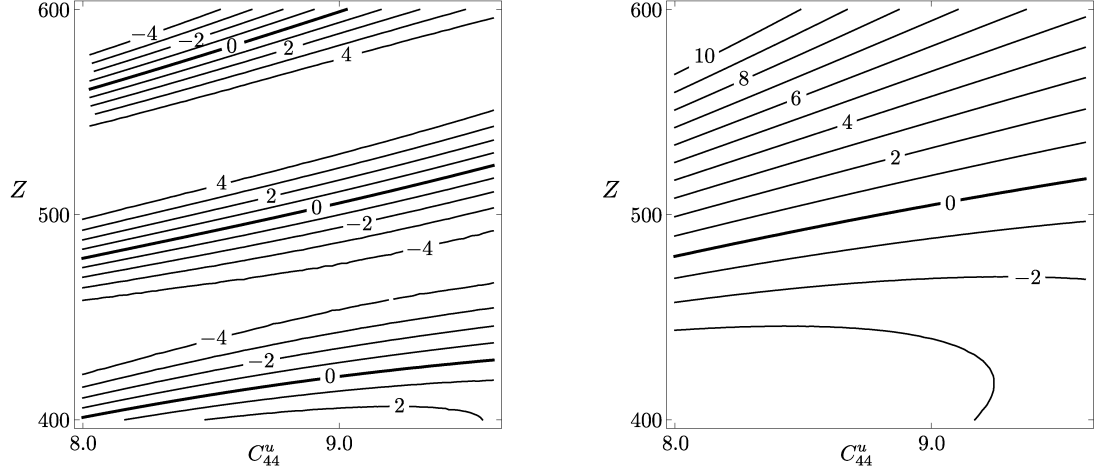Figure 4.15: $D_{r2}/10^{21}$, defined in expression (4.17), as a function of the elasticity parameters, C_{44}^u, and layer thickness, Z, for $\omega = 60$ s^{-1} and $v_r^7 = 3705$ m/s, on the left, and for $\omega = 15$ s^{-1} and $v_r^{10} = 3937$ m/s, on the right. The values on the horizontal axis is to be multiplied by 10^9. The sloping contours indicate sensitivity to both C_{44}^u and Z.

left plot of Figure 4.16 has no sensitivity to Z since, regardless of Z, the fundamental-mode speed is asymptotic to the quasi-Rayleigh wave speed in the layer for higher frequencies.

We consider Figure 4.14 as well, which is the corresponding plot of $D_{r2}/10^{20}$, whose frequency and speed is lower than the right plot of Figure 4.15. In this case, we observe that the determinant is sensitive to both C_{44}^u and C_{44}^d.

Additionally, Figure 4.15 is similar to Figure 4.5. The periodicity that shows up on the left plot of Figure 4.15 is due to the periodicity in D_{r2}. Furthermore, the left plot of Figure 4.16 is distinct from the left plot of Figure 4.6. The distinction is due to differences in asymptotic behaviour of the fundamental mode at high frequencies for the dispersion curves of Love and quasi-Rayleigh waves.
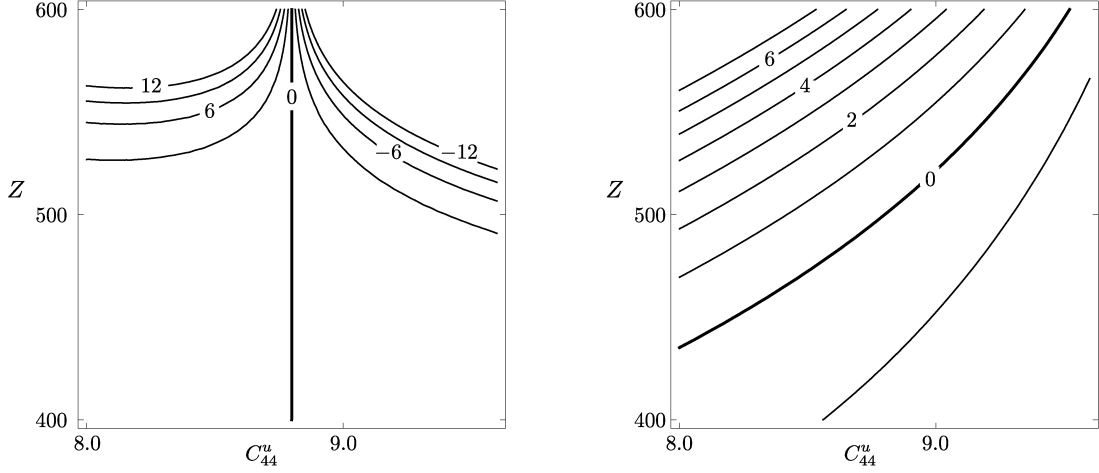
Figure 4.16: $D_{r2}/10^{28}$, on the left, and $D_{r2}/10^{21}$, defined in expression (4.17), on the right, as a function of the elasticity parameter, C_{44}^u, and layer thickness, Z, where $\omega = 60$ s^{-1} and $v_r^1 = 1786$ m/s, and where $\omega = 15$ s^{-1} and $v_r^8 = 1869$ m/s, for the left and right plots, respectively. The values on the horizontal axis is to be multiplied by 10^9. The sloping zero contour in the lower frequency plot indicates sensitivity to both C_{44}^u and Z while the vertical zero contour in the higher frequency plot indicates sensitivity to C_{44}^u but no sensitivity to Z.

4.4 Conclusions

4.4.1 Background examination

In this paper, we study the sensitivity of Love waves and quasi-Rayleigh waves to model parameters based on their exact dispersion relations. Both are guided waves in an elastic layer constrained by a vacuum and an elastic halfspace. According to presented computations, and as illustrated in Figures 4.2 and 4.10, the dispersion relations for the Love and quasi-Rayleigh waves imply that their speeds vary with frequency and differ from one another. Thus, their arrival times should be distinct on a seismic record, which—together with the fact that their polarizations are orthogonal to one other—makes them independent sources of information to infer model parameters.

The speeds of both Love and quasi-Rayleigh waves, whose roots are depicted in Figures 4.1 and 4.9, respectively, are obtained from their dispersion relations. In the high-

frequency case, the fundamental Love-wave mode has a speed that is slightly greater than the S-wave speed in the layer. In the low-frequency case, its speed is slightly lower than the S-wave speed in the halfspace. The highest-mode speeds of both the Love wave and the quasi-Rayleigh wave are smaller than the S-wave speed in the halfspace.

The dispersion curves for Love waves and quasi-Rayleigh waves are given in Figure 4.2 and Figure 4.10, respectively. In the latter figure—and in agreement with Figure 10.14 of Udías [1999]—the fundamental mode has all frequencies, which means that it has no cutoff frequency. For high frequency, the fundamental-mode speed asymptotically approaches the classical Rayleigh-wave speed in the layer, and—in the limit as $\omega \to 0$—that speed approaches the classical Rayleigh-wave speed in the halfspace.

We review the dispersion relation for Love waves and provide the details in appendices of the derivation of the dispersion relation for quasi-Rayleigh waves, including details of the expansion of the 6×6 matrix and its determinant. We compare our results to several past studies, including the one of Love [1911], which assumes incompressibility, and the one of Udías [1999], in which we found typos in the equations, though not in the dispersion-curve plots. Unlike Love [1911], who assumes incompressibility, Udías [1999], who assumes a Poisson's ratio of $1/4$, and Fu [1946], who studies limiting cases, we do not make any simplifying assumptions prior to calculations for the study of sensitivity.

In the case of quasi-Rayleigh waves, and in the context of the 6×6 determinant, we have shown that the solutions $r^u = 0$ and $s^u = 0$ have zero displacements, and hence, can be considered trivial solutions.

4.4.2 Sensitivity results

Our results demonstrate the sensitivity of the Love wave and quasi-Rayleigh wave dispersion relations to elasticity parameters and layer thickness. We conclude that the fundamental mode is mainly sensitive to the upper layer properties while higher modes are sensitive

to both the upper layer and lower halfspace properties. Within each mode the lower frequencies are more sensitive to the lower halfspace than are higher frequencies.

We do not consider sensitivity to C_{11} since we remain within the elasticity parameters common for both the Love and quasi-Rayleigh waves, nor do we examine the sensitivity to ρ. Sensitivities to C_{11} and ρ are obtainable by similar procedures. However, according to Lucena and Taioli [2014], the dispersion curves are sensitive to neither of them.

In the case of Love waves, we formulate and examine the absolute value of a dimensionless sensitivity coefficient given in terms of partial derivatives of the Love-wave dispersion relation with respect to dimensionless variables, v and θ. From these results, we perform an analysis to deduce the optimum frequency, ω_0, to obtain Z from a given mode.

Our results, in particular, Figures 4.2, 4.7, 4.8 and 4.10, allow us to infer data-acquisition information. This can be achieved by considering frequencies required to increase the number of modes. Using this information, we may calibrate sources and receivers to record different modes. For example, at $\omega = 30 \text{ s}^{-1}$, we can see two Love-wave modes and four quasi-Rayleigh-wave modes. That angular frequency would correspond to $f = 5$ Hz, which is low for exploration seismology, very low for geotechnical seismology, and very high for earthquake seismology.. In real data it is probably not possible to see four quasi-Rayleigh-wave modes.

4.5   Future work

Given dispersion relations of the Love and the quasi-Rayleigh waves, we expect to invert the measurements of speed for elasticity parameters and mass densities of both the layer and the halfspace, as well as for the layer thickness. Explicit expressions presented in this paper allow us to formulate the inverse problem and examine the sensitivity of its solution. In particular, the presence of two types of waves lends itself to the formulation of a joint

inversion, which exploits the redundancy of information, since both waves are described in terms of the same model parameters, and can be jointly inverted to obtain those parameters, which is studied in Chapter 5. The presented study of the Love and quasi-Rayleigh wave sensitivities allows us to gain an insight into their combination, which appears explicitly in such an inversion.

In further studies, we could formulate dispersion relations for the case of an anisotropic layer and an anisotropic halfspace. Such a formulation would require modified boundary conditions and equations of motion. Further insights into such issues are given by Babich and Kiselev [2014].

Acknowledgments

4.6   References

V. M. Babich and A. P. Kiselev. *Elastic waves: High-frequency theory (in Russian)*. BHV St. Petersburg, 2014.

A. Ben-Menahem and S. J. Singh. *Seismic waves and sources*. Dover, Mineola, N.Y., 2nd edition, 2000.

C. Y. Fu. Studies on seismic waves: II. Rayleigh waves in a superficial layer. *Geophysics*, 11(1):10–23, 1946.

A. W. Lee. The effect of geological structure upon microseismic disturbance. *Geophysical Journal International*, 3:85–105, 1932.

A. E. H. Love. *Some problems of geodynamics*. Cambridge University Press, 1911.

R. F. de Lucena and F. Taioli. Rayleigh wave modeling: A study of dispersion curve sensitivity and methodology for calculating an initial model to be included in an inversion algorithm. *Journal of Applied Geophysics*, 108:140–151, 2014.

O. Novotný. Methods of computing the partial derivatives of dispersion curves. *Pageoph*, 114:765–774, 1976.

M. A. Slawinski. *Waves and rays in seismology: Answers to unasked questions*. World Scientific, 2nd edition, 2018.

A. Udías. *Principles of seismology*. Cambridge University Press, 1999.

4.A   Formulation of quasi-Rayleigh waves

4.A.1   Material properties and wave equations

* Using the Helmholtz decomposition theorem, we express the displacements as

$$u^\mu = \nabla \mathscr{P}^\mu + \nabla \times \mathscr{S}^\mu, \quad u_1^\mu = \frac{\partial \mathscr{P}^\mu}{\partial x_1} - \frac{\partial \mathscr{S}^\mu}{\partial x_3}, \quad u_3^\mu = \frac{\partial \mathscr{P}^\mu}{\partial x_3} + \frac{\partial \mathscr{S}^\mu}{\partial x_1}, \quad u_2^\mu = 0, \ \mu = u,d,$$

(4.18)

---

*The formulation in this section is similar to that of Udías [1999, Section 10.4] except that we set x_3 to be positive downwards with the free surface at $x_3 = 0$ and interface at $x_3 = Z$, whereas Udías [1999] sets x_3 to be positive upwards with the free surface at $x_3 = H$ and interface at $x_3 = 0$. More importantly, unlike Udías [1999], we do not restrict Poisson's ratio in the layer and in the halfspace to $1/4$. Also we found some errors in Udías's equations.

where we use the gauge condition outlined in Slawinski [2018, Section 6.2] and set $\mathscr{S}_2^\mu = \mathscr{S}^\mu$, for brevity. $\mathscr{P}^\mu$ denotes the scalar potential and $\mathscr{S}^\mu = [\mathscr{S}_1^\mu, \mathscr{S}_2^\mu, \mathscr{S}_3^\mu]$ denotes the vector potential, which herein is $\mathscr{S}^\mu = [0, \mathscr{S}^\mu, 0]$. Potentials allow us to consider the coupling between the *P* and *SV* waves. The pertinent wave equations are

$$\nabla^2 \mathscr{P}^\mu - \frac{1}{(\alpha^\mu)^2} \frac{\partial^2 \mathscr{P}^\mu}{\partial t^2} = 0 \,, \quad \nabla^2 \mathscr{S}^\mu - \frac{1}{(\beta^\mu)^2} \frac{\partial^2 \mathscr{S}^\mu}{\partial t^2} = 0 \,, \quad \mu = u, d, \qquad (4.19)$$

which correspond to the *P* waves and *SV* waves, respectively.

4.A.2 Solutions of wave equations

Let the trial solutions for the corresponding wave equations be

$$\mathscr{P}^\mu = A^\mu(x_3) \exp(\iota(\kappa x_1 - \omega t)) \,, \quad \mu = u, d \,, \qquad (4.20)$$

$$\mathscr{S}^\mu = B^\mu(x_3) \exp(\iota(\kappa x_1 - \omega t)) \,, \quad \mu = u, d \,. \qquad (4.21)$$

Inserting solutions (4.20) and (4.21) into equations (4.19) leads to

$$\frac{d^2 A^\mu}{dx_3^2} + \left(\frac{\omega^2}{(\alpha^\mu)^2} - \kappa^2 \right) A^\mu = 0 \,, \quad \frac{d^2 B^\mu}{dx_3^2} + \left(\frac{\omega^2}{(\beta^\mu)^2} - \kappa^2 \right) B^\mu = 0 \,, \quad \mu = u, d \,,$$

which are ordinary differential equations for amplitudes A^μ and B^μ. Similarly to the derivation of Love waves, we require displacements to decay within the halfspace. Expressions (4.18), which denote displacements, entail

$$\kappa^2 - \omega^2/(\alpha^d)^2 > 0 \quad \text{and} \quad \kappa^2 - \omega^2/(\beta^d)^2 > 0 \,.$$

Thus, we obtain four general solutions, which we write as

$$A^u = C_1 \exp\left(-\iota \sqrt{\frac{\omega^2}{(\alpha^u)^2} - \kappa^2} x_3\right) + C_2 \exp\left(\iota \sqrt{\frac{\omega^2}{(\alpha^u)^2} - \kappa^2} x_3\right),\tag{4.22}$$

$$A^d = C_4 \exp\left(-\sqrt{\kappa^2 - \frac{\omega^2}{(\alpha^d)^2}} x_3\right),$$

$$B^u = D_1 \exp\left(-\iota \sqrt{\frac{\omega^2}{(\beta^u)^2} - \kappa^2} x_3\right) + D_2 \exp\left(\iota \sqrt{\frac{\omega^2}{(\beta^u)^2} - \kappa^2} x_3\right),$$

$$B^d = D_4 \exp\left(-\sqrt{\kappa^2 - \frac{\omega^2}{(\beta^d)^2}} x_3\right).$$

Our assumption about the behaviour of solutions in the halfspace forces r^d and s^d to be real. Thus, we write the nonzero components of the displacement vector as

$$\begin{aligned} u_1^d &= \frac{\partial \mathscr{P}^d}{\partial x_1} - \frac{\partial \mathscr{S}^d}{\partial x_3} \\ &= \left[\iota \kappa C_4 \exp\left(-\kappa r^d x_3\right) + D_4 \kappa s^d \exp\left(-\kappa s^d x_3\right)\right] \exp(\iota(\kappa x_1 - \omega t)), \end{aligned} \tag{4.23}$$

$$\begin{aligned} u_3^d &= \frac{\partial \mathscr{P}^d}{\partial x_3} + \frac{\partial \mathscr{S}^d}{\partial x_1} \\ &= \left[-C_4 \kappa r^d \exp\left(-\kappa r^d x_3\right) + \iota \kappa D_4 \exp\left(-\kappa s^d x_3\right)\right] \exp(\iota(\kappa x_1 - \omega t)), \end{aligned} \tag{4.24}$$

$$\begin{aligned} u_1^u &= \frac{\partial \mathscr{P}^u}{\partial x_1} - \frac{\partial \mathscr{S}^u}{\partial x_3} \\ &= [\iota \kappa C_1 \exp(-\iota \kappa r^u x_3) + \iota \kappa C_2 \exp(\iota \kappa r^u x_3) \\ &\qquad + \iota \kappa s^u D_1 \exp(-\iota \kappa s^u x_3) - \iota \kappa s^u D_2 \exp(\iota \kappa s^u x_3)] \exp(\iota(\kappa x_1 - \omega t)), \end{aligned} \tag{4.25}$$

105

$$u_3^u = \frac{\partial \mathscr{P}^u}{\partial x_3} + \frac{\partial \mathscr{S}^u}{\partial x_1} \tag{4.26}$$

$$= [-\iota \kappa r^u C_1 \exp(-\iota \kappa r^u x_3) + \iota \kappa r^u C_2 \exp(\iota \kappa r^u x_3)$$

$$+ \iota \kappa D_1 \exp(-\iota \kappa s^u x_3) + \iota \kappa D_2 \exp(\iota \kappa s^u x_3)] \exp(\iota (\kappa x_1 - \omega t)),$$

which allows us to apply the boundary conditions.

4.A.3   Boundary conditions

Let us examine expressions (4.23)–(4.26) in view of Hooke's law,

$$\sigma_{ij} = \lambda \delta_{ij} \sum_{k=1}^{3} \varepsilon_{kk} + 2\mu \varepsilon_{ij} = (C_{11} - 2C_{44}) \delta_{ij} \sum_{k=1}^{3} \frac{\partial u_k}{\partial x_k} + C_{44} \left(\frac{\partial u_i}{\partial x_j} + \frac{\partial u_j}{\partial x_i} \right), \tag{4.27}$$

and the boundary conditions at $x_3 = 0$, which are $\sigma_{33}^u = \sigma_{31}^u = 0$; hence, the first condition implies

$$\sigma_{31}^u \big|_{x_3=0} = 0 \Rightarrow \frac{\partial u_1^u}{\partial x_3} \bigg|_{x_3=0} = -\frac{\partial u_3^u}{\partial x_1} \bigg|_{x_3=0}.$$

Factoring out $\exp(\iota (\kappa x_1 - \omega t))$, we write

$$\kappa^2 r^u C_1 - \kappa^2 r^u C_2 + \kappa^2 (s^u)^2 D_1 + \kappa^2 (s^u)^2 D_2 = -\kappa^2 r^u C_1 + \kappa^2 r^u C_2 + \kappa^2 D_1 + \kappa^2 D_2,$$

which, upon rearranging and factoring out κ^2, we rewrite as

$$2r^u (C_1 - C_2) + [(s^u)^2 - 1](D_1 + D_2) = 0. \tag{4.28}$$

The second condition implies

$$\sigma_{33}^u \big|_{x_3=0} = 0 \Rightarrow \left[(C_{11}^u - 2C_{44}^u) \left(\frac{\partial u_1^u}{\partial x_1} + \frac{\partial u_3^u}{\partial x_3} \right) + 2C_{44}^u \left(\frac{\partial u_3^u}{\partial x_3} \right) \right] \bigg|_{x_3=0} = 0,$$

106

which can be rearranged to

$$\left[(C_{11}^u - 2C_{44}^u)\left(\frac{\partial u_1^u}{\partial x_1}\right) + C_{11}^u\left(\frac{\partial u_3^u}{\partial x_3}\right)\right]\Bigg|_{x_3=0} = 0,$$

and, upon factoring out $\kappa^2 \exp(\iota(\kappa x_1 - \omega t))$, further reduces to

$$(C_{11}^u - 2C_{44}^u)\left[-(C_1 + C_2) - s^u(D_1 - D_2)\right] + C_{11}^u\left[-(r^u)^2(C_1 + C_2) + s^u(D_1 - D_2)\right] = 0.$$

$$(4.29)$$

At $x_3 = Z$, the boundary conditions are

$$u_1^u|_{x_3=Z} = u_1^d|_{x_3=Z}, \quad u_3^u|_{x_3=Z} = u_3^d|_{x_3=Z},$$

$$\sigma_{33}^u|_{x_3=Z} = \sigma_{33}^d|_{x_3=Z}, \quad \sigma_{31}^u|_{x_3=Z} = \sigma_{31}^d|_{x_3=Z}.$$

Factoring out $\kappa \exp(\iota(\kappa x_1 - \omega t))$, the first condition becomes

$$\iota C_1 \exp(-\iota \kappa r^u Z) + \iota C_2 \exp(\iota \kappa r^u Z) + \iota s^u D_1 \exp(-\iota \kappa s^u Z) - \iota s^u D_2 \exp(\iota \kappa s^u Z)$$

$$= \iota C_4 \exp(-\kappa r^d Z) + s^d D_4 \exp(-\kappa s^d Z).$$

$$(4.30)$$

Similarly, the second condition implies

$$-\iota r^u C_1 \exp(-\iota \kappa r^u Z) + \iota r^u C_2 \exp(\iota \kappa r^u Z) + \iota D_1 \exp(-\iota \kappa s^u Z) + \iota D_2 \exp(\iota \kappa s^u Z)$$

$$= -r^d C_4 \exp(-\kappa r^d Z) + \iota D_4 \exp(-\kappa s^d Z).$$

$$(4.31)$$

The third condition,

$$\left[(C_{11}^u - 2C_{44}^u)\left(\frac{\partial u_1^u}{\partial x_1}\right) + C_{11}^u\left(\frac{\partial u_3^u}{\partial x_3}\right)\right]\Bigg|_{x_3=Z} = \left[(C_{11}^d - 2C_{44}^d)\left(\frac{\partial u_1^d}{\partial x_1}\right) + C_{11}^d\left(\frac{\partial u_3^d}{\partial x_3}\right)\right]\Bigg|_{x_3=Z},$$

upon factoring out $\kappa^2 \exp(\iota(\kappa x_1 - \omega t))$, becomes

$$(C_{11}^u - 2C_{44}^u)\left[-C_1 \exp(-\iota\kappa r^u Z) - C_2 \exp(\iota\kappa r^u Z) - s^u D_1 \exp(-\iota\kappa s^u Z) + s^u D_2 \exp(\iota\kappa s^u Z)\right]$$

$$+ C_{11}^u\left[-(r^u)^2 C_1 \exp(-\iota\kappa r^u Z) - (r^u)^2 C_2 \exp(\iota\kappa r^u Z) + s^u D_1 \exp(-\iota\kappa s^u Z) - s^u D_2 \exp(\iota\kappa s^u Z)\right]$$

$$= (C_{11}^d - 2C_{44}^d)\left[-C_4 \exp(-\kappa r^d Z) + \iota s^d D_4 \exp(-\kappa s^d Z)\right]$$

$$+ C_{11}^d\left[(r^d)^2 C_4 \exp(-\kappa r^d Z) - \iota s^d D_4 \exp(-\kappa s^d Z)\right].$$

The fourth condition,

$$C_{44}^u\left(\frac{\partial u_1^u}{\partial x_3} + \frac{\partial u_3^u}{\partial x_1}\right)\bigg|_{x_3=Z} = C_{44}^d\left(\frac{\partial u_1^d}{\partial x_3} + \frac{\partial u_3^d}{\partial x_1}\right)\bigg|_{x_3=Z},$$

implies

$$C_{44}^u\left[r^u C_1 \exp(-\iota\kappa r^u Z) - r^u C_2 \exp(\iota\kappa r^u Z) + (s^u)^2 D_1 \exp(-\iota\kappa s^u Z) + (s^u)^2 D_2 \exp(\iota\kappa s^u Z)\right.$$

$$+ r^u C_1 \exp(-\iota\kappa r^u Z) - r^u C_2 \exp(\iota\kappa r^u Z) - D_1 \exp(-\iota\kappa s^u Z) - D_2 \exp(\iota\kappa s^u Z)\big]$$

$$= C_{44}^d\left[-\iota r^d C_4 \exp(-\kappa r^d Z) - (s^d)^2 D_4 \exp(-\kappa s^d Z) - \iota r^d C_4 \exp(-\kappa r^d Z) - D_4 \exp(-\kappa s^d Z)\right].$$

(4.32)

For a notational convenience, we let

$$a' := \kappa r^u Z, a = \kappa r^d Z, C_1' := C_1 e^{-\iota a'}, C_2' := C_2 e^{\iota a'}, C_4' := C_4 e^{-a}, \qquad (4.33)$$

$$b' := \kappa s^u Z, b = \kappa s^d Z, D_1' := D_1 e^{-\iota b'}, D_2' := D_2 e^{\iota b'}, D_4' := D_4 e^{-b}. \qquad (4.34)$$

Thus, conditions (4.28) to (4.32) can be written as

$$2r^u e^{\iota a'} C_1' - 2r^u e^{-\iota a'} C_2' + [(s^u)^2 - 1] e^{\iota b'} D_1' + [(s^u)^2 - 1] e^{-\iota b'} D_2' = 0, \qquad (4.35)$$

108

$$[-(C_{11}^u - 2C_{44}^u) - C_{11}^u(r^u)^2]\,e^{\iota a'}C_1' + [-(C_{11}^u - 2C_{44}^u) - C_{11}^u(r^u)^2]\,e^{-\iota a'}C_2'$$

$$+ 2C_{44}^u s^u\,e^{\iota b'}D_1' - 2C_{44}^u s^u\,e^{-\iota b'}D_2' = 0\,, \tag{4.36}$$

$$\iota C_1' + \iota C_2' + \iota s^u D_1' - \iota s^u D_2' - \iota C_4' - s^d D_4' = 0\,, \tag{4.37}$$

$$-\iota r^u C_1' + \iota r^u C_2' + \iota D_1' + \iota D_2' + r^d C_4' - \iota D_4' = 0\,, \tag{4.38}$$

$$-(C_{11}^u - 2C_{44}^u)C_1' - (C_{11}^u - 2C_{44}^u)C_2' - (C_{11}^u - 2C_{44}^u)s^u D_1' + (C_{11}^u - 2C_{44}^u)s^u D_2'$$

$$- C_{11}^u(r^u)^2 C_1' - C_{11}^u(r^u)^2 C_2' + C_{11}^u s^u D_1' - C_{11}^u s^u D_2' + (C_{11}^d - 2C_{44}^d)C_4'$$

$$- \iota(C_{11}^d - 2C_{44}^d)s^d D_4' - C_{11}^d(r^d)^2 C_4' + \iota C_{11}^d s^d D_4' = 0\,, \tag{4.39}$$

$$C_{44}^u r^u C_1' - C_{44}^u r^u C_2' + C_{44}^u(s^u)^2 D_1' + C_{44}^u(s^u)^2 D_2' + C_{44}^u r^u C_1' - C_{44}^u r^u C_2' - C_{44}^u D_1' - C_{44}^u D_2'$$

$$+ \iota r^d C_{44}^d C_4' + C_{44}^d(s^d)^2 D_4' + \iota r^d C_{44}^d C_4' + C_{44}^d D_4' = 0\,. \tag{4.40}$$

Simplifying, we write conditions (4.39) and (4.40) as

$$-[C_{11}^u - 2C_{44}^u + (r^u)^2 C_{11}^u]C_1' - [C_{11}^u - 2C_{44}^u + (r^u)^2 C_{11}^u]C_2' + 2C_{44}^u s^u D_1' - 2C_{44}^u s^u D_2'$$

$$+ [C_{11}^d - 2C_{44}^d - (r^d)^2 C_{11}^d]C_4' + 2\iota s^d C_{44}^d D_4' = 0\,, \tag{4.41}$$

$$2C_{44}^u r^u C_1' - 2C_{44}^u r^u C_2' + C_{44}^u[(s^u)^2 - 1]D_1' + C_{44}^u[(s^u)^2 - 1]D_2'$$

$$+ 2\iota r^d C_{44}^d C_4' + C_{44}^d[(s^d)^2 + 1]D_4' = 0\,. \tag{4.42}$$

109

4.A.4 Dispersion relation

The six boundary conditions stated in equations (4.35), (4.36), (4.37), (4.38), (4.41) and (4.42) form a linear system of six equations for six unknowns, C_1', C_2', D_1', D_2', C_4' and D_4'. For a nontrivial solution, the determinant of the coefficient matrix, M_r, must be zero. Upon factoring ι from the third and fourth rows, we write

$$
M_r =
\begin{bmatrix}
2r^u e^{\iota a'} & -2r^u e^{-\iota a'} & \dfrac{v_r^2 \rho^u - 2C_{44}^u}{C_{44}^u} e^{\iota b'} \\[2mm]
\left[2C_{44}^u - \rho^u v_r^2\right] e^{\iota a'} & \left[2C_{44}^u - \rho^u v_r^2\right] e^{-\iota a'} & 2C_{44}^u s^u e^{\iota b'} \\[2mm]
1 & 1 & s^u \\[2mm]
-r^u & r^u & 1 \\[2mm]
2C_{44}^u - \rho^u v_r^2 & 2C_{44}^u - \rho^u v_r^2 & 2C_{44}^u s^u \\[2mm]
2C_{44}^u r^u & -2C_{44}^u r^u & v_r^2 \rho^u - 2C_{44}^u
\end{bmatrix}
$$

$$
\left.
\begin{matrix}
\dfrac{v_r^2 \rho^u - 2C_{44}^u}{C_{44}^u} e^{-\iota b'} & 0 & 0 \\[2mm]
-2C_{44}^u s^u e^{-\iota b'} & 0 & 0 \\[2mm]
-s^u & -1 & \iota s^d \\[2mm]
1 & -\iota r^d & -1 \\[2mm]
-2C_{44}^u s^u & v_r^2 \rho^d - 2C_{44}^d & 2\iota C_{44}^d s^d \\[2mm]
v_r^2 \rho^u - 2C_{44}^u & 2\iota C_{44}^d r^d & 2C_{44}^d - v_r^2 \rho^d
\end{matrix}
\right], \quad (4.43)
$$

where we use

$$
C_{11}^u \left((r^u)^2 + 1\right) = C_{11}^u \frac{v_r^2}{(\alpha^u)^2} = \rho^u v_r^2, \quad (s^u)^2 - 1 = \frac{v_r^2 \rho^u - 2C_{44}^u}{C_{44}^u},
$$

$$
C_{11}^d \left(1 - (r^d)^2\right) - 2C_{44}^d = v_r^2 \rho^d - 2C_{44}^d, \quad C_{44}^d \left((s^d)^2 + 1\right) = 2C_{44}^d - v_r^2 \rho^d.
$$

4.B   Details of dispersion relation derivation

In this appendix, for the reader's convenience, we present operations to compute the determinant of the 6×6 matrix stated in expression (4.43). We invoke several algebraic properties that allow us to obtain a 2×2 matrix. In this process, we use the following notational abbreviations.

- $C1, \ldots, C6$ denotes columns $1, \ldots, 6$

- $R1, \ldots, R6$ denotes rows $1, \ldots, 6$

- $C1 \mapsto C1 + C2$ denotes replacement of $C1$ by $C1 + C2$, etc.

- $A' := \sin a'/r^u$

- $B' := \sin b'/s^u$

- $u_\beta := v_r/\beta^u$

Using this notation, we perform the the following sequence of operations.

1. Factor out $1/C_{44}^u$ from $R1$

2. $C1 \mapsto C1 - C2$

3. Factor out 2 from $C1$

4. $C2 \mapsto C2 + C1$

5. $C3 \mapsto C3 - C4$

6. Factor out 2 from $C3$

7. $C4 \mapsto C3 + C4$

8. Factor out r^u from $C1$ and s^u from $C3$

9. $C2 \mapsto C2 - C3$

10. $C4 \mapsto C4 + C1$

11. $R6 \mapsto R6 - 2C_{44}^u R4$

12. $R5 \mapsto R5 - 2C_{44}^u R3$

13. Factor out $\imath$ from $C2, C3, C5$

14. Factor out $-\imath$ from $R3, R2, R5$

15. Factor out C_{44}^u from $R1$ and $R2$

16. Move $C3$ to the first column and shift the former first column and second column to the right; in other words, let $C1' = C1$, $C2' = C2$, $C1 \mapsto C3$, $C2 \mapsto C1'$, $C3 \mapsto C2'$.

112

$$\det[M_r] = 4r^u s^u C_{44}^u \det \begin{bmatrix} ((u_\beta)^2-2)B' & 2\cos a' & 2(r^u)^2A'-((u_\beta)^2-2)B' \\ 2\cos b' & ((u_\beta)^2-2)A' & -2\cos b'-((u_\beta)^2-2)\cos a' \\ 1 & 0 & 0 \\ 0 & -1 & 0 \\ 0 & 0 & -v_r^2\rho^u \\ 0 & 0 & 0 \end{bmatrix}$$

$$\begin{bmatrix} ((u_\beta)^2-2)\cos b'+2\cos a' & 0 & 0 \\ ((u_\beta)^2-2)A'-2(s^u)^2B' & 0 & 0 \\ 0 & -1 & -s^d \\ 0 & -r^d & -1 \\ 0 & v_r^2\rho^d-2(C_{44}^d-C_{44}^u) & -2s^d(C_{44}^d-C_{44}^u) \\ v_r^2\rho^u & 2r^d(C_{44}^d-C_{44}^u) & 2(C_{44}^d-C_{44}^u)-v_r^2\rho^d \end{bmatrix}.$$

Let us write the above matrix in the block form,

$$\begin{bmatrix} B & 0 \\ A & C \end{bmatrix},$$

where

$$B := \begin{bmatrix} ((u_\beta)^2-2)B' & 2\cos a' & 2(r^u)^2A'-((u_\beta)^2-2)B' & ((u_\beta)^2-2)\cos b'+2\cos a' \\ 2\cos b' & ((u_\beta)^2-2)A' & -2\cos b'-((u_\beta)^2-2)\cos a' & ((u_\beta)^2-2)A'-2(s^u)^2B' \end{bmatrix},$$

$$A := \begin{bmatrix} 1 & 0 & 0 & 0 \\ 0 & -1 & 0 & 0 \\ 0 & 0 & -v_r^2\rho^u & 0 \\ 0 & 0 & 0 & v_r^2\rho^u \end{bmatrix}, \quad C := \begin{bmatrix} -1 & -s^d \\ -r^d & -1 \\ v_r^2\rho^d-2(C_{44}^d-C_{44}^u) & -2s^d(C_{44}^d-C_{44}^u) \\ 2r^d(C_{44}^d-C_{44}^u) & 2(C_{44}^d-C_{44}^u)-v_r^2\rho^d \end{bmatrix}.$$

Since A is invertible, we have

$$
\begin{bmatrix} B & 0 \\ A & C \end{bmatrix} = \begin{bmatrix} 0 & I_2 \\ I_4 & 0 \end{bmatrix} \begin{bmatrix} A & C \\ B & 0 \end{bmatrix} = \begin{bmatrix} 0 & I_2 \\ I_4 & 0 \end{bmatrix} \begin{bmatrix} A & 0 \\ 0 & I_2 \end{bmatrix} \begin{bmatrix} I_4 & 0 \\ B & -I_2 \end{bmatrix} \begin{bmatrix} I_4 & A^{-1}C \\ 0 & BA^{-1}C \end{bmatrix},
$$

and, hence,

$$
\det \begin{bmatrix} B & 0 \\ A & C \end{bmatrix} = \det[A]\det[BA^{-1}C] \det \begin{bmatrix} 0 & I_2 \\ I_4 & 0 \end{bmatrix} \det \begin{bmatrix} I_4 & 0 \\ B & -I_2 \end{bmatrix} = \det[A]\det[BA^{-1}C].
$$

Finally, we can write the determinant of the coefficient matrix as

$$
\det[M_r] = 4r^u s^u C_{44}^u (XY - ST) = 4C_{44}^u \det \begin{bmatrix} s^u X & s^u S \\ r^u T & r^u Y \end{bmatrix},
$$

where X, Y, S, T are given after equation (4.15).

4.C   Comparison to results in literature

In this appendix, we present the notational translations for the quasi-Rayleigh waves in the literature, and compare differences found among them. Herein, for convenience, we use definitions (4.33) and (4.34).

Love [1911] considered the same problem but with the assumption of incompressibility. Lee [1932], Fu [1946] and Udías [1999] considered the same problem without the assumption of incompressibility but made other simplifying assumptions.

4.C.1 Comparison with Love [1911]

Love [1911] simplifies his formulation by assuming incompressibility, which implies that $\alpha^u \to \infty$ and $\alpha^d \to \infty$. As a consequence, $r^u = \iota$ and $r^d = 1$. It follows that

$$\cos(a') = \cos(\kappa r^u Z) = \cos(\iota \kappa Z) = \cosh(\kappa Z),$$

$$\sin(a') = \sin(\kappa r^u Z) = \sin(\iota \kappa Z) = \iota \sinh(\kappa Z),$$

$$\cosh(\iota \kappa s^u Z) = \cosh(\iota b') = \cos(b'),$$

$$\sinh(\iota \kappa s^u Z) = \sinh(\iota b') = \iota \sin(b').$$

Consequently, his

$$\xi \eta' - \xi' \eta = 0$$

becomes

$$\frac{\iota s^u}{(C_{44}^u)^2}(XY - ST) = \frac{\iota s^u}{(C_{44}^u)^2}(\mathrm{D}_{r2}) = \frac{\iota \,\mathrm{D}_r}{4(C_{44}^u)^3 \, r^u} = 0,$$

in our notation, where D_r is defined by expression (4.15). Under the assumption of incompressibility, r^u becomes ι, and thus

$$\xi \eta' - \xi' \eta = \frac{\mathrm{D}_r}{4(C_{44}^u)^3} \,.$$

4.C.2 Comparison with Lee [1932]

Lee [1932] obtains a determinantal equation in terms of trigonometric functions. In our notation, his determinantal equation,

$$\xi \eta' - \xi' \eta = 0,$$

becomes

$$\frac{XY - ST}{(C^u_{44})^2} = \frac{\mathrm{D}_{r2}}{(C^u_{44})^2} = \frac{\mathrm{D}_r}{4 r^u s^u (C^u_{44})^3} = 0 \,.$$

In other words, our expressions differ by a multiplicative factor.

4.C.3   Comparison with Fu [1946]

Fu [1946] obtains a determinantal equation in terms of hyperbolic functions. Invoking standard expressions,

$$\cosh(\iota a') = \cos(a'), \quad \cosh(\iota b') = \cos(b'), \quad \sinh(\iota a') = \iota \sin(a'), \quad \sinh(\iota b') = \iota \sin(b') \,,$$

we write his determinantal equation,

$$\zeta \eta' - \zeta' \eta = 0 \,,$$

as

$$(XY - ST) \, \kappa^8 = \mathrm{D}_{r2} \, \kappa^8 = \frac{\kappa^8 \, \mathrm{D}_r}{4 \, C^u_{44} \, r^u \, s^u} = 0 \,,$$

in our notation.

4.C.4   Comparison with Udías [1999]

Referring to Udías [1999], his determinantal equation,

$$\xi \eta' - \xi' \eta = 0 \,,$$

becomes

$$\frac{XY - ST}{(C^u_{44})^2} = \frac{\mathrm{D}_{r2}}{(C^u_{44})^2} = \frac{\mathrm{D}_r}{4 \, (C^u_{44})^3 \, r^u \, s^u} = 0 \,,$$

116

where we use the following six corrections to Udías's formulæ.

1. The second term of formula (10.87), $Zr' \sin a'$, should be $(Z/r') \sin a'$.

2. In the third term of formula (10.87), $\sin a'$ should be $\sin b'$.

3. In the fourth term of formula (10.86), $\sin b'$ should be $\cos b'$.

4. The $(\beta')^2$ in the first denominator of formula (10.92) should be β^2.

5. Instead of r and s, Udías [1999] should have $\bar{r}$ and $\bar{s}$, which are the magnitudes of r and s.

6. Our determinant, with the above corrections to Udías [1999], is $4(C_{44}^u)^3 r^u s^u$ times his formula (10.85); thus, formula (10.85) does not include solutions $r^u = 0$ and $s^u = 0$. However, as we discuss in Section 4.3, those solutions exhibit zero displacements, which might be the reason why Lee [1932], Fu [1946], Udías [1999] and Ben-Menahem and Singh [2000, Section 3.6.5] omit them.

4.C.5 Comparison with Ben-Menahem and Singh [2000]

Translation of the notation of Ben-Menahem and Singh [2000, Section 3.6.5] into our notation results in

$$\Delta_R = \frac{-\kappa^8}{(C_{44}^u)^2}(XY - ST) = \frac{-\kappa^8 D_{r2}}{(C_{44}^u)^2} = \frac{-\kappa^8 D_r}{4(C_{44}^u)^3 r^u s^u} = 0. \tag{4.44}$$

Chapter 5

On Pareto Joint Inversion of guided waves*

Abstract

We use the Pareto Joint Inversion, together with the Particle Swarm Optimization, to invert Love and quasi-Rayleigh surface-wave speeds, obtained from dispersion curves, to infer the elasticity parameters, mass densities and layer thickness of the model for which these curves are generated. For both waves, we use the dispersion relations derived by Dalton et al. [2017]. All computations are done for three angular frequencies, 15, 60 and 100 s^{-1}, and for two, five and seven modes, respectively. Results for all these frequencies are similar so detailed results and their discussion are presented for 15 s^{-1} and 60 s^{-1} selected solutions as representative examples. Comparisons of the model parameters with the values inverted with error-free input indicate an accurate process with potential for practical application. If, however, we introduce a constant error to the input, the results become significantly less

---

accurate, which indicates that the inverse operation is error-sensitive. The results suggest that the layer parameters are more sensitive to input errors than the halfspace parameters. In agreement with Dalton et al. [2017], the fundamental mode is mainly sensitive to the layer parameters whereas higher modes are sensitive to both the layer and halfspace properties; for the second mode, the results for the halfspace are more accurate for low frequencies. Additionally, strong correlations are observed between the inverted elasticity parameters for the layer.

Keywords

Pareto Joint Inversion, Particle Swarm Optimization, guided waves, surface waves

5.1   Introduction

Two types of guided waves can propagate in an elastic layer overlying an elastic halfspace (e.g., Dalton et al. [2017]). At the surface, though the displacements for both waves are parallel to the surface, the displacement of one of them is perpendicular to the direction of propagation and, for the other, parallel to that direction. The former is called the Love wave and the latter the quasi-Rayleigh wave, where the prefix distinguishes it from the Rayleigh wave that exists in the halfspace alone and, in contrast to its guided counterpart, is not dispersive. The orthogonal polarization of the displacement vectors on the surface allows us to identify each wave and to distinguish between them. We can use the propagation speeds of Love and quasi-Rayleigh waves on the surface to infer information about the model in which they propagate. To do so, we use the Pareto Joint Inversion.

5.2 Previous work

There are several important contributions to inversion of dispersion relations of guided waves for model parameters. Let us comment on ones with a particular relevance to our work.

A common technique to obtain quasi-Rayleigh-wave dispersion curves is the Multichannel Analysis of Surface Waves technique [Park et al., 1999]. An approach to inverting such curves for multiple layers is given in Xia et al. [1999], who use the Levenberg-Marquardt and singular-value decomposition techniques to analyze the Jacobian matrix of the model with respect to the *S*-wave velocity, and demonstrate sensitivity of material properties to the dispersion curve.

Wathelet et al. [2004] use a neighbourhood algorithm, which is a stochastic direct-search technique, to invert quasi-Rayleigh-wave dispersion curves obtained from ambient vibration measurements. Lu et al. [2007] invert quasi-Rayleigh waves in the presence of a low-velocity layer, using a genetic algorithm. Boxberger et al. [2011] perform a joint inversion, based on a genetic algorithm, using quasi-Rayleigh and Love wave dispersion curves and Horizontal-to-Vertical Spectral Ratio curves obtained from seismic noise array measurements. Fang et al. [2015] invert dispersion data without generating phase or group velocity maps, using raytracing and a tomographic inversion. Xie and Liu [2015] do Love-wave inversion for a near-surface transversely isotropic structure, using the Very Fast Simulated Annealing algorithm.

Wang et al. [2015] use phase velocity inversion, based on first-order perturbation theory, including multiple modes and both quasi-Rayleigh and Love waves, to examine intrinsic versus extrinsic radial anisotropy in the Earth; the latter anisotropy refers to a homogenized model. Wang et al. [2015] use the classical iterative quasi-Newton method to minimize the L_2 norm misfit and introduce the Generalized Minimal Residual Method.

Dal Moro and Ferigo [2011] carry out a Pareto Joint Inversion of synthetic quasi-Rayleigh and Love-wave dispersion curves for a multiple-layer model using an evolutionary algorithm optimization scheme. Dal Moro [2010] examines a Pareto Joint Inversion using an evolutionary algorithm of the combined quasi-Rayleigh and Love wave dispersion curves and Horizontal-to-Vertical Spectral Ratio data. Dal Moro et al. [2015] perform a three-target Pareto Joint Inversion based on full velocity spectra, using an evolutionary algorithm optimization scheme.

Unlike Dal Moro and his colleagues, we use Particle Swarm Optimization instead of an evolutionary algorithm.

5.3   Dispersion relations

To derive dispersion relations, Dalton et al. [2017] consider an elastic layer of thickness Z overlying an elastic halfspace. Using Cartesian coordinates, we set the surface at $x_3 = 0$, and the interface at $x_3 = Z$, with the x_3-axis positive downward. The layer consists of mass density, ρ^u, and elasticity parameters, C_{11}^u and C_{44}^u. The same quantities of the halfspace are denoted with superscript d. These quantities can be expressed in terms of the P and S wave speeds,

$$\alpha^{(\cdot)} = \sqrt{\frac{C_{11}^{(\cdot)}}{\rho^{(\cdot)}}}, \qquad \beta^{(\cdot)} = \sqrt{\frac{C_{44}^{(\cdot)}}{\rho^{(\cdot)}}}.$$

For the Love wave, the dispersion relation is

$$D_\ell(v_\ell) = \det \begin{bmatrix} e^{\imath b_\ell'} & -e^{-\imath b_\ell'} & 0 \\ -\imath s_\ell^u C_{44}^u & \imath s_\ell^u C_{44}^u & s_\ell^d C_{44}^d \\ 1 & 1 & -1 \end{bmatrix} = 2s_\ell^u C_{44}^u \sin b_\ell' - 2s_\ell^d C_{44}^d \cos b_\ell' = 0, \quad (5.1)$$

where

$$\kappa_\ell = \omega/v_\ell, \quad s_\ell^u = \sqrt{\frac{v_\ell^2}{(\beta^u)^2} - 1}, \quad s_\ell^d = \sqrt{1 - \frac{v_\ell^2}{(\beta^d)^2}}, \quad b_\ell' = \kappa_\ell s_\ell^u Z.$$

This equation has real solutions, v_ℓ, for $\beta^u < v_\ell < \beta^d$, which are referred to as modes; each solution can be represented by a dispersion curve of v_ℓ plotted against ω, along which D_ℓ is zero. The solution with the lowest value of v_ℓ, for a given ω, is called the fundamental mode.

Formally, the dispersion relation for the quasi-Rayleigh wave is given in terms of the determinant of a 6×6 matrix, which, as shown by Dalton et al. [2017], can be reduced to the determinant of a 2×2 matrix,

$$D_r(v_r) = 4C_{44}^u \det \begin{bmatrix} s^u X & s^u S \\ r^u T & r^u Y \end{bmatrix} = 4C_{44}^u r^u s^u (XY - ST) =: 4C_{44}^u r^u s^u D_{r2}, \tag{5.2}$$

where the entries of D_{r2} are

$$X := \left[(s^u)^2) - 1\right] \left[-(v_r^2 q + 2p)B' + 2pr^d \cos b'\right] + 2\left[r^u(2p - v_r^2 \rho^d) \sin a' + r^d(2p + v_r^2 \rho^u) \cos a'\right],$$

$$Y := \left[(s^u)^2) - 1\right] \left[(v_r^2 q + 2p)A' - 2ps^d \cos a'\right] + 2\left[-s^d(2p + v_r^2 \rho^u) \cos b' - s^u(2p - v_r^2 \rho^d) \sin b'\right],$$

$$S := \left[(s^u)^2) - 1\right] \left[-(v_r^2 \rho^u + 2p)s^d B' + (2p - v_r^2 \rho^d) \cos b'\right] + 2\left[(2p + v_r^2 q) \cos a' + 2pr^u s^d \sin a'\right],$$

$$T := \left[(s^u)^2) - 1\right] \left[r^d(v_r^2 \rho^u + 2p)A' - (2p - v_r^2 \rho^d) \cos a'\right] - 2\left[(2p + v_r^2 q) \cos b' + 2s^u r^d p \sin b'\right],$$

with $\kappa, q, p, A', B', r^u, s^u, r^d, s^d, a', b', a, b$, given by $\kappa = \omega/v_r$, $q := \rho^u - \rho^d$, $p := C_{44}^d -$

C_{44}^u,

$$A' := \begin{cases} \dfrac{\sin a'}{r^u} & r^u \neq 0 \\[2mm] \kappa Z & r^u = 0 \end{cases}, \qquad B' := \begin{cases} \dfrac{\sin b'}{s^u} & s^u \neq 0 \\[2mm] \kappa Z & s^u = 0 \end{cases},$$

$$r^u = \sqrt{\frac{v_r^2}{(\alpha^u)^2} - 1}, \quad s^u = \sqrt{\frac{v_r^2}{(\beta^u)^2} - 1}, \quad r^d = \sqrt{1 - \frac{v_r^2}{(\alpha^d)^2}}, \quad s^d = \sqrt{1 - \frac{v_r^2}{(\beta^d)^2}}$$

and

$$a' = \kappa r^u Z, \quad b' = \kappa s^u Z, \quad a = \kappa r^d Z, \quad b = \kappa s^d Z.$$

These equations include several corrections to the formulas of Udías [1999, p. 200] [Dalton et al., 2017]. Values of D_r can be imaginary if the product of r^u and s^u is imaginary.

For modes other than the fundamental mode, equation (5.2) has a solution only for $\beta^u < v_r < \beta^d < \alpha^d$. For the fundamental mode there is a solution for $v_r < \beta^u$, for higher values of ω. For $v_r > \alpha^u$, the determinant is real; for $\beta^u < v_r < \alpha^u$, the determinant is imaginary; for $v_r < \beta^u$ the determinant is real.

5.4 Pareto Joint Inversion

In this study, the dispersion relations of the Love and quasi-Rayleigh waves are the two target functions to be examined together by the Pareto Joint Inversion. In general, we search for

$$\min[f_1(x), f_2(x), \dots, f_n(x)], \qquad x \in S, \tag{5.3}$$

where f_i are target functions and S is the space of acceptable solutions. Herein, $f_1 = D_{r2}$ and $f_2 = D_\ell$, given, respectively, in expression (5.1) and expression (5.2), above. Every solution is

$$C = \{y \in \mathbb{R}^n : y = f(x) : x \in S\}. \tag{5.4}$$

Among them, a Pareto solution is vector $x^* \in S$, such that all other vectors of this type return a higher value of at least one of the functions, f_i.

The set of all Pareto optimal solutions is $\mathscr{P}^*$ and $\mathscr{P}\mathscr{F}^* = (f_1(x), f_2(x), \ldots, f_n(x))$, where $x \in \mathscr{P}^*$, is the Pareto front. Each iteration of the algorithm generates a single Pareto solution to be added to a tradeoff curve that is called the Pareto front. In this paper, the Particle Swarm Optimization algorithm [Kennedy and Eberhart, 1995, Parsopoulos and Vrahatis, 2002] is used to obtain each element of the Pareto front.

The target function for Love waves is a solution of equation (5.1). Since its domain and range consist of real numbers, computations involving imaginary numbers are not necessary.

We use a solution of D_{r2} as the target function for quasi-Rayleigh waves. It is real for the input values of C_{11}^u, C_{44}^u, ρ^u, C_{11}^d, C_{44}^d, ρ^d and Z. However, since the parameters do not have any constraints in randomization, complex numbers appear. Using $\sin(\iota x) = \iota \sinh(x)$ and $\cos(\iota x) = \cosh(x)$, we restrict our computations to real numbers.

5.5   Numerical results and discussion

Figure 5.1 illustrates the dispersion curves for the quasi-Rayleigh and Love waves, which are used as input data for the inversion. Each curve corresponds to a single mode, with the lowest curve being the fundamental mode. The dashed lines correspond to the angular frequencies for which we perform the inversion. Their intercepts with dispersion curves correspond to propagation speeds—along the surface—for distinct modes of a guided wave.

In our extensive tests, we use the first two modes for $\omega = 15 \text{ s}^{-1}$, the first five modes for $\omega = 60 \text{ s}^{-1}$, and the first seven modes for $\omega = 100 \text{ s}^{-1}$. The results for all these frequencies and modes are similar to each other. To illustrate these results, in Figures 5.2–5.4 and 5.8–5.10, we use $\omega = 15 \text{ s}^{-1}$, and in Figures 5.5–5.7, we use $\omega = 60 \text{ s}^{-1}$.
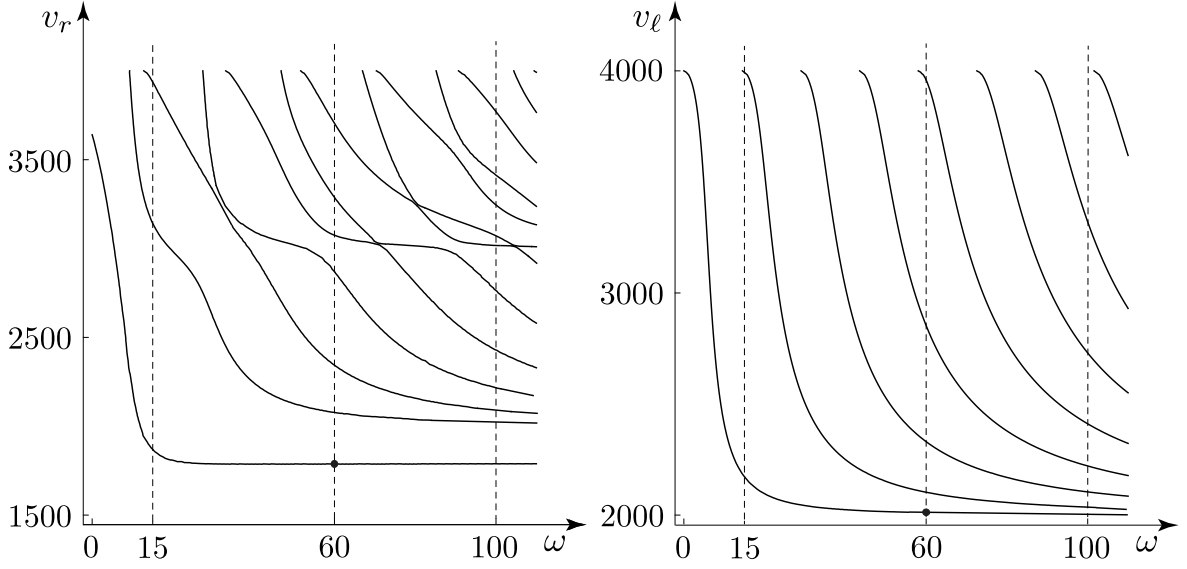
Figure 5.1: Dispersion curves of quasi-Rayleigh wave, in the left-hand plot, and of Love wave, in the right-hand plot. The solid dots correspond to the error-free values of v_r and v_ℓ for the fundamental mode at $\omega = 60$ s^{-1}.

In Figure 5.2, a Pareto front exhibits a rectangular shape, for a large range of values. It means that an optimal value for one target function corresponds to a wide range of values of the other function. Thus, if one target function is minimized the other can—for the same parameters—exhibit substantial values. To study this phenomenon, we plot histograms for model parameters obtained for all solutions constituting a Pareto front and contrast it with histograms obtained for its separated branches. The results are presented in Figures 5.3 and 5.4. The spread in values is not due to perturbations, as is commonly the case for histograms, but shows the range of Pareto optimal solutions along the Pareto front and its two branches. Each Pareto optimal is chosen either when a certain number of iterations is reached or a certain precision is reached, and given error-free data an increase in that precision should result in the corner of the Pareto front being closer to the true model, and in the histogram width being narrower.

For each parameter, there is a good match between the values obtained by the inverse process and the values used in the original dispersion relations. It is visible that, in the case
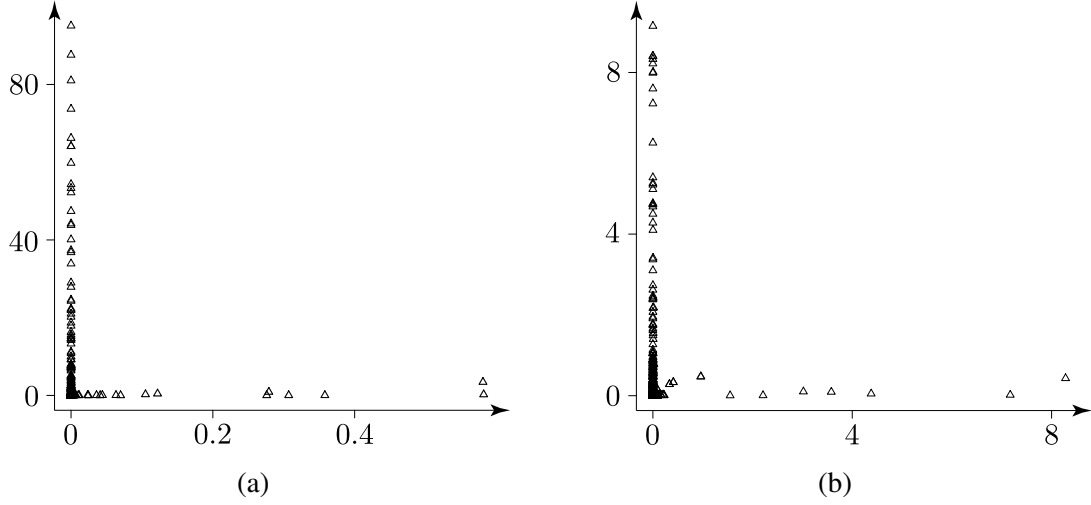
Figure 5.2: Pareto fronts for $\omega = 15\,\text{s}^{-1}$; plots (a) and (b): first mode and second mode. The horizontal axis measures the quasi-Rayleigh wave target function misfit, which is $|D_{r2}|^2$, and the vertical axis measures the Love wave target function misfit, which is $|D_\ell|^2$. Values on both axes are to be scaled by 10^{-5}.

of guided waves, inversion information provided by both sources is complementary and proper application of joint inversion allows the recognition of correct parameters. More precisely, constraining the quasi-Rayleigh wave inversion with quasi-Love waves stabilizes the whole solution. This behaviour is visible in Figure 5.2, where proposed solutions, marked by dark triangles, are more concentrated near $(0,0)$, along the horizontal axis, which corresponds to quasi-Rayleigh waves, and more spread out along the vertical axis, which corresponds to the Love waves. It means that quasi-Rayleigh waves lend themselves particularly well to such an optimization and, if a satisfactory solution for Love waves is found, the quasi-Rayleigh target function can be adjusted.

To present results for all frequencies and all modes in a concise manner, let us examine Table 5.1, which contains the model and estimated values, as well as Table 5.2, where the ratio of the estimated to model values is expressed in terms of percentages. The values of all parameters are inverted satisfactorily, with discrepancies that might be caused by differences in positions of global minima of target functions and by occasional spurious

126
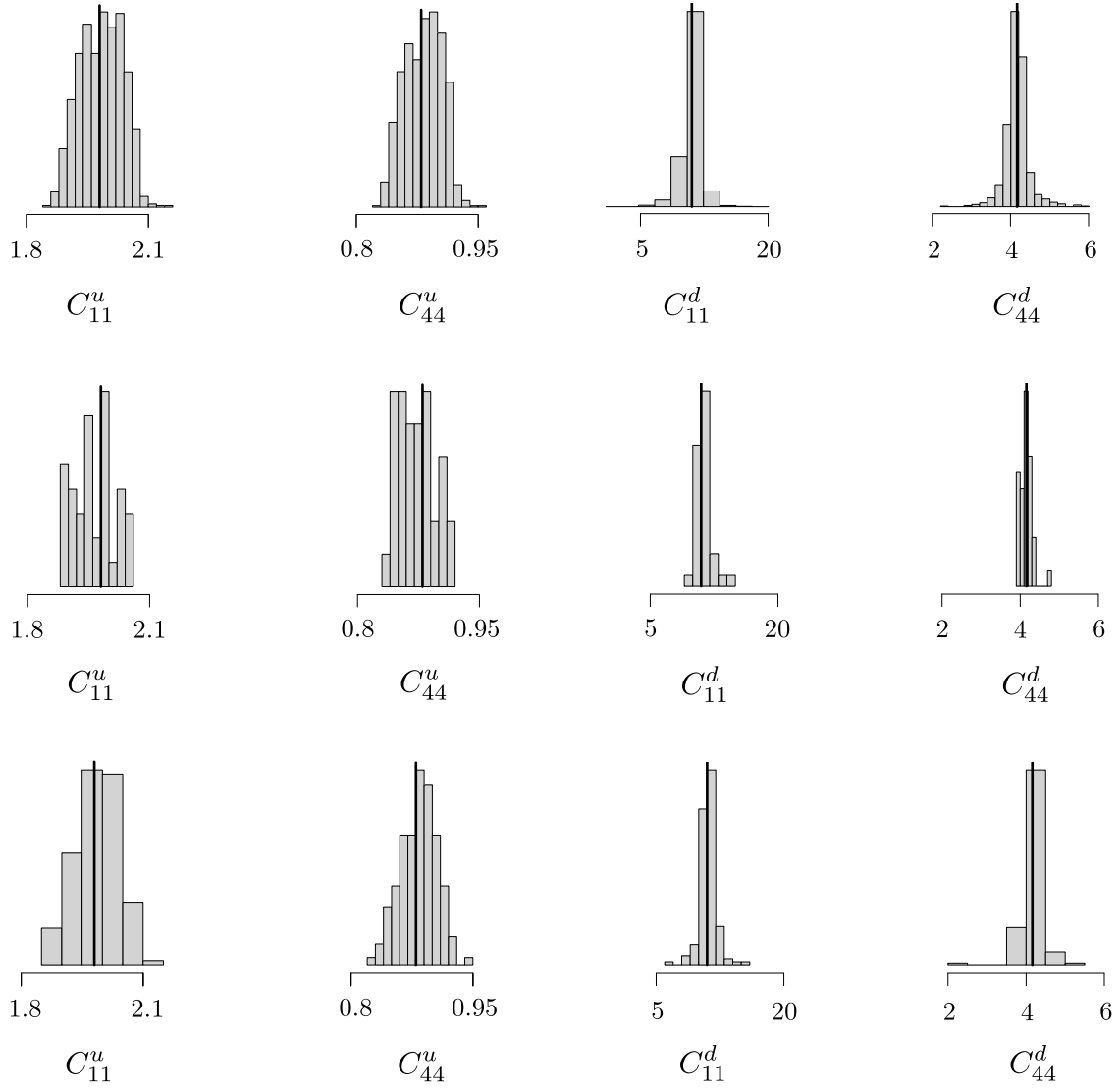
Figure 5.3: Histograms of elasticity parameters in 10^{10} N/m^2 ; top row: the Pareto front; middle row: Love branch of the Pareto front; bottom row: Rayleigh branch of the Pareto front; vertical black lines represent the model values from Table 5.1

Figure 5.4: Histograms of layer thickness, in metres, and mass densities, in 10^3 kg/m^3 ; top row: Pareto front; middle row: Love branch of the Pareto front; bottom row: Rayleigh branch of the Pareto front; vertical black lines represent the model values from Table 5.1
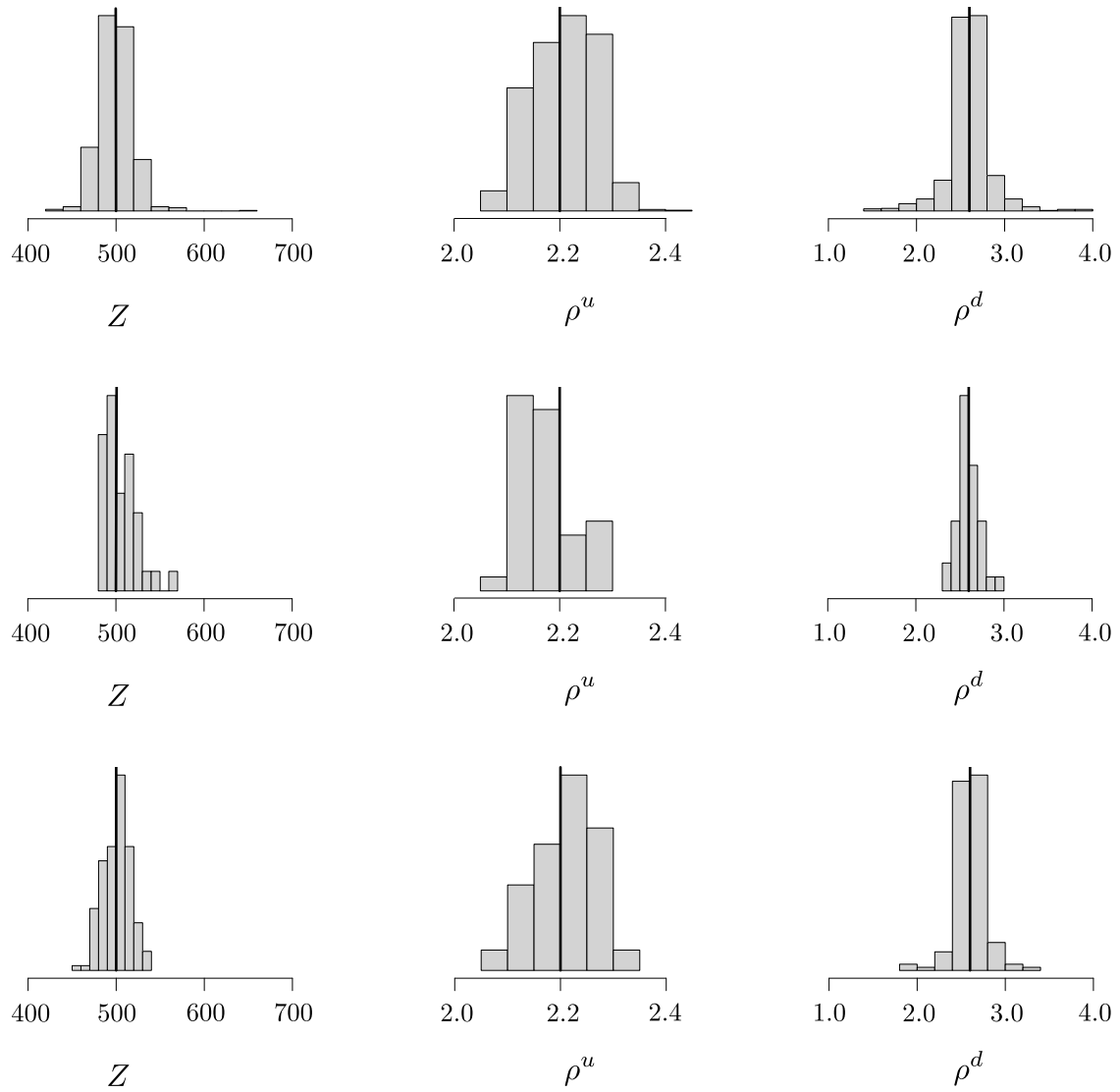
128

	C_{11}^u	C_{44}^u	C_{11}^d	C_{44}^d	ρ^u	ρ^d	Z
Model	1.980	0.880	10.985	4.160	2.200	2.600	500.0
$\omega = 15\ \mathrm{s}^{-1}$							
2nd mode	2.211	0.875	10.958	4.215	2.234	2.605	522.7
1st mode	1.999	0.893	10.405	3.919	2.254	2.578	480.3
$\omega = 60\ \mathrm{s}^{-1}$							
5th mode	2.026	0.919	10.919	4.354	2.240	2.690	512.0
4th mode	2.035	0.893	10.707	4.128	2.256	2.464	494.9
3rd mode	2.022	0.878	11.307	4.258	2.184	2.743	505.1
2nd mode	2.009	0.881	11.239	3.805	2.221	2.667	476.2
1st mode	1.992	0.884	11.030	3.951	2.212	2.632	491.5
$\omega = 100\ \mathrm{s}^{-1}$							
7th mode	2.015	0.751	10.089	4.168	2.177	2.724	517.4
6th mode	1.949	0.871	10.848	4.285	2.174	2.563	501.1
5th mode	1.981	0.878	10.846	4.074	2.192	2.682	500.4
4th mode	2.038	0.912	10.683	4.079	2.283	2.561	498.0
3rd mode	1.954	0.872	10.882	4.210	2.174	2.538	506.1
2nd mode	2.046	0.906	10.547	4.334	2.265	2.579	499.9
1st mode	2.123	0.857	11.089	4.315	2.197	2.052	548.8

Table 5.1: Summary of results: Elasticity parameters are in units of $10^{10}\mathrm{N/m^2}$, mass densities in $10^3\mathrm{kg/m^3}$ and layer thickness in metres.

results due to local minima and the numerical complexity of the algorithm, whereby each Pareto optimal solution is obtained by an application of Particle Swarm Optimization to minimizing fairly complicated target function D_ℓ and very complicated target function D_{r2} with the Pareto Joint Inversion criterion determining the stopping point. In general, the presented results support the idea of possible application of the presented method for practical application if high quality data are available.

We wish to perform an analysis of the possible impact of measurements errors on Pareto joint inversion. However, in the case of guided waves, standard perturbation methods are not feasible. First, a single front is already a collection of hundreds of individual solutions, so a perturbation approach would lead to parameter distributions expressing both the Pareto-front and perturbation effects. An interpretation of such a combination might be exceedingly difficult. Secondly, obtaining perturbed results for all frequencies and modes

	C_{11}^u	C_{44}^u	C_{11}^d	C_{44}^d	ρ^u	ρ^d	Z
Model	100.0	100.0	100.0	100.0	100.0	100.0	100.0
$\omega = 15\ \text{s}^{-1}$							
2nd mode	111.7	99.4	99.8	101.3	101.6	100.2	104.5
1st mode	100.9	101.5	94.7	94.2	102.5	99.2	96.1
$\omega = 60\ \text{s}^{-1}$							
5th mode	102.3	104.4	99.4	104.7	101.8	103.4	102.4
4th mode	102.8	101.5	97.5	99.2	102.6	94.8	99.0
3rd mode	102.1	99.8	102.9	102.4	99.3	105.5	101.0
2nd mode	101.5	100.1	102.3	91.5	101.0	102.6	95.2
1st mode	100.6	100.5	100.4	95.0	100.5	101.2	98.3
$\omega = 100\ \text{s}^{-1}$							
7th mode	101.8	85.3	91.8	100.2	99.0	104.8	103.5
6th mode	98.4	99.0	98.8	103.0	98.8	98.6	100.2
5th mode	100.0	99.7	98.7	97.9	99.6	103.1	100.1
4th mode	102.9	103.6	97.3	98.1	103.8	98.5	99.6
3rd mode	98.7	99.1	99.1	101.2	98.8	97.6	101.2
2nd mode	103.3	103.0	96.0	104.2	103.0	99.2	100.0
1st mode	107.2	97.4	100.9	103.7	99.8	78.9	109.8

Table 5.2: Estimated values compared to model values, in percentages

would require enormous computational time, though it might be feasible with cluster computing.

Thus, to examine the sensitivity of the proposed method, for all modes and frequencies, we examine the effects of fixed errors: $\pm 1\%$, $\pm 3\%$ and $\pm 5\%$ in propagation speeds of the quasi-Rayleigh and Love waves. This allows us to gain an insight into effects of inaccuracies of the input on the estimation of model parameter, without performing a perturbation study.

Tables 5.3 and 5.4 contain the best solutions from the combination of all Pareto-optimal solutions for input errors of $\pm 5\%$. These values are to be compared with Tables 5.1 and 5.2, which contain the best solutions obtained from the error-free input. Figures 5.5–5.7 are kernel densities, which are akin to smoothed histograms, of model parameters along the Pareto fronts for the fundamental mode at $\omega = 60\,\mathrm{s}^{-1}$, obtained with input errors. For each case a different number of solutions is accepted so only maximum positions and spread of distributions have interpretational value. The dots in Figure 5.1 correspond to the error-free values of v_r and v_ℓ.

In Figures 5.5–5.7, the dotted lines correspond to the error of $\pm 1\%$, dashed lines of $\pm 3\%$ and solid lines of $\pm 5\%$. Therein, the black colour corresponds to a negative value and the grey to a positive one.

Examining the tables, we see that even relatively low errors lead to a significant loss of accuracy. Examining the kernel densities, we see that the peak values are shifted from the model values, and the kernel densities have a greater spread than original histograms, especially for ρ^u and C_{44}^u. To explain the last statement, consider the fact that—as seen in Figure 5.1 and as discussed by Udías [1999]—the fundamental-mode dispersion curve of the quasi-Rayleigh wave is asymptotic to the propagation speed of a Rayleigh wave in a halfspace with the same properties as the layer, which is affected by the shear-wave speed in the layer, $\beta^u = \sqrt{C_{44}^u/\rho^u}$. Thus, an error in v_r affects particularly the inverted values of

	C_{11}^u	C_{44}^u	C_{11}^d	C_{44}^d	ρ^u	ρ^d	Z
Model	1.980	0.880	10.985	4.160	2.200	2.600	500.0
$\omega = 15 \text{ s}^{-1}$							
2nd mode	1.899	0.856	10.440	4.002	2.296	2.748	509.4
1st mode	2.121	0.943	10.736	4.061	2.135	2.435	524.4
$\omega = 60 \text{ s}^{-1}$							
5th mode	2.312	0.899	11.017	3.861	2.091	2.679	535.7
4th mode	2.178	0.859	9.541	3.969	2.022	2.593	504.1
3rd mode	1.921	0.917	11.139	3.992	2.119	2.231	505.9
2nd mode	1.711	0.843	10.956	4.328	2.296	2.522	523.5
1st mode	2.113	0.933	15.211	4.004	2.120	2.929	482.9
$\omega = 100 \text{ s}^{-1}$							
7th mode	2.219	0.890	10.854	3.753	1.263	2.660	527.2
6th mode	1.907	0.863	9.640	4.177	2.177	2.024	530.0
5th mode	2.495	0.849	11.556	4.208	2.246	2.492	513.9
4th mode	1.952	0.923	12.543	4.031	2.117	2.665	508.5
3rd mode	1.937	0.864	10.480	4.291	2.239	2.549	491.5
2nd mode	2.066	0.837	11.757	4.232	2.322	2.463	470.0
1st mode	2.068	0.863	11.633	4.353	2.488	2.613	560.9

Table 5.3: Summary of results for input errors of $\pm 5\%$: Elasticity parameters are in units of 10^{10}N/m^2, mass densities in 10^3kg/m^3 and layer thickness in metres.

ρ^u and C_{44}^u. We also note that, while the peak values of the kernel densities are those for which there are the most Pareto-optimal solutions, those values are not necessarily the best solutions, which are the solutions at the corner of the Pareto fronts.

To gain an additional insight into the effects of input errors on the inverse process, we examine correlations between the inverted values of C_{11} and C_{44}, in the layer and in the halfspace, for input with and without errors. In Figures 5.8–5.10, the left-hand plot corresponds to the layer and the right-hand plot to the halfspace. For each case, we consider only the fundamental mode and $\omega = 15 \text{ s}^{-1}$.

In Figure 5.8, we illustrate the correlation for input without errors. In Figures 5.9 and 5.10, we illustrate the correlation for the speed perturbed by $\pm 5\%$. The values along the axes for the left-hand and right-hand plots are to be scaled as follows. Figure 5.8: $\times 10^9$,

	C_{11}^u	C_{44}^u	C_{11}^d	C_{44}^d	ρ^u	ρ^d	Z
Model	100.0	100.0	100.0	100.0	100.0	100.0	100.0
$\omega = 15\ \mathrm{s}^{-1}$							
2nd mode	95.9	97.2	95.08	96.28	104.4	105.7	101.9
1st mode	107.1	107.2	97.7	97.6	97.0	93.7	104.9
$\omega = 60\ \mathrm{s}^{-1}$							
5th mode	116.8	102.1	100.3	92.8	95.0	103.0	107.1
4th mode	110.0	97.6	86.9	95.4	91.9	99.7	100.8
3rd mode	97.0	104.2	101.4	96.0	96.3	85.8	101.2
2nd mode	86.4	95.8	99.7	104.0	104.4	97.0	104.7
1st mode	106.7	106.1	138.5	96.2	96.4	112.6	96.6
$\omega = 100\ \mathrm{s}^{-1}$							
7th mode	112.1	101.2	98.8	90.2	57.4	102.3	105.4
6th mode	96.3	98.0	87.8	100.4	97.0	77.8	106.0
5th mode	126.0	96.4	105.2	101.1	102.1	95.9	102.8
4th mode	98.6	104.9	114.2	96.9	96.2	102.5	101.7
3rd mode	97.8	98.1	95.4	103.1	101.8	98.0	98.3
2nd mode	104.4	95.2	107.0	101.7	105.5	94.7	94.0
1st mode	104.5	98.0	105.9	104.6	113.1	100.5	112.2

Table 5.4: Estimated values compared to model values, in percentages, for input errors of $\pm 5\%$
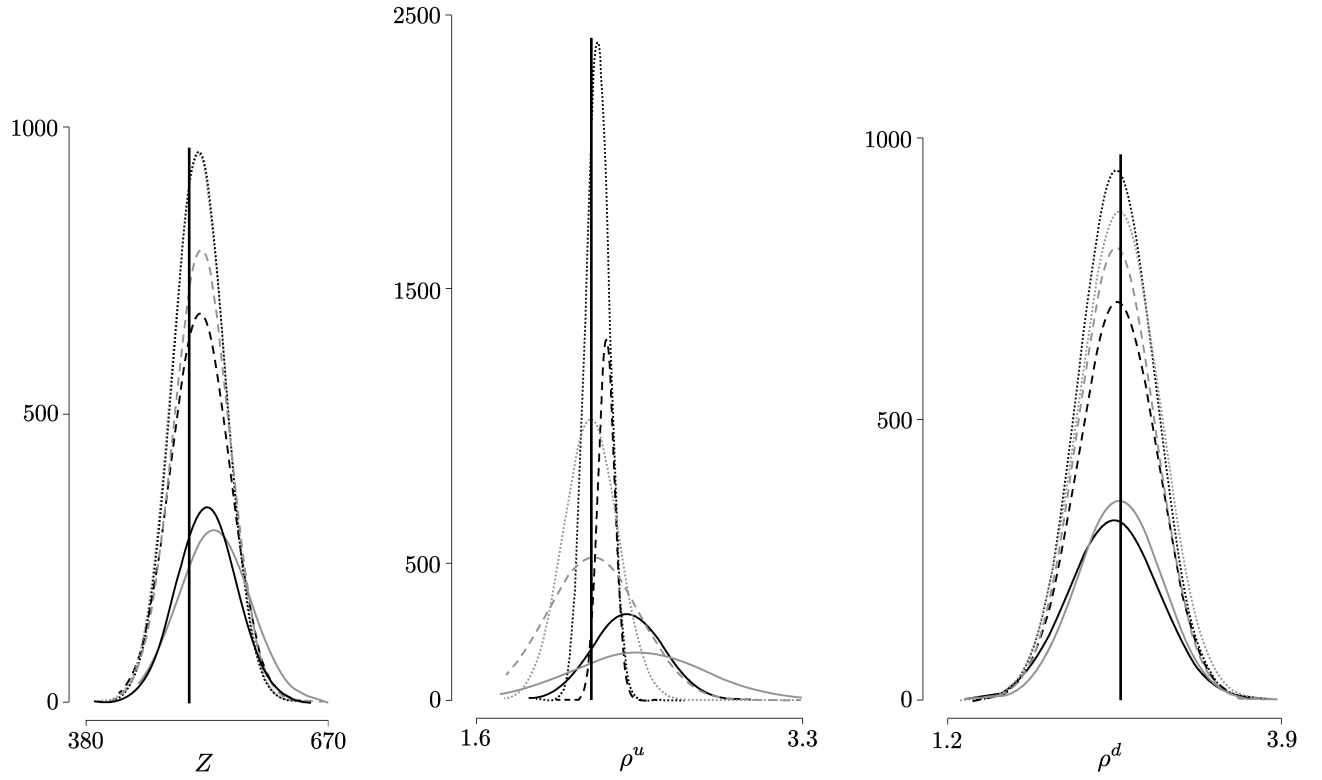
Figure 5.5: Distributions of layer thickness, in metres, and mass densities, in 10^3 kg/m^3, for input errors of $\pm 1\%$, $\pm 3\%$, $\pm 5\%$; vertical lines represent the model values from Table 5.1

134

Figure 5.6: Distributions of elasticity parameters, in 10^{10} N/m^2, for input errors of $\pm 1\%$, $\pm 3\%$, $\pm 5\%$; vertical lines represent the model values from Table 5.1
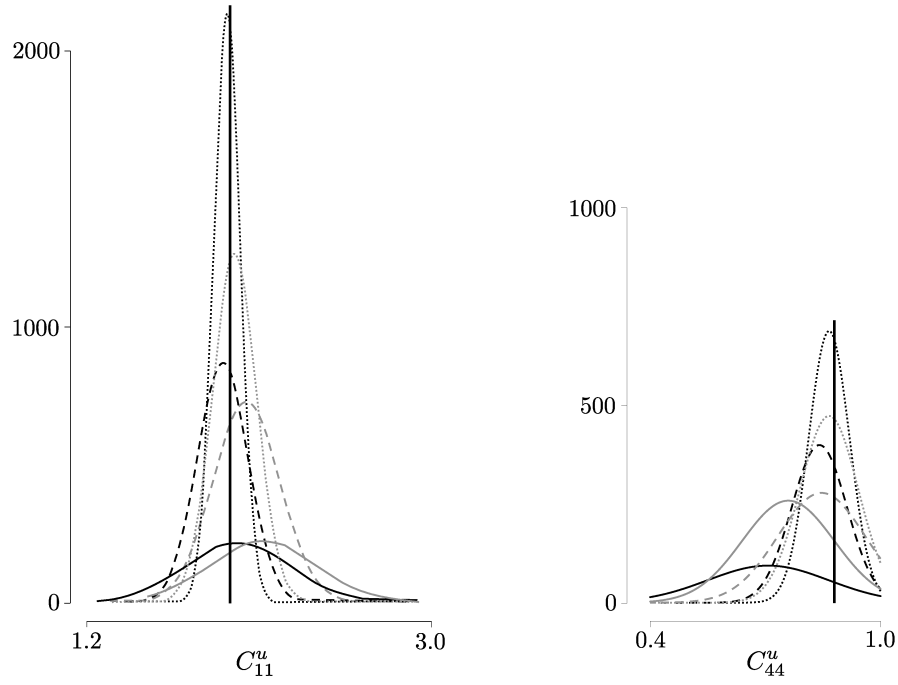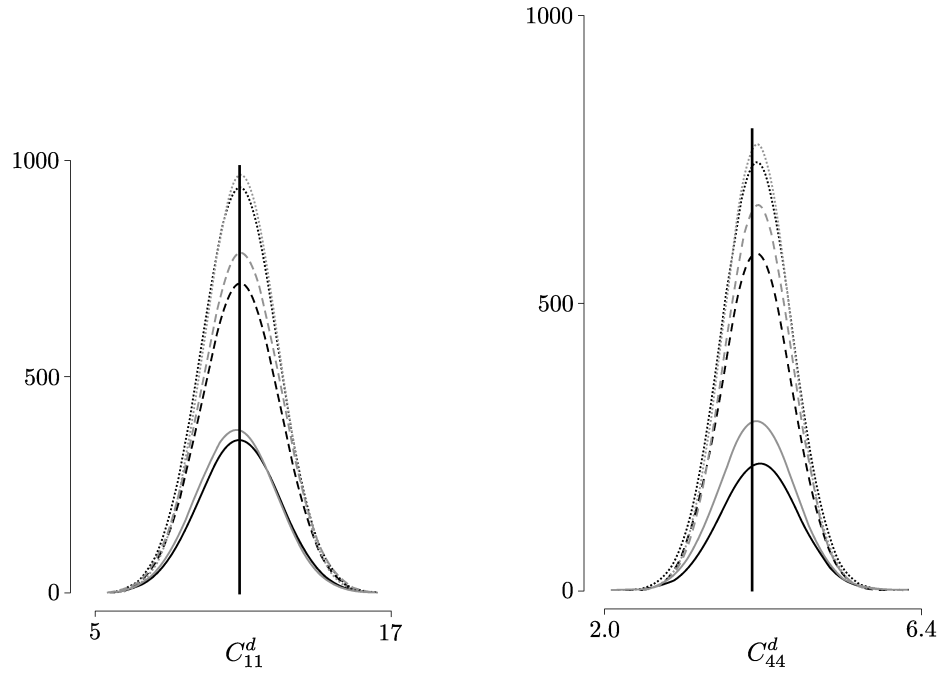

Figure 5.7: Distributions of elasticity parameters, in 10^{10} N/m^2, for input errors of $\pm 1\%$, $\pm 3\%$, $\pm 5\%$; vertical lines represent the model values from Table 5.1

$\times 10^{11}$; Figure 5.9: $\times 10^{10}$, $\times 10^{11}$; Figure 5.10: $\times 10^{10}$, $\times 10^{11}$.

The three left-hand plots, which refer to the layers, exhibit a linear relation between C_{11} and C_{44}. In each plot, the black triangle corresponds to the optimal Pareto solution. In units of 10^{10} N/m^2, they are as follows. Figure 5.8: $C_{11}^u = 1.999$, $C_{44}^u = 0.893$, $C_{11}^d = 10.405$, $C_{44}^d = 3.919$, as in Table 5.1; Figure 5.9: $C_{11}^u = 2.121$, $C_{44}^u = 0.943$, $C_{11}^d = 10.736$, $C_{44}^d = 4.061$, as in Table 5.3; Figure 5.10: $C_{11}^u = 1.894$, $C_{44}^u = 0.838$, $C_{11}^d = 11.066$, $C_{44}^d = 4.042$, which do not appear in any table.

Let us consider a linear regression,

$$C_{44}^u = 0.43\,C_{11}^u + 2.97 \times 10^8,$$

$$C_{44}^u = 0.37\,C_{11}^u + 1.63 \times 10^9,$$

$$C_{44}^u = 0.42\,C_{11}^u + 3.96 \times 10^8,$$

for each left-hand plot, respectively. The slope is similar for each case, the intercept varies slightly more. These results show that the ratio of elasticity parameters is preserved along the Pareto front.

The linear relation between C_{11}^u and C_{44}^u might be due to the asymptotic behaviour of the fundamental mode, which—for both quasi-Rayleigh waves and Love waves—depends on the values of C_{44}^u. Hence, the value of C_{11}^u has to adjust itself, in accordance with solutions along the Pareto front. A similar effect can be observed in Figure 5.3.

The three right-hand plots, which refer to the halfspace, exhibit neither the linear relation nor a significant shift of the optimal Pareto solution, marked by a black triangle. These results suggest that, herein, the layer elasticity parameters are more sensitive to the input errors than are the halfspace parameters, which is consistent with results listed in Table 5.4.
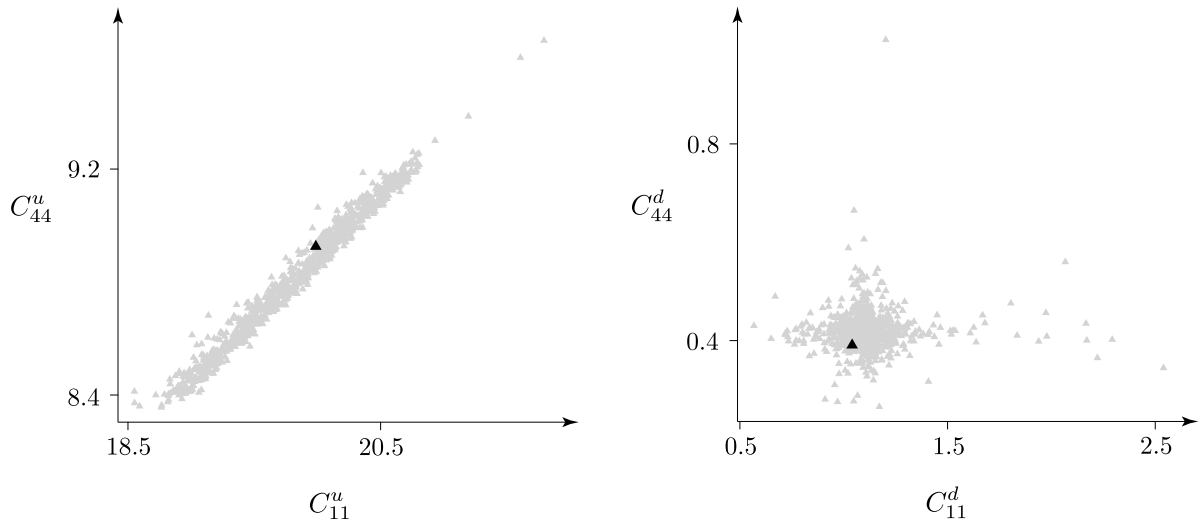
Figure 5.8: Relationships between elasticity parameters for input without errors
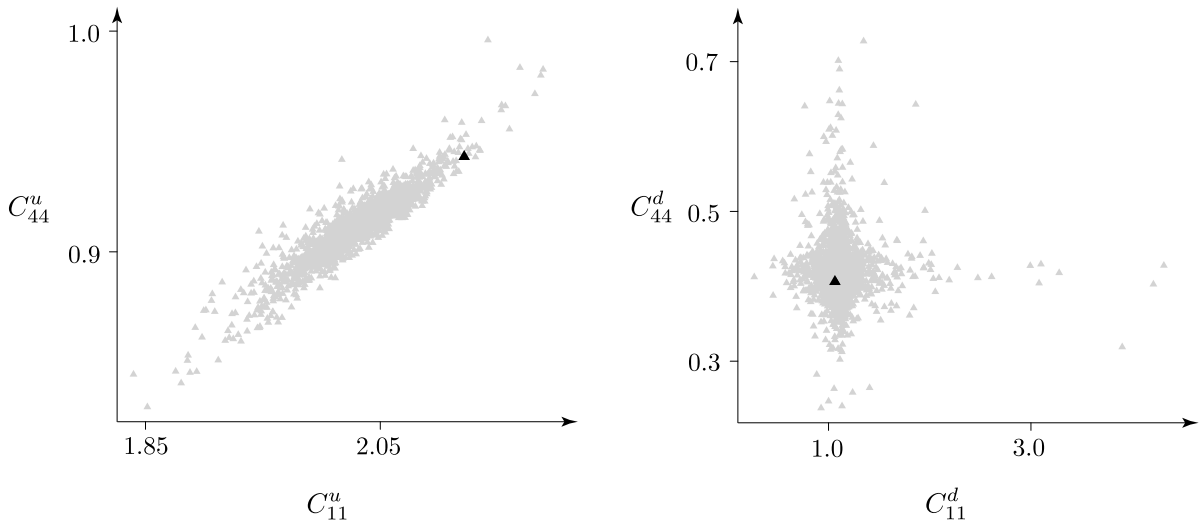

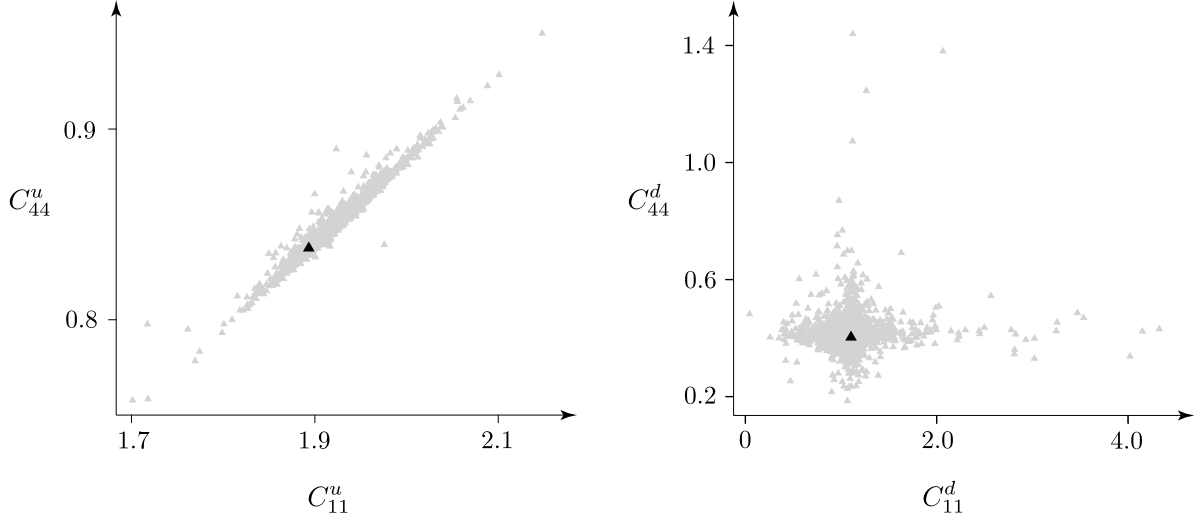Figure 5.9: Relations between elasticity parameters for the input error of $+5\%$

137

Figure 5.10: Relations between elasticity parameters for for the input error of -5%

5.6 Conclusion

In this paper, we discuss a guided-wave joint inversion using a formulation based on dispersion relations proposed by Dalton et al. [2017]. To eliminate common joint-inversion problems, such as choosing target-functions weights, we use a Pareto inversion. The results are promising for possible practical applications, especially if mode velocities are provided with high accuracy. For input with low accuracy, inverted parameters become significantly less reliable, which indicates the error-sensitivity of the process, with the layer parameters being more sensitive to input errors than the halfspace parameters. Also, presented results suggest that such inversion should be based on quasi-Rayleigh waves supported by additional information provided by Love waves. In agreement with Dalton et al. [2017], the fundamental mode is more sensitive to the layer parameters whereas higher modes are sensitive to both the layer and halfspace properties; for the second mode, the results for the halfspace are more accurate for low frequencies. Future work could involve relating the error in the data to the error in the inverted parameters.

Acknowledgments

5.7 References

T. Boxberger, M. Picozzi, and S. Parolai. Shallow geology characterization using Rayleigh and Love wave dispersion curves derived from seismic noise array measurements. *Journal of Applied Geophysics*, 75:345–354, 2011.

G. Dal Moro. Insights on surface wave dispersion and HVSR: Joint analysis via Pareto optimality. *Journal of Applied Geophysics*, 72:129–140, 2010.

G. Dal Moro and F. Ferigo. Joint analysis of Rayleigh- and Love-wave dispersion: Issues, criteria and improvements. *Journal of Applied Geophysics*, 75:573–589, 2011.

G. Dal Moro, R. M. M. Moura, and S. S. R. Moustafa. Multi-component joint analysis of surface waves. *Journal of Applied Geophysics*, 119:128–138, 2015.

D. R. Dalton, M. A. Slawinski, P. Stachura, and T. Stanoev. Sensitivity of Love and quasi-Rayleigh waves to model parameters. *The Quarterly Journal of Mechanics and Applied Mathematics*, 70(2):103–130, 2017.

H. Fang, H. Yao, H. Zhang, Y-C. Huang, and R. D. van der Hilst. Direct inversion of surface

wave dispersion for three-dimensional shallow crustal structure based on ray tracing: methodology and application. *Geophys. J. Int.*, 201:1251–1263, 2015.

J. Kennedy and R. Eberhart. Particle swarm optimization. *Proc. IEEE Conf. on Neural Networks*, pages 1942–1948, 1995.

L. Lu, C. Wang, and B. Zhang. Inversion of multimode Rayleigh waves in the presence of a low-velocity layer: numerical and laboratory study. *Geophys. J. Int.*, 168:1235–1246, 2007.

C. B. Park, R. D. Miller, and J. Xia. Multichannel analysis of surface waves. *Geophysics*, 64(3):800–808, 1999.

K. Parsopoulos and M. Vrahatis. Particle swarm optimization method in multiobjective problems. *Proceedings of the ACM Symposium on Applied Computing (SAC)*, pages 603–607, 2002.

A. Udías. *Principles of seismology*. Cambridge University Press, 1999.

N. Wang, J-P. Montagner, G. Burgos, Y. Capdeville, and D. Yu. Intrinsic *versus* extrinsic seismic anisotropy: Surface wave phase velocity inversion. *Comptes Rendus Geoscience*, 347:66–76, 2015.

M. Wathelet, D. Jongmans, and M. Ohrnberger. Surface-wave inversion using a direct search algorithm and its application to ambient vibration measurements. *Near Surface Geophysics*, 2:211–221, 2004.

J. Xia, R. D. Miller, and C. B. Park. Estimation of near-surface shear-wave velocity by inversion of Rayleigh waves. *Geophysics*, 64(3):691–700, 1999.

H. Xie and L. Liu. Near-surface anisotropic structure characterization by Love wave inversion for assessing ground conditions in urban areas. *Journal of Earth Science*, 26(6): 807–812, 2015.

Chapter 6

On Backus average in modelling guided waves[*]

Abstract

We study the Backus [1962] average of a stack of layers overlying a halfspace to examine its applicability for the quasi-Rayleigh and Love wave dispersion curves. We choose these waves since both propagate in the same model. We compare these curves to values obtained for the stack of layers using the propagator matrix. In contrast to the propagator matrix, the Backus [1962] average is applicable only for thin layers or low frequencies. This is true for both a weakly inhomogeneous stack of layers resulting in a weakly anisotropic medium and a strongly inhomogeneous stack of alternating layers resulting in a strongly anisotropic medium. We also compare the strongly anisotropic and weakly anisotropic media, given by the Backus [1962] averages, to results obtained by the isotropic Voigt [1910] averages of these media. As expected, we find only a small difference between these results

---

[*]This chapter is a modified version of D.R. Dalton, T.B. Meehan, and M.A. Slawinski. On Backus average in modelling guided waves. arXiv:1801.05464v2 [physics.geo-ph], 2018. Submitted to *Journal of Applied Geophysics*, March, 2018.

for weak anisotropy and a large difference for strong anisotropy. We perform the Backus [1962] average for a stack of alternating transversely isotropic layers that is strongly inhomogeneous to evaluate the dispersion relations for the resulting medium. We compare the resulting dispersion curves to values obtained using a propagator matrix for that stack of layers. Again, there is a good match only for thin layers or low frequencies. Finally, we perform the Backus [1962] average for a stack of nonalternating transversely isotropic layers that is strongly inhomogeneous, and evaluate the quasi-Rayleigh wave dispersion relations for the resulting transversely isotropic medium. We compare the resulting curves to values obtained using the propagator matrix for the stack of layers. In this case, the Backus [1962] average performs less well, but—for the fundamental mode—remains adequate for low frequencies or thin layers.

Keywords

Backus average, surface waves, propagator matrix, Thomsen parameters

6.1   Introduction

This paper is an examination of the applicability of the Backus [1962] average to guided-wave-dispersion modelling. We compare the dispersion relations of both Love and quasi-Rayleigh waves for the Backus [1962] average of a stack of layers to the dispersion relations for these layers obtained using the propagator-matrix method. The prefix distinguishes quasi-Rayleigh waves, which are guided waves, from classical Rayleigh waves, which propagate within a halfspace. We examine the effects of strength of inhomogeneity, anisotropy and layer thickness.

The focus on examining both Love and quasi-Rayleigh waves is motivated by their existence in the same model. This is a consequence of compatibility of their wave equations

and boundary conditions, as discussed by Dalton et al. [2017].

Similar work—for Love waves in a stack of alternating isotropic layers—was done by Anderson [1962], in which the author drew on the results of Postma [1955]. Herein, we broaden this work to quasi-Rayleigh waves and, drawing on the work of Backus [1962], to a nonalternating stack of isotropic layers. We extend the scope to include Love waves for a stack of alternating transversely isotropic layers and quasi-Rayleigh waves for stacks of alternating and nonalternating transversely isotropic layers.

We begin this paper by providing background information for the Backus [1962] and Voigt [1910] averages, as well as the Thomsen [1986] parameters. The essence of this paper consists of numerical results and their discussion, where we consider the effects of strength of inhomogeneity, anisotropy and layer thickness on different modes and frequencies of the dispersion relations for the quasi-Rayleigh and Love waves.

6.2 Background

Backus [1962] shows that—in parallel isotropic layers whose thicknesses are much smaller than the wavelength—waves behave as if they were travelling through a single transversely isotropic medium. An examination and extension of the Backus [1962] average, as well as its limitations, are discussed by Bos et al. [2017a,b].

The parameters of this medium are (e.g., Slawinski [2018, equations (4.37)–(4.42)])

$$c_{1111}^{\overline{\mathrm{TI}}} = \overline{\left(\frac{c_{1111} - 2c_{2323}}{c_{1111}}\right)}^2 \; \overline{\left(\frac{1}{c_{1111}}\right)}^{-1} + \overline{\left(\frac{4(c_{1111} - c_{2323})c_{2323}}{c_{1111}}\right)}, \qquad (6.1)$$

$$c_{1133}^{\overline{\mathrm{TI}}} = \overline{\left(\frac{c_{1111} - 2c_{2323}}{c_{1111}}\right)} \; \overline{\left(\frac{1}{c_{1111}}\right)}^{-1}, \qquad (6.2)$$

$$c_{1212}^{\overline{\mathrm{TI}}} = \overline{c_{2323}}, \qquad (6.3)$$

$$c_{2323}^{\overline{\text{TI}}} = \overline{\left(\frac{1}{c_{2323}}\right)}^{-1}, \tag{6.4}$$

$$c_{3333}^{\overline{\text{TI}}} = \overline{\left(\frac{1}{c_{1111}}\right)}^{-1}, \tag{6.5}$$

where $c_{ijk\ell}$ are the elasticity-tensor components for an isotropic Hookean solid and the overline indicates an average. These expressions constitute a medium equivalent to a stack of layers, which we refer to as the Backus medium. In this paper, we use an arithmetic average, whose weight is the layer thickness, which we take to be the same for all averaged layers; for example, in equation (6.3),

$$c_{1212}^{\overline{\text{TI}}} = \overline{c_{2323}} = \frac{1}{n}\sum_{i=1}^{n}(c_{2323})_i, \tag{6.6}$$

where n is the number of layers.

Backus [1962] also shows that waves travelling through parallel transversely isotropic layers behave as if they were travelling through a single transversely isotropic medium. The parameters of such a medium are (e.g., Slawinski [2018, equations (4.56)–(4.61)])

$$c_{1111}^{\overline{\text{TI}}} = \overline{\left(c_{1111} - \frac{c_{1133}^2}{c_{3333}}\right)} + \overline{\left(\frac{c_{1133}}{c_{3333}}\right)}^2 \overline{\left(\frac{1}{c_{3333}}\right)}^{-1}, \tag{6.7}$$

$$c_{1133}^{\overline{\text{TI}}} = \overline{\left(\frac{c_{1133}}{c_{3333}}\right)} \overline{\left(\frac{1}{c_{3333}}\right)}^{-1}, \tag{6.8}$$

$$c_{1212}^{\overline{\text{TI}}} = \overline{c_{1212}}, \tag{6.9}$$

$$c_{2323}^{\overline{\text{TI}}} = \overline{\left(\frac{1}{c_{2323}}\right)}^{-1}, \tag{6.10}$$

$$c_{3333}^{\overline{\text{TI}}} = \overline{\left(\frac{1}{c_{3333}}\right)}^{-1}, \tag{6.11}$$

where $c_{ijk\ell}$ are the elasticity-tensor components of a transversely isotropic Hookean solid.

This result is also referred to as the Backus medium. The parameters in expressions (6.1)–(6.5) and in expressions (6.7)–(6.11) are denoted by $c_{ijk\ell}^{\overline{\text{TI}}}$. However—even though the former are a special case of the latter and both share the same material symmetry—they correspond to distinct media, as shown by different expressions on the right-hand sides of the corresponding equations in systems (6.1)–(6.5) and (6.7)–(6.11).

To quantify the strength of anisotropy of transversely isotropic media, we invoke the three Thomsen [1986] parameters that are zero for isotropy and have absolute values much less than one for weak anisotropy,

$$\gamma := \frac{c_{1212}^{\overline{\text{TI}}} - c_{2323}^{\overline{\text{TI}}}}{2c_{2323}^{\overline{\text{TI}}}}, \tag{6.12}$$

$$\delta := \frac{\left(c_{1133}^{\overline{\text{TI}}} + c_{2323}^{\overline{\text{TI}}}\right)^2 - \left(c_{3333}^{\overline{\text{TI}}} - c_{2323}^{\overline{\text{TI}}}\right)^2}{2c_{3333}^{\overline{\text{TI}}} \left(c_{3333}^{\overline{\text{TI}}} - c_{2323}^{\overline{\text{TI}}}\right)}, \tag{6.13}$$

$$\varepsilon := \frac{c_{1111}^{\overline{\text{TI}}} - c_{3333}^{\overline{\text{TI}}}}{2c_{3333}^{\overline{\text{TI}}}}. \tag{6.14}$$

To examine the effects of anisotropy, we study dispersion curves for the closest isotropic counterpart, as formulated by Voigt [1910]; this formulation is an isotropic case of the Gazis et al. [1963] average. The two elasticity parameters of the isotropic counterpart of a Backus medium are [Slawinski, 2018, equations (4.96) and (4.97)]

$$c_{1111}^{\overline{\text{iso}}} = \frac{1}{15}\left(8c_{1111}^{\overline{\text{TI}}} + 4c_{1133}^{\overline{\text{TI}}} + 8c_{2323}^{\overline{\text{TI}}} + 3c_{3333}^{\overline{\text{TI}}}\right) \tag{6.15}$$

and

$$c_{2323}^{\overline{\text{iso}}} = \frac{1}{15}\left(c_{1111}^{\overline{\text{TI}}} - 2c_{1133}^{\overline{\text{TI}}} + 5c_{1212}^{\overline{\text{TI}}} + 6c_{2323}^{\overline{\text{TI}}} + c_{3333}^{\overline{\text{TI}}}\right); \tag{6.16}$$

henceforth, this result is referred to as the Voigt medium.

6.3 Isotropic layers

6.3.1 Introduction

Our study of quasi-Rayleigh and Love waves is conducted by examining their dispersion relations. For a Voigt medium of thickness Z, density ρ^u, S-wave speed $\beta^u = \sqrt{c^u_{2323}/\rho^u}$ and P-wave speed $\alpha^u = \sqrt{c^u_{1111}/\rho^u}$, overlying an isotropic halfspace with density ρ^d, S-wave speed $\beta^d = \sqrt{c^d_{2323}/\rho^d}$ and P-wave speed $\alpha^d = \sqrt{c^d_{1111}/\rho^d}$, the dispersion relations for Love and quasi-Rayleigh waves are given in equations (2) and (17), respectively, of Dalton et al. [2017]. Herein, these relations are coded in Mathematica® and the dispersion curves are plotted as zero contours of the respective dispersion relations, which are purely real.

For the Backus [1962] average of a stack of isotropic layers, the dispersion relations for quasi-Rayleigh and Love waves are given by setting to zero the determinants of the matrices in equations (29) and (30), respectively, of Khojasteh et al. [2008]. These relations can also be derived by setting to zero the thickness of the liquid layer in equations (22) and (23) of Bagheri et al. [2015]. In a manner analogous to expressions (2) and (17) of Dalton et al. [2017], the properties of the Backus medium consist of its thickness, mass density and five elasticity parameters of a transversely isotropic continuum, c_{1111}, c_{1133}, c_{1133}, c_{1212}, c_{2323}. Again, these relations are coded in Mathematica®, but the dispersion curves are plotted as zero contours of the sum of the real and imaginary parts of the respective determinants.

An insight into the dispersion relations based on the Backus [1962] average is provided by comparing their curves to the dispersion curves computed for a stack of layers from which the Backus medium is obtained by averaging their properties. For a stack of isotropic layers overlying an isotropic halfspace, the dispersion relations for Love and quasi-Rayleigh waves are based on a propagator matrix, more specifically, on the delta-matrix solution
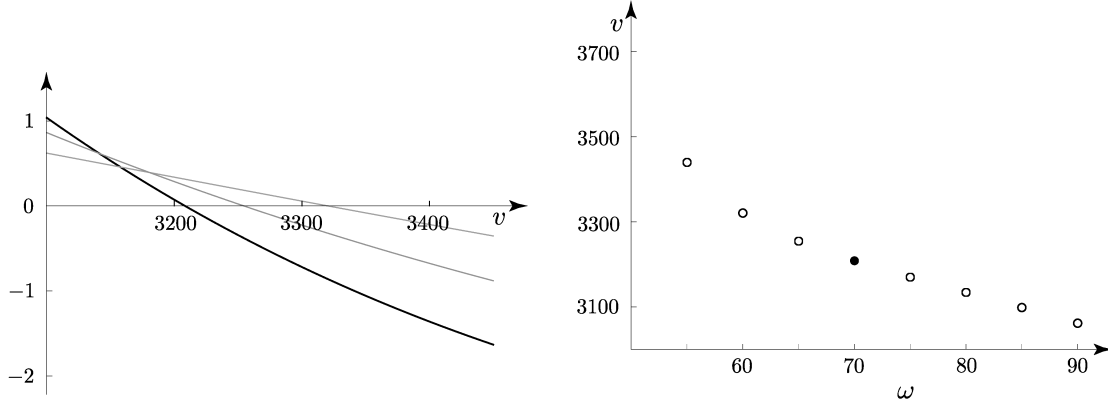
Figure 6.1: Dispersion curve obtained by solving the dispersion relation for v, with a given value of ω

reviewed by Buchen and Ben-Hador [1996]. These relations are coded in Python®.

In contrast to the Backus [1962] average, the propagator matrix allows us to combine information about all layers while retaining their individual properties. To illustrate the root-finding process, we consider, in the left-hand plot of Figure 6.1, the values of the determinant for the dispersion relation as a function of speed. Each curve corresponds to a distinct value of ω; the black curve corresponds to $\omega = 70\,\mathrm{s}^{-1}$. For each curve, the solution corresponds to v for which the determinant is equal to zero. The right-hand plot is a dispersion curve, where each point, (ω, v), is a solution from the left-hand plot; the black dot at $\omega = 70\,\mathrm{s}^{-1}$ corresponds to the zero intercept of the black curve. More details are included in Meehan [2017, 2018].

6.3.2 Weak inhomogeneity

Let us consider a weakly inhomogeneous stack of isotropic layers, whose elasticity parameters and corresponding velocities are given in Table 6.1.

Following expressions (6.1)–(6.5), we obtain $c^{\overline{\mathrm{TI}}}_{1111} = 18.84$, $c^{\overline{\mathrm{TI}}}_{1133} = 10.96$, $c^{\overline{\mathrm{TI}}}_{1212} = 3.99$, $c^{\overline{\mathrm{TI}}}_{2323} = 3.38$ and $c^{\overline{\mathrm{TI}}}_{3333} = 18.43$; these values are to be multiplied by 10^6, and their units are $\mathrm{m}^2\,\mathrm{s}^{-2}$.

148

layer	c_{1111}	c_{2323}	v_P	v_S
1	10.56	2.02	3.25	1.42
2	20.52	4.45	4.53	2.11
3	31.14	2.89	5.58	1.70
4	14.82	2.62	3.85	1.62
5	32.15	2.92	5.67	1.71
6	16.00	2.56	4.00	1.60
7	16.40	6.35	4.05	2.52
8	18.06	4.33	4.25	2.08
9	31.47	8.01	5.61	2.83
10	17.31	3.76	4.16	1.94

Table 6.1: Density-scaled elasticity parameters, $\times 10^6\,\mathrm{m^2\,s^{-2}}$, for a weakly inhomogeneous stack of isotropic layers, and the corresponding *P*-wave and *S*-wave velocities, $\mathrm{km\,s^{-1}}$ [Brisco, 2014, Slawinski, 2018]

The nearest isotropic tensor, whose parameters are $c_{1111}^{\overline{\mathrm{iso}}} = 18.46 \times 10^6$ and $c_{2323}^{\overline{\mathrm{iso}}} = 3.71 \times 10^6$, is obtained using expressions (6.15) and (6.16). The corresponding *P*-wave and *S*-wave speeds—which are the square roots of these parameters—are $v_P = 4.30\,\mathrm{km\,s^{-1}}$ and $v_S = 1.93\,\mathrm{km\,s^{-1}}$.

Following expressions (6.12), (6.13) and (6.14), we obtain $\gamma = 0.09$, $\delta = -0.04$ and $\varepsilon = 0.01$. Since these values are close to zero, we conclude that—for the layer parameters in Table 6.1—the resulting Backus medium is only weakly anisotropic, as expected in view of Adamus et al. [2018].

6.3.3 Strong inhomogeneity

Let us consider a strongly inhomogeneous stack of alternating isotropic layers, whose elasticity parameters and velocities are given in Table 6.2.

Following expressions (6.1)–(6.5), we obtain $c_{1111}^{\overline{\mathrm{TI}}} = 26.79$, $c_{1133}^{\overline{\mathrm{TI}}} = 3.48$, $c_{1212}^{\overline{\mathrm{TI}}} = 10.00$, $c_{2323}^{\overline{\mathrm{TI}}} = 6.40$ and $c_{3333}^{\overline{\mathrm{TI}}} = 15.21$; these values are to be multiplied by 10^6, and their units are $\mathrm{m^2\,s^{-2}}$. Following expressions (6.15) and (6.16), we obtain $c_{1111}^{\overline{\mathrm{iso}}} = 21.67 \times$

layer	c_{1111}	c_{2323}	v_P	v_S
1	9	4	3	2
2	49	16	7	4
3	9	4	3	2
4	49	16	7	4
5	9	4	3	2
6	49	16	7	4
7	9	4	3	2
8	49	16	7	4
9	9	4	3	2
10	49	16	7	4

Table 6.2: Density-scaled elasticity parameters, $\times 10^6 \, \mathrm{m}^2 \, \mathrm{s}^{-2}$, for a strongly inhomogeneous stack of alternating isotropic layers, and the corresponding P-wave and S-wave velocities, $\mathrm{km \, s}^{-1}$
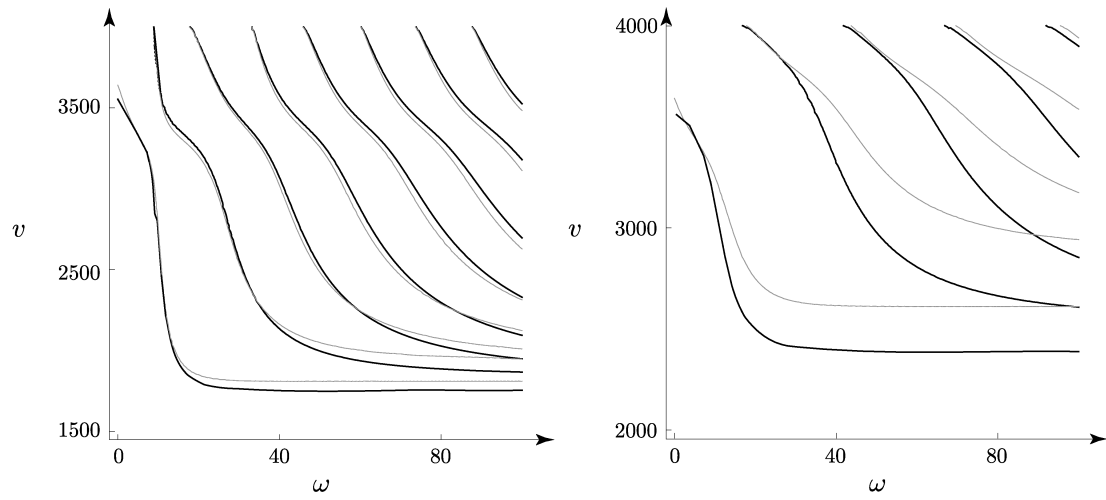

Figure 6.2: quasi-Rayleigh wave dispersion curves for the Backus medium and the Voigt medium, shown as black and grey lines, respectively.
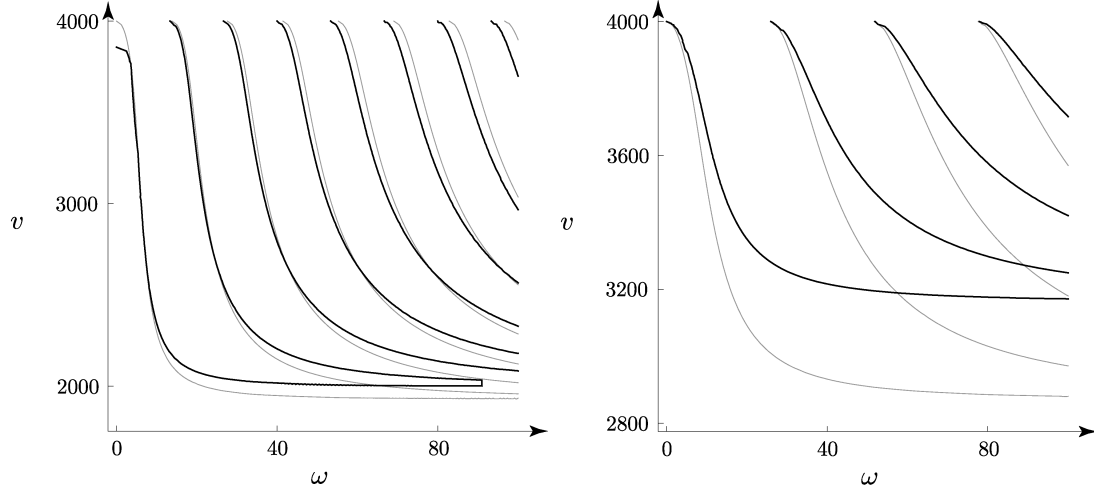
Figure 6.3: Love wave dispersion curves for the Backus medium and the Voigt medium, shown as black and grey lines, respectively

10^6 and $c_{2323}^{\overline{\text{iso}}} = 8.23 \times 10^6$, and the corresponding P-wave and S-wave speeds are $v_P = 4.66\,\text{km}\,\text{s}^{-1}$ and $v_S = 2.87\,\text{km}\,\text{s}^{-1}$.

Following expressions (6.12), (6.13) and (6.14), we obtain $\gamma = 0.28$, $\delta = 0.08$ and $\varepsilon = 0.38$. Since these values are not close to zero, we conclude that—for the layer parameters in Table 6.2—the resulting Backus medium is strongly anisotropic, as expected in view of Adamus et al. [2018].

6.3.4 Discussion

Figures 6.2–6.9 illustrate the dispersion relations for Love and quasi-Rayleigh waves for Backus media that are averages of isotropic layers, for Voigt media that are averages of these Backus media, and for delta-matrix solutions for the stack of these layers. In each figure, the left-hand plot is for a weakly anisotropic Backus medium and the right-hand plot is for a strongly anisotropic Backus medium; they are compared with either a Voigt medium or a delta-matrix solution.

In each plot, the lowest curve corresponds to the fundamental mode of a guided wave,
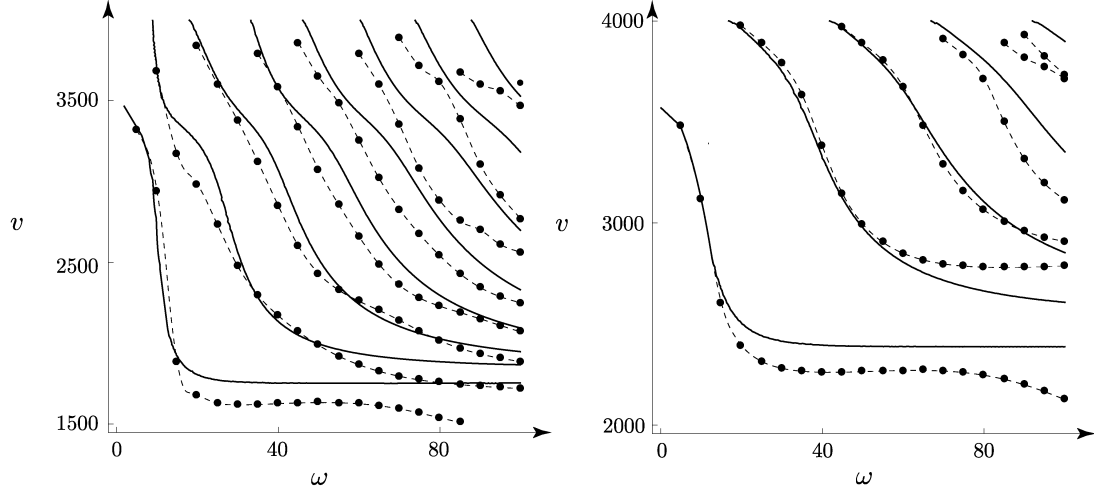
Figure 6.4: quasi-Rayleigh wave dispersion curves for the Backus medium and the delta-matrix solution, shown as black lines and points, respectively, for layers that are 50 m thick

the next curve to its first mode, and so on. For the fundamental mode, the speed values correspond to all frequencies, $(0, \infty)$; higher modes have cutoff frequencies; the speeds of these modes correspond to (ω_0, ∞), where $\omega_0 > 0$. At the zero-frequency limit, the dispersion relation is affected only by properties of the halfspace; at the high-frequency limit, it is affected only by properties of the overlying medium; the intermediate region is affected by properties of the entire model. For the quasi-Rayleigh wave, the lower limit is the value of the Rayleigh-wave speed in the halfspace. For the Love wave, it is the S-wave speed in the halfspace. These issues are discussed by Dalton et al. [2017] and Udías [1999, p. 201]. However, even the highest frequency available in a seismic signal might not allow us to observe the effects due only to the overlying medium.

For both weakly and strongly anisotropic media, the mass density of the halfspace, which is isotropic, is $\rho^d = 2600 \text{ kg/m}^3$, and its elasticity parameters are $c^d_{1111} = 10.99 \times 10^{10} \text{ N/m}^2$ and $c^d_{2323} = 4.16 \times 10^{10} \text{ N/m}^2$. The mass density of the layers—and, hence, of the resulting medium—is $\rho^u = 2200 \text{ kg/m}^3$. In Figures 6.2–6.5, the medium overlying the isotropic halfspace is 500 m thick; in Figures 6.6 and 6.7, it is 100 m thick; in Figures 6.8

Figure 6.5: Love wave dispersion curves for the Backus medium and the delta-matrix solution, shown as black lines and points, respectively, for layers that are 50 m thick
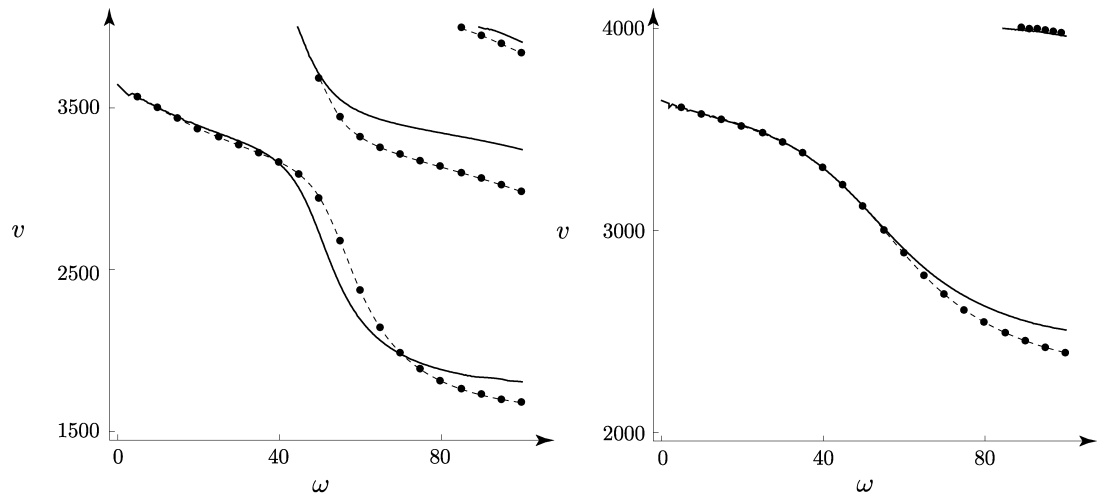
Figure 6.6: quasi-Rayleigh wave dispersion curves for the Backus medium and the delta-matrix solution, shown as black lines and points, respectively, for layers that are 10 m thick

153

Figure 6.7: Love wave dispersion curves for the Backus medium and the delta-matrix solution, shown as black lines and points, respectively, for layers that are 10 m thick

Figure 6.8: quasi-Rayleigh wave dispersion curves for the Backus medium and the delta-matrix solution, shown as black lines and points, respectively, for layers that are 5 m thick
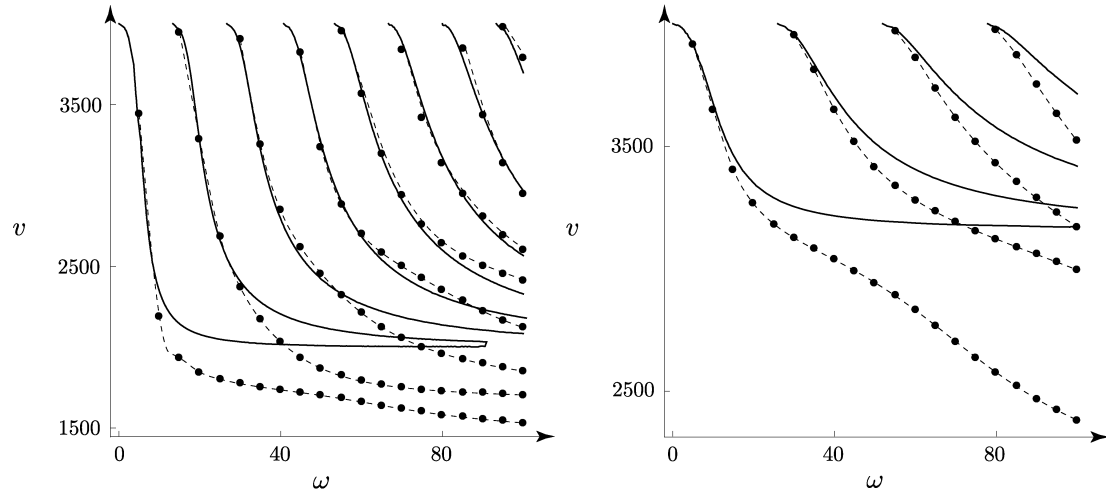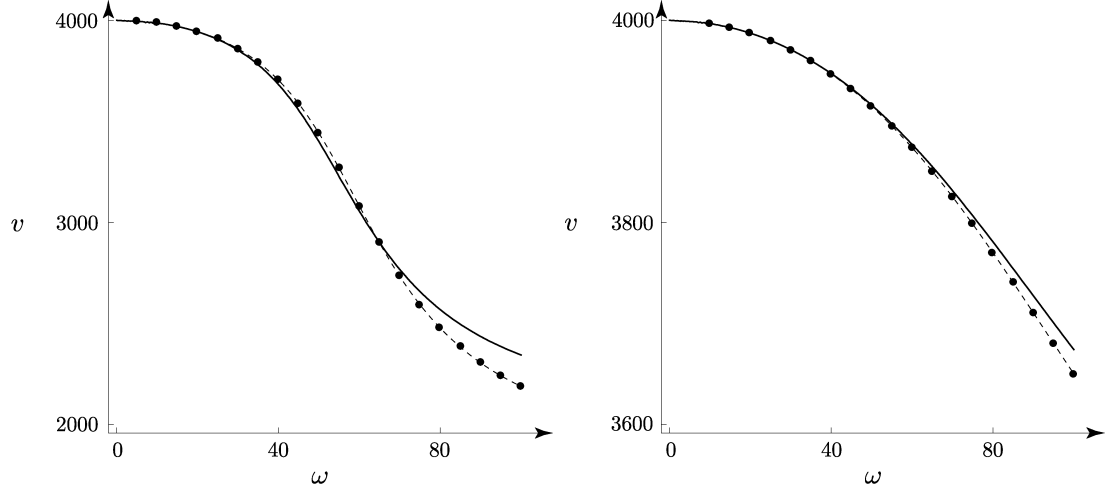
Figure 6.9: Love wave dispersion curves for the Backus medium and the delta-matrix solution, shown as black lines and points, respectively, for layers that are 5 m thick
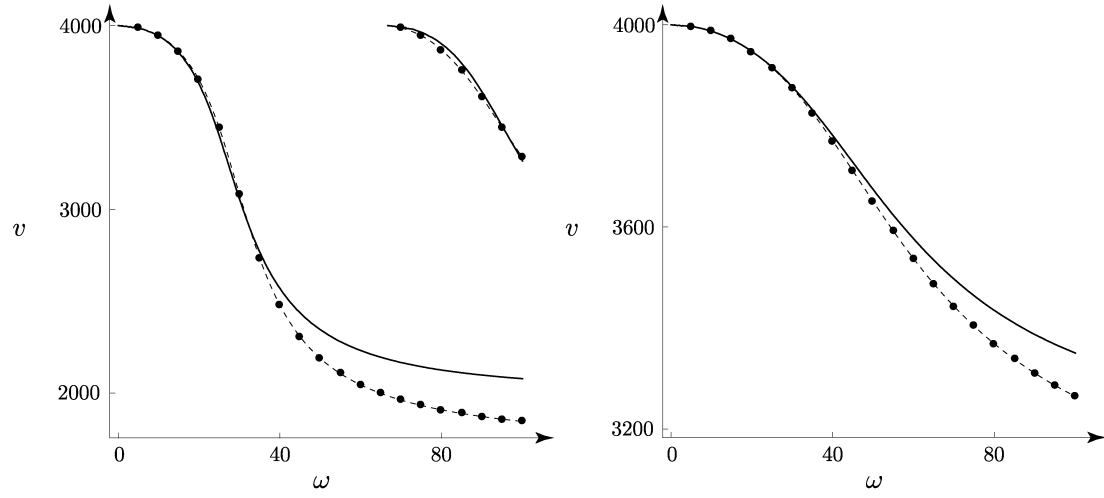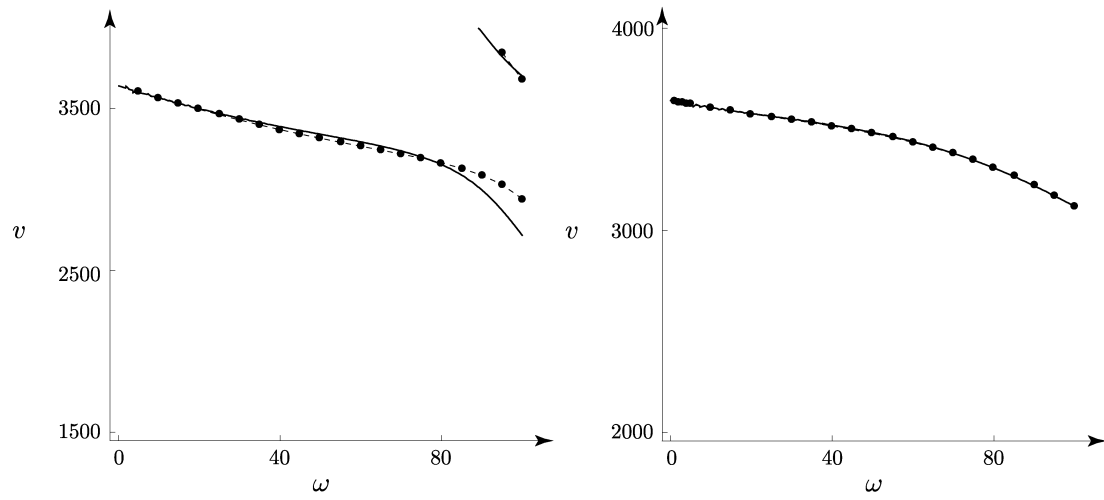
and 6.9, it is 50 m thick. Since, in each case, the Backus [1962] average is taken over ten layers, the resulting Backus-medium parameters are not affected by the value of the total thickness, as illustrated by expression (6.6). This value, however, affects the dispersion relations, as exemplified—for the isotropic case—by the presence of Z in expressions (2) and (17) of Dalton et al. [2017].

Examining Figures 6.2 and 6.3, we observe the effect of inhomogeneity on the dispersion curves of the quasi-Rayleigh and Love waves. As illustrated by the similarity of curves for the Backus and Voigt media, in the left-hand plots, the effect is negligible under weak inhomogeneity, which—for the Backus [1962] average—becomes weak anisotropy. As indicated by the discrepancy between these curves, in the right-hand plots, the effect, which is negligible near the cutoff frequency, becomes pronounced with the increase of frequency. The match is good at lower frequencies, since the dispersion relation is dominated by properties of the halfspace.

Examining Figures 6.4, 6.6 and 6.8, we see that there is a good match between the Backus media—both weakly and strongly anisotropic—and the delta-matrix solutions, but

only for thinner layers or lower frequencies. Also, there is a good match in the second, third, and fourth modes for frequencies near the cutoff frequency for the thick layers in Figure 6.4, where the speed approaches the *S*-wave speed in the halfspace. A similar pattern appears in Figures 6.5, 6.7 and 6.9.

Since both quasi-Rayleigh and Love waves exist in the model consisting of the same parameters, we can examine distinct dispersion relations that correspond to the same model. These are shown in Figures 6.4 and 6.5, Figures 6.6 and 6.7, Figures 6.8 and 6.9; each respective pair corresponds to a model of 50 m, 10 m and 5 m thick layers. Examining Figures 6.4 and 6.5, for instance, we see that—for both weak and strong inhomogeneity— the match between the results of the Backus [1962] average and the propagator matrix appears to be better for all modes of the Love wave, only at lower frequencies, but, in the case of the quasi-Rayleigh wave, extends to higher frequencies.

6.4 Transversely isotropic layers

6.4.1 Introduction

As in Section 6.3, for the Backus [1962] average of a stack of transversely isotropic layers, the dispersion relations for quasi-Rayleigh and Love waves are given by setting to zero the determinants of the matrices in equations (29) and (30), respectively, of Khojasteh et al. [2008]. The halfspace can be isotropic, in which case its properties are the same as in expressions (2) and (17) of Dalton et al. [2017], or transversely isotropic.

For a stack of transversely isotropic layers overlying a transversely isotropic halfspace, the dispersion relation for quasi-Rayleigh waves is based on the reduced-delta-matrix solution of Ikeda and Matsuoka [2013], and the dispersion relation for Love waves is based on the delta-matrix solution reviewed by Buchen and Ben-Hador [1996], but with pseudorigidity and pseudothickness defined by Anderson [1962]. These relations are coded in Python[®].

layer	c_{1111}	c_{1133}	c_{3333}	c_{2323}	c_{1212}
1	8.06	2.46	7.08	1.86	2.35
2	13.73	5.75	16.77	5.55	3.56
3	8.06	2.46	7.08	1.86	2.35
4	13.73	5.75	16.77	5.55	3.56
5	8.06	2.46	7.08	1.86	2.35
6	13.73	5.75	16.77	5.55	3.56
7	8.06	2.46	7.08	1.86	2.35
8	13.73	5.75	16.77	5.55	3.56
9	8.06	2.46	7.08	1.86	2.35
10	13.73	5.75	16.77	5.55	3.56

Table 6.3: Density-scaled elasticity parameters, whose units are $10^6 \, \mathrm{m^2 s^{-2}}$, for a stack of alternating transversely isotropic layers

The algorithm is similar to the delta-matrix solution, except for expressions of transversely isotropic continua, which contain five elasticity parameters, as derived by Anderson [1962] and Ikeda and Matsuoka [2013].

6.4.2 Alternating layers on isotropic halfspace

Let us consider a stack of alternating transversely isotropic layers, given in Table 6.3, where the parameters of the odd-numbered layers are from tensor C_a^{TI} of Danek et al. [2018] and the parameters of the even-numbered layers are twice those of the tensor C_{bb}^{TI} of Danek et al. [2018]. We chose these parameters to illustrate varying levels of anisotropy, quantified by parameters (6.12), (6.13) and (6.14). We set the mass density of the layers to $2200 \, \mathrm{kg/m^3}$, and use the same halfspace parameters as in Section 6.3.

Following expressions (6.7)–(6.11), we obtain $c_{1111}^{\overline{\mathrm{TI}}} = 10.67$, $c_{1133}^{\overline{\mathrm{TI}}} = 3.44$, $c_{1212}^{\overline{\mathrm{TI}}} = 2.95$, $c_{2323}^{\overline{\mathrm{TI}}} = 2.79$ and $c_{3333}^{\overline{\mathrm{TI}}} = 9.96$; these values are multiplied by 10^6, and their units are $\mathrm{m^2 s^{-2}}$. Following expressions (6.15) and (6.16), we have $c_{1111}^{\overline{\mathrm{iso}}} = 10.09 \times 10^6$ and $c_{2323}^{\overline{\mathrm{iso}}} = 3.02 \times 10^6$, respectively, which correspond to $v_P = 3.27 \, \mathrm{km \, s^{-1}}$ and $v_S = 1.74 \, \mathrm{km \, s^{-1}}$. According to expressions (6.12), (6.13) and (6.14), $\gamma = 0.03$, $\delta = -0.09$ and $\varepsilon = 0.04$, re-
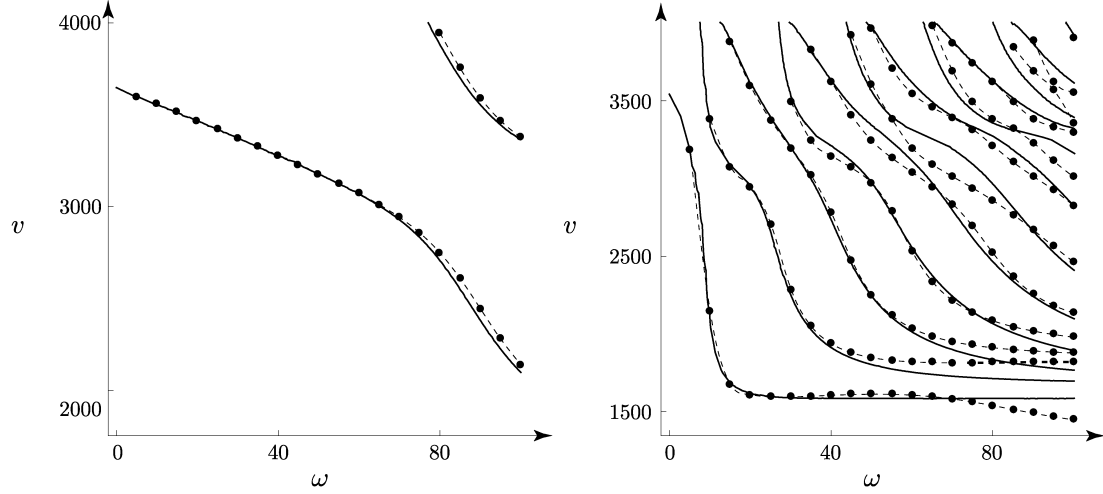
Figure 6.10: quasi-Rayleigh wave dispersion curves for the Backus medium and reduced-delta-matrix solution, shown as black lines and points, respectively

spectively. Since these values are close to zero, we conclude that—for the layer parameters in Table 6.3—the resulting Backus medium is only weakly anisotropic.

The quasi-Rayleigh wave dispersion curves for the stack of layers given in Table 6.3 are calculated using a Python[®] code [Meehan, 2017] based on the reduced-delta-matrix solution of Ikeda and Matsuoka [2013]. We compare these results to those obtained for the Backus medium of that stack by setting to zero the determinant of the matrix in equation (29) of Khojasteh et al. [2008]. The left-hand plot of Figure 6.10 depicts the results for a stack of layers that are 5 m thick and the right-hand plot for a stack of layers that are 50 m thick. As expected, the match is better for thin layers or low frequencies, and also near cutoff frequencies.

We also calculate Love wave dispersion curves for the same stack of layers using the delta-matrix solution reviewed by Buchen and Ben-Hador [1996], but with the pseudo-rigidity and pseudothickness defined by Anderson [1962]. We compare these results to those obtained for the Backus medium of that stack by setting the determinant of the matrix in equation (30) of Khojasteh et al. [2008] to zero. The left-hand plot of Figure 6.11 depicts
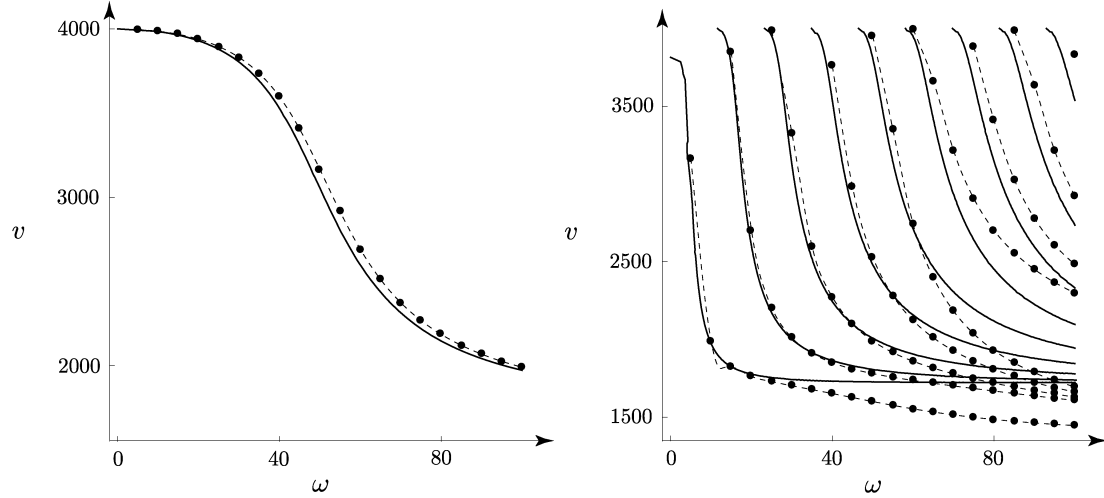
158

Figure 6.11: Love wave dispersion curves for the Backus medium and delta-matrix solution, shown as black lines and points, respectively

the results for a stack of layers that are 5 m thick and the right-hand plot for a stack of layers that are 50 m thick. Again, as expected, the match is better for thin layers or low frequencies, and it is also good near cutoff frequencies.

The left-hand plots of Figures 6.10 and 6.11 correspond to one model; the right-hand plots correspond to another model. Thus, we can examine the match between the results of the Backus [1962] average and the propagator matrix for stacks of layers that are 5 m and 50 m thick. For 5 m layers, the match is good, at all frequencies, for both quasi-Rayleigh and Love waves. For 50 m layers, the match is good for both waves at lower frequencies; at higher frequencies, the match is better for the quasi-Rayleigh wave.

6.4.3 Nonalternating layers on transversely isotropic halfspace

Let us examine the model of twenty transversely isotropic layers overlying a transversely isotropic halfspace used in Harkrider and Anderson [1962] and in Ikeda and Matsuoka [2013]. The mass densities and elasticity parameters of this model are given in Table 6.4.[*]

---

[*]In calculating c_{1133}, we note an error in Anderson [1961]. In his formula for c_{13}, on page 2955, $(1/2)(c_{11} - c_{33})^2$ should be $\left((1/2)(c_{11} - c_{33})\right)^2$. It can be confirmed by equations (9.2.19) and (9.2.23)

159

To compute the mean density, we use

$$\rho^{\overline{\text{TI}}} = \overline{\rho} = \frac{1}{n}\sum_{i=1}^{n}\rho_i.$$ (6.17)

We examine Figure 6.12 to see that—for the case of layers that are 1 m thick, illustrated in the left-hand plot—the results for the Backus medium match the results for the delta-matrix solution for $\omega < 70 \text{ s}^{-1}$. This frequency corresponds to the wavelength of about 160 m, which is greater than the thickness of the twenty-layer stack and much greater than the thickness of individual layers. For the case of layers that are 5 m thick, illustrated in the right-hand plot, the results match only for the fundamental mode and for $\omega < 15 \text{ s}^{-1}$, which corresponds to a wavelength of about 700 m. Again, this wavelength is greater than the thickness of the twenty-layer stack and much greater than the thickness of individual layers.

Backus [1962] derives the average under the assumption of $\kappa\ell' \ll 1$, where $\kappa = \omega/v$ and ℓ' is the averaging width, as discussed by Bos et al. [2017a]. However note that, as discussed on page 19, if the arithmetic average is used over a stack of layers that has a height of Z, so that the averaging function is a boxcar with a height of Z, then $\ell' = Z/(2\sqrt{3})$. For 1 m layers, $\omega = 70 \text{ s}^{-1}$ and $v = 1760 \text{ m/s}$, we have $\kappa Z = 0.80$ and $\kappa\ell' = 0.24$. For 5 m layers, $\omega = 15 \text{ s}^{-1}$ and $v = 1760 \text{ m/s}$, we have $\kappa Z = 0.85$ and $\kappa\ell' = 0.25$. In both cases, the Backus [1962] average performs better than could be expected in view of its underlying assumption.

This model does not include values of c_{1212} or c_{1122}, so we are unable to generate its Love-wave dispersion curves, which would be the counterparts of Figure 6.12. Thus, herein, we cannot compare the behaviours of the quasi-Rayleigh and Love waves for non-alternating layers overlying a transversely isotropic halfspace.

---

of Slawinski [2015], with $n_3 = \sqrt{2}/2$.

layer	ρ	c_{1111}	c_{1133}	c_{3333}	c_{2323}
1	2000	2.90	2.63	2.90	0.14
2	2000	4.43	3.62	4.43	0.40
3	2000	3.88	1.74	3.88	1.07
4	2250	5.80	1.30	5.80	2.25
5	2250	6.50	8.37	5.89	2.65
6	2250	6.50	1.06	5.89	2.54
7	2250	7.25	1.64	6.57	2.54
8	2250	7.25	1.23	6.57	2.01
9	2250	7.83	2.04	4.92	2.25
10	2250	7.83	1.44	4.92	2.54
11	2250	9.00	-4.27	5.65	4.52
12	2250	11.33	-1.98	7.12	4.52
13	2500	37.97	20.69	36.07	6.45
14	2500	73.12	51.02	69.46	6.83
15	2500	73.12	54.84	62.15	6.64
16	2500	73.12	54.84	62.15	6.64
17	2500	81.00	49.94	68.85	10.31
18	2500	78.32	52.56	66.57	7.84
19	2500	75.71	51.81	68.14	8.48
20	2500	93.54	70.12	84.19	7.43
H	2600	101.08	71.02	90.97	10.40

Table 6.4: Mass densities, in kg/m^3, and elasticity parameters, in $10^9 \, N/m^2$, of the Harkrider and Anderson [1962] model
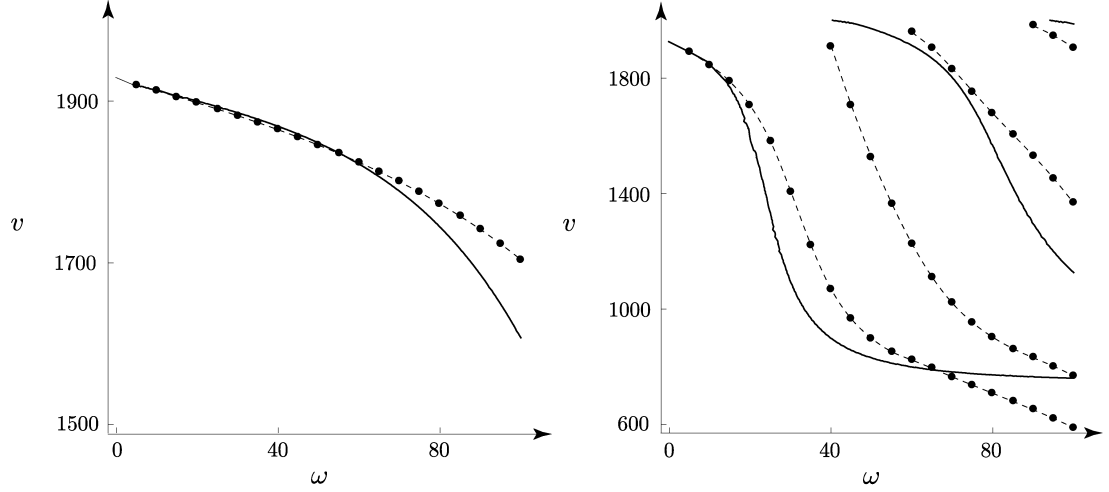
Figure 6.12: quasi-Rayleigh wave dispersion curves for the Backus medium of the Harkrider and Anderson [1962] model and the Ikeda and Matsuoka [2013] reduced-delta-matrix solution, shown as black lines and points, respectively

6.5   Conclusion

Comparing the modelling of guided waves using the Backus [1962] average to modelling of these waves based on the propagator matrix, we obtain a good match for the fundamental mode in a weakly inhomogeneous stack of layers and, as expected, for low frequencies or thin layers.

For alternating layers, which is a common occurrence in sedimentary basins, the discrepancy between these two methods remains small, even for strong inhomogeneity. For higher modes, the difference remains small near the cutoff frequency.

For a stack of nonalternating transversely isotropic layers that is strongly inhomogeneous, the discrepancy is small only for the fundamental mode and for low frequencies or thin layers. The results become similar—even for higher frequencies—if the layers become thinner. Also, in such a case, similar results are obtained for $\kappa\ell' \lesssim 0.25$, in spite of the underlying assumption, $\kappa\ell' \ll 1$.

Let us comment on the results, in the context of conclusions presented in previous

162

works. Liner and Fei [2006] recommend the averaging length be less than or equal to one-third of the dominant seismic wavelength, which corresponds to $\kappa Z \leqslant 2$ or $\kappa \ell' \leqslant 0.6$. This is the point at which the fundamental mode solutions shown in the right-hand plot of Figure 6.6 begin to diverge from one another. However, upon examining Figures 6.4–6.12, we conclude that we do not have a single maximum value of κZ at which the solutions begin to diverge; it depends on the degree of inhomogeneity of the stack of layers and on whether it is an alternating or nonalternating stack of layers. For instance, for the fundamental mode, the maximum value of κZ ranges from 0.80, as is the case in the left-hand plot of Figure 6.12, to 20, in the right-hand plot of Figure 6.10. Yet, for Figures 6.4–6.12, the median value of κZ at which the solutions begin to diverge is 2, which is the value suggested by Liner and Fei [2006].

Mavko et al. [1998] suggest the necessity for layers to be at least ten times smaller than the seismic wavelength, $\lambda/h > 10$, where $\lambda = 2\pi v/\omega$, with v standing for the propagation speed of the quasi-Rayleigh or Love wave, and h being the layer thickness. Again, examining Figures 6.4–6.12, we conclude that we do not have a single minimum λ/h ratio, at which the solutions begin to diverge. For instance, for the fundamental mode, the minimum value of λ/h ranges from 3, in the right-hand plot of Figure 6.10, to 150, in the left-hand plot of Figure 6.12. For Figures 6.4–6.12, the median value of λ/h at which the solutions begin to diverge is 28, which is of the same order of magnitude as the value suggested by Mavko et al. [1998].

Capdeville et al. [2013] state that the Backus [1962] average is applicable only to a fine-scale layered medium, far from the free surface and from the source. Our results are consistent with the first part of that statement. However, in contrast to the middle part of that statement, for most cases, we obtain satisfactory results, even in proximity of the free surface. Results are degraded for the Harkrider and Anderson [1962] model due to near-surface low-velocity layers. In this study, we cannot examine the last part of that statement,

which is the issue of source proximity.

In Bos et al. [2017a], which is, in slightly modified form, Chapter 2 of this thesis, we say that the Backus [1962] average is applicable only for perpendicular incidence, or nearly so. However some testing in Dalton and Slawinski [2016] indicates that the traveltimes for oblique incidence are not much in error if the weighting is by layer thickness, but are more accurate if the weighting is by distance travelled in each layer. But why then do we get results for guided waves almost as good as those for body waves discussed by Mavko et al. [1998]? Perhaps it is because the guided waves can be considered as the result of interference of totally internally reflected upgoing and downgoing obliquely propagating body waves.

In comparing the results obtained for a Backus medium to the results obtained for a Voigt medium, we can treat the latter as an approximation of the former. Both are viewed as analogies for the behaviour of seismic waves in thinly layered media. It is not the case in comparing the results obtained for a Backus medium to the results obtained with a propagator matrix. The latter is not restricted to the assumption of $\kappa \ell' \ll 1$, which is essential for the Backus [1962] average. The purpose of this average is not to provide information about the material itself, but to model the response of a seismic signal. As such, the frequency at which the discrepancy between the results obtained for a Backus medium and the results obtained with a propagator matrix becomes significant can be interpreted as the frequency beyond which the Backus [1962] average ceases to be empirically adequate in the context of seismology. The adequacy of the propagator matrix, on the other hand, depends on the frequency content of a seismic signal, but is not limited by it.

Results of this study, in particular empirical adequacy of modelling techniques, allow us to gain an insight, especially in regard to how good an approximation by a single layer over a halfspace is, into the reliability of a joint inverse of the quasi-Rayleigh and Love dispersion curves for obtaining model parameters. A work on that subject is presented by

Bogacz et al. [2018], which is, in slightly modified form, Chapter 5 of this thesis.

In this chapter the propagator matrix results are more accurate for all frequencies, but the Backus average results are adequate for low frequencies and would result in a saving in computation time for a large number of layers at low frequencies. Also the Backus average approach allows us to determine how good the model of a single layer over a halfspace is. This chapter proves quantitatively, not just qualitatively, that for low frequencies and/or thin layers the dispersion curves for a stack of layers are equivalent to those for the Backus medium.

Acknowledgments

6.6 References

F. P. Adamus, M. A. Slawinski, and T. Stanoev. On effects of inhomogeneity on anisotropy in Backus average. *arXiv*, 1802.04075([physics.geo-ph]):1–9, 2018.

D. L. Anderson. Elastic wave propagation in layered anisotropic media. *J. Geophys. Res.*, 66:2953–2964, 1961.

D. L. Anderson. Love wave dispersion in heterogeneous anisotropic media. *Geophysics*, 27(4):445–454, 1962.

G. E. Backus. Long-wave elastic anisotropy produced by horizontal layering. *J. Geophys. Res.*, 67(11):4427–4440, 1962.

A. Bagheri, S. Greenhalgh, A. Khojasteh, and M. Rahimian. Dispersion of Rayleigh, Scholte, Stoneley and Love waves in a model consisting of a liquid layer overlying a two-layer transversely isotropic solid medium. *Geophys. J. Int.*, 203:195–212, 2015.

A. Bogacz, D. R. Dalton, T. Danek, K. Miernik, and M. A. Slawinski. On Pareto Joint Inversion of guided waves. *arXiv*, 1712.09850:[physics.geo–ph], 2018.

L. Bos, D. R. Dalton, M. A. Slawinski, and T. Stanoev. On Backus average for generally anisotropic layers. *Journal of Elasticity*, 127(2):179–196, 2017a.

L. Bos, T. Danek, M. A. Slawinski, and T. Stanoev. Statistical and numerical considerations of Backus-average product approximation. *Journal of Elasticity*, DOI 10.1007/s10659-017-9659-9:1–16, 2017b.

C. Brisco. Anisotropy vs. inhomogeneity: Algorithm formulation, coding and modelling. Honours thesis, Memorial University, 2014.

P. W. Buchen and R. Ben-Hador. Free-mode surface-wave computations. *Geophys. J. Int.*, 124:869–887, 1996.

Y. Capdeville, É. Stutzmann, N. Wang, and J.-P. Montagner. Residual homogenization for seismic forward and inverse problems in layered media. *Geophys. J. Int.*, 194:470–487, 2013.

D. R. Dalton and M. A. Slawinski. On Backus average for oblique incidence. *arXiv*, [physics.geo-ph](1601.02966v1), 2016.

D. R. Dalton, M. A. Slawinski, P. Stachura, and T. Stanoev. Sensitivity of Love and quasi-Rayleigh waves to model parameters. *The Quarterly Journal of Mechanics and Applied Mathematics*, 70(2):103–130, 2017.

T. Danek, A. Noseworthy, and M. A. Slawinski. Effects of norms on general Hookean solids for their isotropic counterparts. *Dolomites research notes on approximation*, 11: 15–28, 2018.

D. C. Gazis, I. Tadjbakhsh, and R. A. Toupin. The elastic tensor of given symmetry nearest to an anisotropic elastic tensor. *Acta Crystallographica*, 16(9):917–922, 1963.

D. G. Harkrider and D. L. Anderson. Computation of surface wave dispersion for multilay-ered anisotropic media. *Bulletin of the Seismological Society of America*, 52(2):321–332, 1962.

T. Ikeda and T. Matsuoka. Computation of Rayleigh waves on transversely isotropic media by the reduced delta matrix method. *Bulletin of the Seismological Society of America*, 103(3):2083–2093, 2013.

A. Khojasteh, M. Rahimian, R. Y. S. Pak, and M. Eskandari. Asymmetric dynamic Green's functions in a two-layered transversely isotropic half-space. *J. Eng. Mech.*, 134(9):777–787, 2008.

C. L. Liner and T. W. Fei. Layer-induced seismic anisotropy from full-wave sonic logs: theory, applications and validation. *Geophysics*, 71:D183–D190, 2006.

G. Mavko, T. Mukerji, and J. Dvorkin. *The Rock Physics Handbook*. Cambridge University Press, Cambridge, 1998.

T. B. Meehan. Python[®] code for calculating surface wave dispersion curves. https://github.com/tbmcoding/dispersion, December 2017.

T. B. Meehan. Evolution of the propagator matrix method and its implementation in seismology. *arXiv*, 1801.04635([physics.geo-ph]):1–12, January 2018.

G. W. Postma. Wave propagation in a stratified medium. *Geophysics*, 20:780–806, 1955.

M. A. Slawinski. *Waves and rays in elastic continua*. World Scientific, Singapore, 3rd edition, 2015.

M. A. Slawinski. *Waves and rays in seismology: Answers to unasked questions*. World Scientific, 2nd edition, 2018.

L. Thomsen. Weak elastic anisotropy. *Geophysics*, 51(10):1954–1966, 1986.

A. Udías. *Principles of seismology*. Cambridge University Press, 1999.

W. Voigt. *Lehrbuch der Kristallphysik*. Teubner, Leipzig, 1910.

Chapter 7

Summary and conclusions

7.1 Summary

In this thesis and in the papers on which it is based, we have derived expressions for elasticity parameters of a homogeneous generally anisotropic medium that is long-wave equivalent to a stack of thin generally anisotropic layers. We have shown how the generally anisotropic formulation is simplified in the case of monoclinic layers and in the case of orthotropic layers. We also examine the mathematical underpinnings of the formulation, including the validity of the product approximation. Afterwards, this validity has been extended further by Bos et al. [2017b].

We also examine commutativity and noncommutativity of translational averages over a spatial variable and rotational averages over a symmetry group at a point. There is very near commutativity in the case of weak anisotropy, which is common in near-surface seismology. Indeed, surprisingly, a perturbation of the elasticity parameters about a point of weak anisotropy results in the commutator of the two types of averaging being of the order of the square of the perturbation, when one might expect that it would be just the order of the perturbation itself.

We review forward-modelling expressions for Love and quasi-Rayleigh waves and examine the sensitivity of Love and quasi-Rayleigh waves to model parameters. The fundamental mode is mainly sensitive to upper-layer parameters while higher modes are sensitive to both the upper-layer and halfspace properties. Within each mode the lower frequencies are more sensitive to the halfspace than are the higher frequencies. We also perform an analysis to deduce the optimum frequency to obtain the layer thickness from a given Love-wave mode.

We perform a Pareto Joint Inversion, using Particle Swarm Optimization, of synthetic dispersion-curve data to obtain model parameters including densities, elasticity parameters, and layer thickness. The inverted model parameters are accurate and stable without any further constraints. For velocities with errors, these parameters become significantly less accurate, which indicates the error-sensitivity of the process. Given real data with errors, it might be necessary to incorporate constraints such as estimated values of the layer elasticity parameters and/or thickness.

Finally, we tie together the two topics of Backus [1962] average and guided waves by examining the applicability of the Backus [1962] average in modelling of guided waves. Comparing the modelling of guided waves using the Backus [1962] average to modelling of these waves based on the propagator matrix, we obtain a good match for the fundamental mode in weak inhomogeneity of layers and, as expected, for low frequencies or thin layers. And it turns out that although Backus [1962] required the product of wavenumber and averaging thickness to satisfy $\kappa \ell' \ll 1$, even for our most strongly inhomogeneous model we obtain adequate results for $\kappa \ell' \lesssim 0.25$.

To our knowledge this is the only study since that of Anderson [1962] to test an equivalent medium formulation in the context of dispersion curve modelling. Anderson [1962] drew on the results of Postma [1955] to compare dispersion curves for a laminated (periodic) stack of isotropic layers over a halfspace to those for the equivalent transversely

170

isotropic medium over the same halfspace. We extend this work to quasi-Rayleigh waves and, drawing on the work of Backus [1962], to a nonalternating stack of isotropic layers. We broaden the scope to include Love waves for a stack of alternating transversely isotropic layers and quasi-Rayleigh waves for stacks of alternating and nonalternating transversely isotropic layers.

7.2   Future work

Some of the future work proposed in Section 2.6 has already been published or is in progress. Bos et al. [2017b] consider statistically and numerically the validity of the product approximation. Bos et al. [2018] study whether the Backus [1962] equivalent medium of a stack of strongly anisotropic layers, whose anisotropic properties are randomly different from each other, is isotropic, and determine that it is a very weakly anisotropic transversely isotropic medium. Kaderali, in his Ph.D. thesis, is currently applying the Backus average to well-log data. But the error-propagation analysis, an analysis of the effect of errors in layer parameters on the errors of the equivalent medium, using perturbation techniques, could still be performed.

The future work proposed in Section 4.5 has also been done, the inversion in Chapter 5 and the dispersion curve calculations for transversely isotropic layers in Chapter 6. But the inversion could be extended to transversely isotropic layers and/or more than two layers, and the dispersion curve calculations could be extended to orthotropic, monoclinic, or even generally anisotropic layers, perhaps using the formulation of Crampin [1970], if the problem that has with high frequency instability is solved by using modern computers with more precision.

As mentioned in Section 5.5, our guided-wave inverse solutions are obtained by considering a single mode at a time. Thus a method that could use several modes at once might

improve the results. The guided-wave inverse could also be extended to more than two layers, drawing on the work of Meehan [2017, 2018]. The guided-wave inverse could also be applied to real data.

The most complex case considered in Chapter 6 is a stack of transversely isotropic layers. This could be extended to orthotropic or monoclinic or even generally anisotropic layers, with the Backus [1962] average formulae taken from Chapter 2. The dispersion curves for the stack and for the Backus [1962] average layer could be obtained using the formulation of Crampin [1970]. Results of Chapter 3 could be drawn on to find dispersion curves for an effective medium of higher symmetry, as is done in Chapter 6 for the Voigt [1910] average.

We might be able to extend the results of Chapter 5 by relating the error in the data to the error in the inverted elasticity parameters, densities, and layer thickness.

Some of my coauthors have been examining surface waves in prestressed media and I might get involved in that.

7.3 Conclusions

Again, to our knowledge, this is the only study since that of Anderson [1962] to test an equivalent medium formulation in the context of dispersion curve modelling. But what are the results of our study in terms of the broader context of seismology? As stated in Section 6.5, upon examining Figures 6.4–6.12, we conclude that we do not have a single maximum value of κZ at which the solutions begin to diverge; it depends on the context. For instance, for the fundamental mode, the maximum value of κZ ranges from 0.80, which is equivalent to $\kappa \ell' = 0.24$, as is the case in the left-hand plot of Figure 6.12, to 20, in the right-hand plot of Figure 6.10. Yet, for Figures 6.4–6.12, the median value of κZ at which the solutions begin to diverge is 2, which is the value suggested by Liner and Fei [2006]

for body waves.

Examining Figures 6.4–6.12, we conclude that we do not have a single minimum λ/h ratio, at which the solutions begin to diverge. For instance, for the fundamental mode, the minimum value of λ/h ranges from 3, in the right-hand plot of Figure 6.10, to 150, in the left-hand plot of Figure 6.12. For Figures 6.4–6.12, the median value of λ/h at which the solutions begin to diverge is 28, which is of the same order of magnitude as the value of ten suggested by Mavko et al. [1998] for body waves. The fact that it is greater, and hence the performance of the Backus average is not as good for guided waves as for body waves, may be due to the fact that the Backus average assumes perpendicular incidence or nearly so, and guided waves can be considered as resulting from interference of obliquely propagating upgoing and downgoing totally internally reflected body waves.

Capdeville et al. [2013] state that the Backus [1962] average is applicable only to a fine-scale layered medium, far from the free surface and from the source. Our results are consistent with the first part of that statement. However, in contrast to the middle part of that statement, for most cases, we obtain satisfactory results, even in proximity of the free surface. Results are degraded for *Model HA* due to near-surface low-velocity layers, but even for that case satisfactory results are obtained for $\kappa\ell' \lesssim 0.25$ despite the restriction of $\kappa\ell' \ll 1$ in the theory of Backus [1962].

In conclusion, the Backus [1962] average can be applied in modelling of guided-wave dispersion curves, especially in the case of a weakly inhomogeneous stack of layers and the case of an alternating stack of layers.

Overall Bibliography

F. P. Adamus, M. A. Slawinski, and T. Stanoev. On effects of inhomogeneity on anisotropy in Backus average. *arXiv*, 1802.04075([physics.geo-ph]):1–9, 2018.

D. L. Anderson. Elastic wave propagation in layered anisotropic media. *J. Geophys. Res.*, 66:2953–2964, 1961.

D. L. Anderson. Love wave dispersion in heterogeneous anisotropic media. *Geophysics*, 27(4):445–454, 1962.

V. M. Babich and A. P. Kiselev. *Elastic waves: High-frequency theory (in Russian).* BHV St. Petersburg, 2014.

G. E. Backus. Long-wave elastic anisotropy produced by horizontal layering. *J. Geophys. Res.*, 67(11):4427–4440, 1962.

A. Bagheri, S. Greenhalgh, A. Khojasteh, and M. Rahimian. Dispersion of Rayleigh, Scholte, Stoneley and Love waves in a model consisting of a liquid layer overlying a two-layer transversely isotropic solid medium. *Geophys. J. Int.*, 203:195–212, 2015.

A. Ben-Menahem and S. J. Singh. *Seismic waves and sources.* Dover, Mineola, N.Y., 2nd edition, 2000.

J. G. Berryman. Range of the *P*-wave anisotropy parameter for finely layered VTI media. *Stanford Exploration Project*, 93:179–192, 1997.

A. Bogacz, D. R. Dalton, T. Danek, K. Miernik, and M. A. Slawinski. On Pareto Joint Inversion of guided waves. *arXiv*, 1712.09850:[physics.geo–ph], 2018.

A. Bóna, I. Bucataru, and M. A. Slawinski. Space of $SO(3)$-orbits of elasticity tensors. *Archives of Mechanics*, 60(2):123–138, 2008.

W. L. Bond. The mathematics of the physical properties of crystals. *Bell System Technical Journal*, 22:1–72, 1943.

L. Bos, D. R. Dalton, M. A. Slawinski, and T. Stanoev. On Backus average for generally anisotropic layers. *Journal of Elasticity*, 127(2):179–196, 2017a.

L. Bos, T. Danek, M. A. Slawinski, and T. Stanoev. Statistical and numerical considerations of Backus-average product approximation. *Journal of Elasticity*, DOI 10.1007/s10659-017-9659-9:1–16, 2017b.

L. Bos, M. A. Slawinski, and T. Stanoev. On the Backus average of layers with randomly oriented elasticity tensors. *arXiv*, 1804.06891([physics.geo-ph]), 2018.

T. Boxberger, M. Picozzi, and S. Parolai. Shallow geology characterization using Rayleigh and Love wave dispersion curves derived from seismic noise array measurements. *Journal of Applied Geophysics*, 75:345–354, 2011.

C. Brisco. Anisotropy vs. inhomogeneity: Algorithm formulation, coding and modelling. Honours thesis, Memorial University, 2014.

P. W. Buchen and R. Ben-Hador. Free-mode surface-wave computations. *Geophys. J. Int.*, 124:869–887, 1996.

Y. Capdeville, L. Guillot, and J. J. Marigo. 1-D non-periodic homogenization for the wave equation. *Geophys. J. Int.*, 181:897–910, 2010a.

Y. Capdeville, L. Guillot, and J. J. Marigo. 2D nonperiodic homogenization to upscale elastic media for P-SV waves. *Geophys. J. Int.*, 182:903–922, 2010b.

Y. Capdeville, É. Stutzmann, N. Wang, and J.-P. Montagner. Residual homogenization for seismic forward and inverse problems in layered media. *Geophys. J. Int.*, 194:470–487, 2013.

J. M. Carcione, S. Picott, F. Cavallini, and J. E. Santos. Numerical test of the Schoenberg-Muir theory. *Geophysics*, 77(2):C27–C35, 2012.

C. H. Chapman. *Fundamentals of seismic wave propagation*. Cambridge University Press, 2004.

S. Crampin. The dispersion of surface waves in multilayered anisotropic media. *Geophysical Journal of the Royal Astronomical Society*, 21:387–402, 1970.

G. Dal Moro. Insights on surface wave dispersion and HVSR: Joint analysis via Pareto optimality. *Journal of Applied Geophysics*, 72:129–140, 2010.

G. Dal Moro and F. Ferigo. Joint analysis of Rayleigh- and Love-wave dispersion: Issues, criteria and improvements. *Journal of Applied Geophysics*, 75:573–589, 2011.

G. Dal Moro, R. M. M. Moura, and S. S. R. Moustafa. Multi-component joint analysis of surface waves. *Journal of Applied Geophysics*, 119:128–138, 2015.

D. R. Dalton and M. A. Slawinski. On Backus average for oblique incidence. *arXiv*, [physics.geo-ph](1601.02966v1), 2016.

D. R. Dalton, M. A. Slawinski, P. Stachura, and T. Stanoev. Sensitivity of Love and quasi-Rayleigh waves to model parameters. *The Quarterly Journal of Mechanics and Applied Mathematics*, 70(2):103–130, 2017.

T. Danek and M. A. Slawinski. Backus average under random perturbations of layered media. *SIAM Journal on Applied Mathematics*, 76(4):1239–1249, 2016.

T. Danek, M. Kochetov, and M. A. Slawinski. Uncertainty analysis of effective elasticity tensors using quaternion-based global optimization and Monte-Carlo method. *The Quarterly Journal of Mechanics and Applied Mathematics*, 66(2):253–272, 2013.

T. Danek, M. Kochetov, and M. A. Slawinski. Effective elasticity tensors in the context of random errors. *Journal of Elasticity*, 121(1):55–67, 2015a.

T. Danek, M. Kochetov, and M. A. Slawinski. Effective elasticity tensors in the context of random errors. *Journal of Elasticity*, 121(1):55–67, 2015b.

T. Danek, A. Noseworthy, and M. A. Slawinski. Effects of norms on general Hookean solids for their isotropic counterparts. *Dolomites research notes on approximation*, 11: 15–28, 2018.

H. Fang, H. Yao, H. Zhang, Y-C. Huang, and R. D. van der Hilst. Direct inversion of surface wave dispersion for three-dimensional shallow crustal structure based on ray tracing: methodology and application. *Geophys. J. Int.*, 201:1251–1263, 2015.

C. Y. Fu. Studies on seismic waves: II. Rayleigh waves in a superficial layer. *Geophysics*, 11(1):10–23, 1946.

D. C. Gazis, I. Tadjbakhsh, and R. A. Toupin. The elastic tensor of given symmetry nearest to an anisotropic elastic tensor. *Acta Crystallographica*, 16(9):917–922, 1963.

L. Guillot, Y. Capdeville, and J. J. Marigo. 2-D non periodic homogenization for the SH wave equation. *Geophys. J. Int.*, 182:1438–1454, 2010.

D. G. Harkrider and D. L. Anderson. Computation of surface wave dispersion for multilayered anisotropic media. *Bulletin of the Seismological Society of America*, 52(2):321–332, 1962.

N. A. Haskell. Dispersion of surface waves on multilayered media. *Bulletin of the Seismological Society of America*, 43:17–34, 1953.

K. Helbig. Elastischen Wellen in anisotropen Medien. *Getlands Beitr. Geophys.*, 67:256–288, 1958.

K. Helbig. Layer-induced anisotropy: Forward relations between constituent parameters and compound parameters. *Revista Brasileira de Geofísica*, 16(2–3):103–114, 1998.

K. Helbig. Inversion of compound parameters to constituent parameters. *Revista Brasileira de Geofísica*, 18(2):173–185, 2000.

K. Helbig and M. Schoenberg. Anomalous polarization of elastic waves in transversely isotropic media. *J. Acoust. Soc. Am.*, 81(5):1235–1245, 1987.

T. Ikeda and T. Matsuoka. Computation of Rayleigh waves on transversely isotropic media by the reduced delta matrix method. *Bulletin of the Seismological Society of America*, 103(3):2083–2093, 2013.

G. Ke, H. Dong, Å. Kristensen, and M. Thompson. Modified Thomson-Haskell matrix methods for surface-wave dispersion-curve calculation and their accelerated root-searching schemes. *Bulletin of the Seismological Society of America*, 101(4):1692–1703, 2011.

J. Kennedy and R. Eberhart. Particle swarm optimization. *Proc. IEEE Conf. on Neural Networks*, pages 1942–1948, 1995.

A. Khojasteh, M. Rahimian, R. Y. S. Pak, and M. Eskandari. Asymmetric dynamic Green's functions in a two-layered transversely isotropic half-space. *J. Eng. Mech.*, 134(9):777–787, 2008.

M. Kochetov and M. A. Slawinski. On obtaining effective orthotropic elasticity tensors. *The Quarterly Journal of Mechanics and Applied Mathematics*, 62(2):149–166, 2009a.

M. Kochetov and M. A. Slawinski. On obtaining effective transversely isotropic elasticity tensors. *Journal of Elasticity*, 94:1–13, 2009b.

D. Kumar. Applying Backus averaging for deriving seismic anisotropy of a long-wavelength equivalent medium from well-log data. *J. Geophys. Eng.*, 10:1–15, 2013.

A. W. Lee. The effect of geological structure upon microseismic disturbance. *Geophysical Journal International*, 3:85–105, 1932.

C. L. Liner and T. W. Fei. Layer-induced seismic anisotropy from full-wave sonic logs: theory, applications and validation. *Geophysics*, 71:D183–D190, 2006.

A. E. H. Love. *Some problems of geodynamics*. Cambridge University Press, 1911.

L. Lu, C. Wang, and B. Zhang. Inversion of multimode Rayleigh waves in the presence of a low-velocity layer: numerical and laboratory study. *Geophys. J. Int.*, 168:1235–1246, 2007.

R. F. de Lucena and F. Taioli. Rayleigh wave modeling: A study of dispersion curve sensitivity and methodology for calculating an initial model to be included in an inversion algorithm. *Journal of Applied Geophysics*, 108:140–151, 2014.

G. Mavko, T. Mukerji, and J. Dvorkin. *The Rock Physics Handbook*. Cambridge University Press, Cambridge, 1998.

T. B. Meehan. Python® code for calculating surface wave dispersion curves. https://github.com/tbmcoding/dispersion, December 2017.

T. B. Meehan. Evolution of the propagator matrix method and its implementation in seismology. *arXiv*, 1801.04635([physics.geo-ph]):1–12, January 2018.

O. Novotný. Methods of computing the partial derivatives of dispersion curves. *Pageoph*, 114:765–774, 1976.

C. B. Park, R. D. Miller, and J. Xia. Multichannel analysis of surface waves. *Geophysics*, 64(3):800–808, 1999.

K. Parsopoulos and M. Vrahatis. Particle swarm optimization method in multiobjective problems. *Proceedings of the ACM Symposium on Applied Computing (SAC)*, pages 603–607, 2002.

G. W. Postma. Wave propagation in a stratified medium. *Geophysics*, 20:780–806, 1955.

Y. Y. Riznichenko. On seismic anisotropy. *Invest. Akad. Nauk SSSR, Ser. Geograf. i Geofiz.*, 13:518–544, 1949.

B. Romanowicz. Inversion of surface waves: a review. *International Handbook of Earthquake and Engineering Seismology*, 81A:149–175, 2002.

M. P. Rudzki. Parametrische Darstellung der elastischen Wellen in anisotropischen Medie. *Bull. Acad. Cracovie*, page 503, 1911.

S. M. Rytov. The acoustical properties of a finely layered medium. *Akust. Zhur.*, 2:71, 1956.

M. Schoenberg and F. Muir. A calculus for finely layered anisotropic media. *Geophysics*, 54(5):581–589, 1989.

T. Shermergor. *Theory of elasticity of microinhomogeneous media* (in Russian). Nauka, 1977.

M. A. Slawinski. *Waves and rays in elastic continua*. World Scientific, Singapore, 3rd edition, 2015.

M. A. Slawinski. *Waves and rays in seismology: Answers to unasked questions*. World Scientific, 2nd edition, 2018.

L. Thomsen. Weak elastic anisotropy. *Geophysics*, 51(10):1954–1966, 1986.

W. Thomson. *Mathematical and physical papers: Elasticity, heat, electromagnetism*. Cambridge University Press, 1890.

W. T. Thomson. Transmission of elastic waves through a stratified solid medium. *Journal of Applied Physics*, 21:89–93, 1950.

D. K. Tiwary. *Mathematical modelling and ultrasonic measurement of shale anisotropy and a comparison of upscaling methods from sonic to seismic*. PhD thesis, University of Oklahoma, 2007.

A. Udías. *Principles of seismology*. Cambridge University Press, 1999.

W. Voigt. *Lehrbuch der Kristallphysik*. Teubner, Leipzig, 1910.

N. Waeselmann, J. M. Brown, R. J. Angel, N. Ross, J. Zhao, and W. Kamensky. The elastic tensor of monoclinic alkali feldspars. *American Mineralogist*, 101:1228–1231, 2016.

N. Wang, J-P. Montagner, G. Burgos, Y. Capdeville, and D. Yu. Intrinsic *versus* extrinsic seismic anisotropy: Surface wave phase velocity inversion. *Comptes Rendus Geoscience*, 347:66–76, 2015.

M. Wathelet, D. Jongmans, and M. Ohrnberger. Surface-wave inversion using a direct search algorithm and its application to ambient vibration measurements. *Near Surface Geophysics*, 2:211–221, 2004.

J. E. White and F. A. Angona. Elastic wave velocities in laminated media. *J. Acoust. Soc. Am.*, 27:310–317, 1955.

J. Xia, R. D. Miller, and C. B. Park. Estimation of near-surface shear-wave velocity by inversion of Rayleigh waves. *Geophysics*, 64(3):691–700, 1999.

H. Xie and L. Liu. Near-surface anisotropic structure characterization by Love wave inversion for assessing ground conditions in urban areas. *Journal of Earth Science*, 26(6): 807–812, 2015.